A 3D BACTERIAL SWIMMING MODEL COUPLED WITH EXTERNAL FLUID MECHANICS USING THE IMMERSED BOUNDARY METHOD

By
CHIA-YU HSU

A dissertation submitted in partial fulfillment of
the requirements for the degree of

DOCTOR OF PHILOSOPHY

WASHINGTON STATE UNIVERSITY
Department of Mathematics

AUGUST 2007

To the Faculty of Washington State University:

The members of the Committee appointed to examine the dissertation of **CHIA-YU HSU** find it satisfactory and recommend that it be accepted.

_____
Chair

_____

_____

TABLE OF CONTENTS

List of Tables

List of Figures

This dissertation is dedicated to
my Father and Mother
for their endless love.

Acknowledgements

I would like to thank Professor Robert Dillon, my supervisor, for introducing me to this interdisciplinary computational science. His numerous discussions, endless patience and constant encouragement helped make this work a success. I appreciate the opportunity he provided to pursue research in the field of mathematical and computational biology and for introducing me to the modeling of bacterial swimming and the immersed boundary method. In particular, I appreciate having been provided with a research assistantship so that I could focus on my research projects in the Department of Mathematics at WSU.

I would like to thank all of the faculty in the Department of Mathematics, WSU, for providing me with all of the available facilities and such a warm environment so that I could have enough resources and be able to concentrate on my research and studies. In particular, I would like to thank Professor Mark Schumaker, for his numerous invitations to give talks in the applied mathematics seminars. This provided me with a great chance to talk about my projects and to improve my research results and a great opportunity to practice my oral presentation skills. Special thanks to Pam Guptill, our graduate program coordinator, for her assistance on student affairs and for her friendship. And thanks to Terry Wagoner, Craig Holland and Kevin Cooper for their computer support. I would also like to thank Dr. XingZhou Yang for his discussions, suggestions and software assistance on computational issues while he was in Pullman as a visiting researcher in 2005 and later via email.

Also I would like to thank my friends in Pullman, Ching-Guo Wu and Hao-Yu Chiu, Vincent Kok and his wife Dong-Yun Wang, for their many invitations to join their family activities. Their friendship and spiritual support provided me the strength and energy to overcome the daily affairs I had in living in Pullman and in my dissertation writing period. Beside these, I would like to thank Dr. Alan Genz, Dr. Judith McDonald, Dr. Darrell Kent and his wife Jan, Jeanette and David Martin,

Professor Dillon and Nadine, for their invitations to join Thanksgiving and Christmas parties. Those family parties provided me great chances to join and enjoy traditional family holidays with a lot of nice people. In particular, I would like to thank my parents Hsin-Chang and Hsiu-Mei, and all my family for their love, encouragement, and on support during the my Ph.D study. Most of all, I would like to thank Professor Valipuram S. Manoranjan and Professor Mark Schumaker for being on my thesis committee and for the lectures I took from both of them during my graduate study years.

All the numerical simulations were run on computers at the Center for Computational Science (CCS) at Tulane University. All the figures in this dissertation were created using the NCAR Graphics software which is provided by the National Center for Atmospheric Research (NCAR). The research was supported by a National Science Foundation grant DMS-0201063. The author thanks CCS for their computational facilities, to NCAR for their graphic software, and NSF for the support of this research.

A 3D Bacterial Swimming Model
Coupled With External Fluid Mechanics
Using The Immersed Boundary Method

Abstract

by Chia-Yu Hsu, Ph.D
Washington State University
August 2007

Chair: Robert Dillon

We introduce a 3D motile rod-shaped bacterial model with a single polar flagellum which is based on the configuration of a monotrichous type of bacteria such as Pseudomonas aeruginosa. The structure of the model bacterial cell consists of a cylindrical body together with the flagellar forces produced by the rotation of a helical flagellum. The bacterial cell body is constructed from a set of immersed boundary points and elastic links. The helical flagellum is assumed to be rigid and modeled as a set of discrete points along the helical flagellum and flagellar hook. A set of flagellar forces are applied along this rotating helical curve as the flagellum rotates. An additional set of torque balance forces are applied tangentially on the cell body to drive the counter-revolution of the body and provide torque balance.

The fluid flow that drives the model bacterial cell is governed by the incompressible Navier-Stokes equations with a force density contributed from the elasticity of the cell body, the rotation of the flagellum, and the torque balance forces. The model is based on the immersed boundary method introduced by Peskin to model the fluid flow of the heart. We solve the Navier-Stokes equations numerically for the fluid velocity at each time step by Fast Fourier Transform methods and advect the bacterial cell at the local fluid velocity.

This fully 3D model is loosely based on an earlier 2D model for bacterial swimming introduced by Dillon, Fauci and Gaver in 1995. Numerical simulations of the bacterial swimming model are presented. We show simulations that demonstrate first order convergence as the numerical mesh is refined. We also show simulations of the model helical centroid trajectory, the model behavior in forward and backward swimming and the hydrodynamic interaction of two or more motile cells from various initial configurations as well as the hydrodynamic influence of walls and tubes on the model swimming.

Introduction

Many bacteria commonly found in nature and in the human body are motile. These include many strains of Escherichia coli (E. coli), Salmonella typhimurium, and Pseudomonas aeruginosa which play an important role in human disease. A bacterial flagellum or flagella provides the motility in these and many other types of bacteria. There are alternative forms of bacterial motility including gliding, in bacteria such as Myxobacteria [140, 149, 76, 60], and the complex swimming mechanism of Spirochaetes [33, 151]. Motile bacteria of the flagellated type can swim in viscous fluid environments. E. coli is probably the most widely studied bacteria. Motile forms of E. coli are peritrichously flagellated and have many flagella. In contrast, Pseudomonas aeruginosa [134, 58] typically have a single flagellum at one end of a rod-shaped body or a pair of flagella, one at each end. Pseudomonas aeruginosa is a pathogen of high frequency in nosocomial infections, urinary tract infections, and in cystic fibrosis and can have considerable antibiotic resistance [136, 48].

In this thesis, we introduce a new mathematical model and numerical method for modeling bacterial motility in rod-shaped bacteria with a single polar flagellum such as found in many strains of Pseudomonas aeruginosa. The formulation of this fluid-mechanical model is based on the immersed boundary method, first introduced by Charles Peskin to model the blood flow in the human heart. We include the fully

three-dimensional time dependent fluid dynamics of the Navier-Stokes equations for incompressible fluid flow, the mechanics of the bacterial rod-shaped body and the forces due to the rotation of the bacterial flagellum. The model strictly enforces conservation of momentum, as well as angular momentum, and thus provides a realistic description of bacterial swimming.

In Chapter 1.1, we give some relevant background on bacterial microbiology, the rod-shaped bacterial cell body, the bacterial motor, and flagellum. In Chapter 1.2, we give an overview of flagellar hydrodynamics in bacterial swimming and, in Chapter 1.3, an overview of the immersed boundary method.

The three-dimensional swimming bacterial model will be described in Chapter 2. The bacterial cell body is constructed with a set of immersed boundary points and elastic links. The flagellum is represented by a set of flagellar forces that generate fluid flow and propel the bacterial cell. The torque due to flagellar rotation is offset by torque forces on the body which results in zero net force and zero net torque produced by the bacterium.

In Chapter 3, we present a numerical convergence study, a study of single cell swimming, a study of bacterial swimming with changes in flagellar configuration and the complex interaction of two swimming bacteria. Simulation results of a single swimming bacteria are contrasted with results from the literature. We also consider the motion of a bacterium with the flagellar rotational direction reversed, and the effect of changes in flagellar characteristics such as flagellar length, amplitude, pitch and rotational frequency. The interaction of swimming bacteria in proximity is of particular interest in bioconvection and in chemotaxis. We show that the hydrodynamic interaction of two bacteria swimming can create the illusion of bacterial tumbling.

In Chapter 4, we investigate the interaction a swimming bacterium near a wall, between planar walls, within a cylindrical tube and outside one or two cylinders. In Chapter 5, we summarize and discuss these results and describe future development of this bacterial swimming model.

Chapter 1

Research Background

The swimming of bacteria was first observed by Antony van Leeuwenhoek in the 1670's using his single-lens microscope [8]. Most motile bacteria move by use of a flagellum or flagella [121]. Motile bacteria are able to actively move toward regions that are more suitable for survival. These regions might contain more nutrients. Motile bacteria can also move away from toxic regions [7, 14, 30]. Relevant research on bacterial motility and related topics will be reviewed in Chapter 1.1. The study of flagellar hydrodynamics has a rich history beginning with the work of G.I. Taylor [142, 143]. Lighthill provided a hydrodynamical model of the flagellar force that inspired the bacterial swimming model in this dissertation [101, 102]. In Chapter 1.2, we provide a survey of the relevant studies on the hydrodynamics of flagellated microorganisms.

The immersed boundary method was originally developed by Peskin [123] in 1977 for the study of blood flow in the heart. This method [124] provides both a modeling framework and numerical method for studying the interaction of incompressible fluid flow and immersed elastic structures. The immersed boundary method has been employed in a variety of applications including the study of blood flow in the heart [122, 123, 124], blood vessels [148, 135], deformation of blood cells [29], platelet

aggregation and adhesion in blood clotting [67, 65, 68, 150], signal transduction by cochlea [22, 70] as well as microorganism locomotion [61, 62, 52, 63, 64, 38]. In Chapter 1.3, we provide an overview of this method.

1.1 Bacterial Motility

The investigation of bacterial motility has provided insights into the structure of the bacterial flagellum and its motor, as well as the external fluid mechanics of flagellar hydrodynamics. There are three types of mechanisms that have been identified for bacterial motility. The most common type of motility is produced by the rotation of a flagellum or flagella [15]. The swimming of Spirochaetes is also facilitated by flagella, but in this case the flagella wrap around a central protoplasmic cylindrical body. This cylindrical body and flagella lie inside an outer membrane [121, 151]. In a third type of motility associated with the gram-negative myxobacteria, bacteria are able to glide along a surface on slime produced by the bacteria [140, 149]. We do not consider the motility of spirochetes or of gliding bacteria in this study and shall use the terms "motile" and "flagellated" interchangeably. Flagellated bacteria are classified by the number and distribution of flagella on the bacterial cell body. Flagellated bacteria have been divided into four categories:

(1) Monotrichous: A single flagellum at one end of the body

(2) Amphitrichous: Two flagella, one at each end, or a single flagellum on each end

(3) Lophotrichous: More than two flagella located at one end of the cell body

(4) Peritrichous: More than two flagella distributed over the cell body

In our three-dimensional swimming bacterial model, we shall focus on rod-shaped bacteria of monotrichous type. The bacterial structure associated with flagellated bacterial swimming has been studied by Berg at al [5]-[13]; the hook and MS-ring (motor) of the basal body by DePamphilis and Adler [49, 50]; the flagellar bundle, geometry and flagellar assembly by Macnab [109, 112, 113]; the gradient-sensing

mechanism of bacterial motility and chemotaxis by Macnab and Koshland [110, 111]; signal transduction and torque generation of the reversible motor by Blair [26, 27]; flagellar motor numerology relative to motor rotation by DeRosier [51]; rotational switching by Bren and Eisenbach [31]; and the flagellar structure by Namba et al [120]. In most cases, a peritrichous type of bacteria, such as Escherichia coli or Salmonella typhimurium, has been used as the experimental model organism. However, Roberts and Doetsch [134] investigated flagellar properties of monotrichous bacteria.

In order to observe the movement of bacteria under chemoattractants, Berg and Brown [14] created a tracking microscope in 1972 to track bacterial movement. They created a gradient of chemoattractants by inserting attractants at the wall of the tracking chamber. In 1973, Berg and Anderson [15] showed that bacteria swim by using flagellar rotation. In 1974, Silverman and Simon [138] provided data and further experimental evidence in support of these conclusions. In one of their experiments, Silverman and Simon tethered two bacteria together and observed the counter rotation of the bacteria. The flagellum was found to be the fundamental organelle for bacterial motility. It is a semi-rigid passive appendage and rotates rigidly about the flagellar axis as it protrudes behind the cell body [15, 8]. The flagellum has three major components: a basal body, a hook and a filament [57]. The basal body is a reversible motor composed of several proteinaceous rings with diameters of about 45nm [51, 13]. The motor's rotational frequency can vary from 15Hz when the bacterium is tethered up to 300 Hz when the bacterium is swimming [86, 26]. The hook, with length of about 45-50nm, extends from the motor to the helical filament [49, 86, 138]. The flagellar filament is composed of 11 protofilaments which are comprised of protein monomers known as flagellin. This whip-like hollowed appendage can grow 10-15 μm in length.

Its atomic structure has been studied in detail by Namba and colleagues [120] with X-ray crystallography and electron cryomicroscopy.

This passive bacterial flagellum is very different from the eukaryotic flagellum due to fundamental differences in the flagellar structures [6]. The "9+2" axoneme of a typical eukaryotic flagellum consists of an outer ring of 9 microtubule doublets and two inner microtubules. The bending of the eukaryotic flagellum is induced by sliding between neighboring pairs of doublet microtubules. The sliding of adjacent pairs of doublet microtubules is produced by the activity of thousands of molecular motors known as dyneins. The sliding induced by the dyneins are powered by the hydrolysis of adenosine triphosphate (ATP) [55].

In flagellated bacteria, a rotational motor, embedded in the cell body, turns a rigid helical flagellum. The rotation of the flagellum drives the fluid motion [15, 8]. The motor rotation is generated by a transmembrane flow of proton ions. Many motile bacteria are sensitive to chemical attractants in the environment and have evolved a complex mechanism for moving up (or down) chemical gradients by alternating the flagellar rotational directions between counterclockwise (CCW) and clockwise (CW). By convention, the rotational direction CCW and CW are taken with respect to a viewpoint behind the cell body [26, 144, 146].

A left-handed helix is commonly found in flagellated bacteria as they swim forward with a CCW flagellar rotation. However, this is not a unique flagellar configuration. Some flagellated bacteria have been found to swim forward with a right-handed helical flagellum rotating CW [1, 72]. According to Namba [120], a reversal of the bacterial motor forces the configuration of the flagella's 11 protofilaments to change state from L-type to R-type or from L-type to R-type. This change of state is accompanied by

changes in flagellar handedness as well as changes in amplitude and pitch.

The bacterial response to chemical gradients is known as chemotaxis. Bacterial cells sense chemoattractants or repellent through a complex signal transduction process [139, 27]. Bacteria are unable to sense a chemical gradient directly. Instead, the bacteria sense changes in chemical concentration over time. In the classic run and tumble model for E.coli, a bacterium swims forward under the combined clockwise rotation of its flagella, and undergoes a tumble or change of direction when the flagella reverse rotational direction [5, 13, 91]. In high concentrations of chemoattractants, the attractants bind to chemoreceptors, methyl-accepting chemotaxis proteins (MCPs), and block the function of phosphorylated cytoplasmic protein CheY causing the motor to rotate CCW [30, 115].

The flagellum of monotrichous bacteria such as Pseudomonas aeruginosa are dragged into a left-handed helix in CCW rotation to generate the fluid flow that propels the cell body to forward. For peritrichous bacteria such as Escherichia coli and Salmonella typhimurium, the flagella form a helical bundle and propel the bacteria forward if all the motors rotate CCW [109, 107, 87]. This is known as the running mode. In peritrichous bacteria, a tumble mode occurs when a reversal of flagellar rotation causes the flagellar bundle to unravel. The tumble mode was first photographed in Salmonella in 1965 by Mitani and Iino, and in E. coli by Ramsey and Adler in 1966-1969 [14]. The duration of the run and tumble modes are approximately 1 second and 0.1 seconds respectively [11]. However, this tumble mechanism may not be appropriate for monotrichous bacteria.

The bacterial cell body rotates in the opposite direction of flagellar rotation. This counter rotation of the cell body produces an overall torque balance with the torque

induced by the rotation of the flagellar motor and flagellum [130, 93]. Turner, Berry and Berg [18, 21] have investigated the torque generated by the motor in CW and CCW rotation. Changes in the configuration of the flagellum due to changes in rotational direction have been investigated by Arkhipov, Freddolino, Imada, Namba and Schulten in 2006 [3, 2].

1.2 Flagellar Hydrodynamics

The fluid dynamics of swimming organisms is a complex system and difficult to analyze. In bacterial swimming, the factors involved in motility include the quantity or density of the bacteria in the domain, physiological conditions of the bacteria such as size, mass and elasticity, the structure of the cell body and flagella, the configuration of the flagellum, the bacterial swimming methodology, environmental factors such as the density, viscosity and temperature of the fluid, as well as other conditions such as chemical substrates, particles in the fluid, and gravity.

The Reynolds number is a dimensionless ratio of inertial force and viscous force defined as

$$Re = \frac{LU}{\mu/\rho} = \frac{LU}{\nu} = \frac{Inertial force}{Viscous force}$$

where L is the characteristic length, U is the characteristic velocity, μ is fluid viscosity, ρ is fluid density and $\nu = \mu/\rho$ is kinematic viscosity. We show typical values in Tables 1.1 for bacterial swimming in water.

Symbol	Parameter	Data
L	characteristic length	1 μm
U	characteristic velocity	20 μm/sec
μ	fluid viscosity	10^{-2} g/cm.sec
ρ	fluid density	1g/cm^3
ν	kinematic viscosity	μ/ρ

Table 1.1: Typical parameters for bacterial swimming.

Childress [33] provided a table to show the distinct Reynolds numbers of a variety of animals and organisms with different sizes and swimming velocities, such as spermatozoan with $Re \approx 10^{-2} - 10^{-3}$ and medium sized fish with $Re \approx 10^4$. The Reynolds number for a bacterium is approximately $Re = 10^{-5}$, due to its size and

velocity. Since the fluid viscosity dominates the fluid dynamics of swimming bacteria, the initial forces are typically neglected and the fluid mechanics can be represented by the Stokes equation with momentum equation:

$$-\nabla p + \mu \triangle \mathbf{u} + \mathbf{F} = 0 \tag{1.2.1}$$

and the continuity equation:

$$\nabla \cdot \mathbf{u} = 0 \tag{1.2.2}$$

where $\mathbf{u}$ is the fluid velocity, p denotes the pressure, μ is fluid viscosity, $\mathbf{F}$ is the external force applied to the fluid.

Since the Stokes equations are linear, they are more amenable to mathematical analysis than the Navier-Stokes equations which will be described later. The modern study of the hydrodynamics of swimming organisms and cilia began with Gray [73, 75] in the 1920's. In 1950 and 1952, G.I. Taylor [142, 143] studied the swimming of microscopic organisms in the low Reynolds number regime and interaction of the tails of microscopic organisms. The resistive-force theory of Gray and Hancock [74, 78, 79, 33, 101, 102] provided estimates for the effective normal and tangential resistance coefficients K_T and K_N for a segment of a moving flagellum.

Later, slender-body theory, originally initiated by Burgers in 1938, was developed by Cox [41] and Batchelor [4] for a long slender solid body. Cox investigated the interaction between two or more long slender bodies and the swimming behavior in the neighborhood of solids walls. Batchelor extended this theory from Cox's assumption of a slender body with circular cross-section to a more general noncircular crosssection. Keller and Rubinow [88, 89] used the method of matched asymptotic expansions to study the flow passing a slender body with circular cross section and allowed the slender body to twist. Machin [108], Brokaw [32], Hines and Blum [80] investigated

bending wave propagation in eukaryotic flagellum. Winet, Chwang and Wu [42, 43, 44, 45, 46, 47] have investigated the locomotion of spirochetes which propagate a 3D helical wave along their elongated body. Their analysis of spirochete motility followed the resistive theory of Gray and Hancock and included the counter rotation of the cell body and the torque generated by the flagellum.

Lighthill's [101, 102] refinement of slender body theory led to a modification of the resistance coefficients and an improved analysis of flagellar hydrodynamics. Higdon [81, 82, 83] studied microorganism swimming by flagellar propulsion using stokeslets, dipoles and rotlets to represent the cell body and applied slender body theory to represent the flagellum with a set of the stokeslets and dipoles. Moreover, an image system was used to eliminate the velocity induced by those singularities on the flagellum and represent the fluid velocity as a system of singular integral equations. A similar approach was used by Phan-Thieh, Tran-Cong and Ramia [129] to study the hydrodynamics of microorganism motility. Lighthill provided a detailed description of microorganism motility in his monograph on aquatic animal locomotion at low Reynolds number in his book, *Mathematical Biofluiddynamics* [101]. Childress provided an overview of flagellar hydrodynamics of the swimming flagellated organisms in his book, *Mechanics of swimming and flying* [33].

1.3 The Immersed Boundary Method

The immersed boundary method, was originally developed by Charles Peskin in 1972 and applied to the study of the blood flow of heart valves in 1977 [122, 123, 124]. Peskin and McQueen have extended the method to the three-dimensional biofluid dynamics of the heart [125, 126, 127]. The immersed boundary method has also been used by Eggleton and Popel to study blood cell deformation [59], by Bottino to model viscoelastic networks in the actin cytoskeleton of ameboid cells and in cell deformation [29], by Fogelson and Fauci to model platelet aggregation and adhesion in blood clotting [67, 65, 68, 150], by Vesier and Yoganathan to model blood flow in elastic vessels [148], by Byer to model signal transduction by cochlea in the inner ear [22], by Givelberg and Bunn in a 3D model of the cochlea [70], by Fauci and others to model the swimming of various aquatic animals, organisms and micro-organisms including eels, leech, nematodes, sperm, biflagellated algal cells [61, 62, 52, 63, 64, 38] and, by Dillon, Fauci, Gaver, and Fogelson to model biofilm formation [53, 54].

The immersed boundary method can be described by Equations (1.3.1)-(1.3.4),

$$\rho(\mathbf{u}_t + (\mathbf{u}\cdot\nabla)\mathbf{u}) = -\nabla p + \mu\triangle\mathbf{u} + \mathbf{F}(\mathbf{x},t) \tag{1.3.1}$$

$$\nabla\cdot\mathbf{u} = 0 \tag{1.3.2}$$

$$\mathbf{F}(\mathbf{x},t) = \int \mathbf{f}(\mathbf{s},t)\delta(\mathbf{x}-X(\mathbf{s},t))d\mathbf{s} \tag{1.3.3}$$

$$\frac{\partial X}{\partial t} = \mathbf{u}(X(\mathbf{s},t),t) = \int \mathbf{u}(\mathbf{x},t)\delta(\mathbf{x}-X(\mathbf{s},t))d\mathbf{x} \tag{1.3.4}$$

where $\mathbf{u}$ is the fluid velocity, p is pressure, $\mathbf{x}$ and $\mathbf{s}$ are Eulerian and Lagrangian variables, $\delta(\mathbf{x})$ is the Dirac delta function. ρ is fluid density and μ is fluid viscosity. The first two equations (1.3.1) and (1.3.2) are the Navier-Stokes equations for an incompressible fluid. An elastic structure or organism is represented as an immersed boundary at time t denoted by $X(\mathbf{s}, t)$. The boundary conditions for the fluid domain are typically given as periodic and the domain is a regular parallelepiped in three dimensions. In the basic version of the immersed boundary method, the organism is assumed to have the same density as the fluid. Thus, the immersed boundary $X(\mathbf{s}, t)$ is assumed to be massless. The forces $\mathbf{f}(\mathbf{s}, t)$ due to the organism are applied to the Navier Stokes equations by means of the integral equation (1.3.3) . The Navier-Stokes equations "see" the organism as additional forces F. The system of equations is closed by requiring that the immersed boundary $X(\mathbf{s}, t)$ move at the local fluid velocity in Equation(1.3.4). In typical numerical implementations, the fluid domain is represented as a regular grid. Since the domain shape is a regular parallelepiped, the equations can be solved efficiently using Fast Fourier Transform methods or multigrid.

Originally, Peskin developed the immersed boundary method to study the flow pattern around the heart and solved the incompressible Navier Stokes equations using Chorin's projection method [122, 123]. In this projection method the fluid velocity vector field $\mathbf{u}$ is projected onto the divergence-free vector field according to the Helmholtz-Hodge Decomposition Theorem [35, 36, 34] by applying the condition of incompressibility. Later in 1977, a fast Laplace-solver was incorporated into the immersed boundary method. The spatial discretization was based on a Cartesian mesh for the Eulerian variables and a moving curvilinear mesh for the Lagrangian variables. A second order accurate Runge-Kutta method was used in the temporal

discretization. Several smoothed delta functions [77] used in Equation (1.3.3) and (1.3.4) have been created to interpolate the Lagrangian elastic force density to the Cartesian grid and interpolated on the Eulerian grid to the points on the Lagrangian mesh.

In 1992, Tu and Peskin investigated the stability and instability of the immersed boundary method using Stokes equations. They compared the stability of explicit, approximate-implicit and implicit methods. The body configuration was computed implicitly and the force density term was found by Newton's method from the gradient of the elastic energy function. In 1993, Mayo and Peskin [116] used an iterative scheme defined on the interpolation operator of the boundary configuration and Aitken extrapolation to accelerate the convergence rate. Besides this, volume conservation was studied by Peskin and Printz [128] in 1993.

The improvement of the immersed boundary method's spatial order of accuracy was investigated by Lai and Peskin [90]. A formally second order accurate immersed boundary method was demonstrated in the flow past a cylinder. Other improvements of the immersed boundary method such as high order convergence rate for a sufficiently smooth boundary have also been investigated by Griffith and Peskin [77] using a hybrid numerical scheme in using an approximate projection method for the intermediate velocity and a strong stability-preserving Runge-Kutta method for time integration and evolution of the immersed boundary points.

LeVeque and Li, inspired by the immersed boundary method, developed a fully second order accurate immersed interface method for elliptic and hyperbolic equations. The immersed interface method incorporates jump conditions at the sharp interface [97, 98, 99]. The immersed interface method was extended to the Navier

Stokes equations by Li and Lai in 2001 with the aid of a level set representation for the interface [100]. Lee and LeVeque [95, 96] extended the immersed interface method to the framework of Peskin's immersed boundary method in 2002. Khoo, et.al developed another type of immersed interface method for the Navier-Stokes equations [94].

A blob projection method was developed by Cortez and Minion which use a finite difference method for modeling the interaction of elastic membranes immersed in a viscous incompressible fluid. In the blob projection method, a cutoff or blob function, was used to regularize the force field [40]. More properties of this blob function are found in Cortez's "Method of Regularized Stokeslets" [39] and its applications to the study of the flagellar bundle [66] by Flores, et al..

Chapter 2

A 3D Bacterial Swimming Model

We introduce a three-dimensional model for a motile rod-shaped bacterium with a single polar flagellum. The formulation of the model is based on the immersed boundary method. The structure of the model bacterial cell consists of a cylindrical body together with flagellar forces. A 3D bacterial cell body is constructed from a set of points and elastic links. The bacterial flagellum, and the rotational forces due to the bacterial motor are represented in an idealized fashion. The helical flagellum is modeled as set of discrete points along its helix and its flagellar hook. We assume that the flagellum is rigid and impose a fixed rotational velocity. The flagellar forces on each of the discrete flagellar immersed boundary points are derived by considering the drag force on each small segment of the rotating flagellum [11, 33] The counter rotation of the bacterial cell body is induced by torque balance forces applied to the cell body. At each point in time, the model bacterial cell applies a zero net force and a zero net rotational force or torque to the surrounding fluid. The net force and net torque are obtained by a summation of the individual contributions to the force and torque over the entire bacterial model organism. The flagellar forces drive the fluid motion and the swimming of the bacterial cell. We represent the fluid mechanics

by means of the fully three-dimensional time dependent Navier-Stokes equations for incompressible flow. We note that the Reynolds number for bacterial swimming is very low and that the Stokes equations could be used for this model. We show a detailed description of the bacterial structure in Chapter 2.1.

In Chapter 2.2, we discuss Lighthill's analysis of flagellar hydrodynamics and describe the flagellar force structure of our 3D model. The flagellar force structure and its mathematical representation will be provided. The immersed boundary model will be introduced in Chapter 2.3 along with the numerical algorithm for this model.

2.1 The Rod-Shaped Bacterial Cell Body

Figure 2.1: A 3D bacterium with a helical flagellum shown from two viewpoints.

The 3D rod-shaped bacterial model, as shown in Figure 2.1, is designed to model the motility of a neutrally buoyant bacterium with a single polar flagellum. The bacterial cell body is modeled by a set of immersed boundary points connected by elastic links to form the cylindrical structure of a rod-shaped bacterium. The rigidity of the cell body is obtained by employing elastic links with sufficient stiffness. Figure 2.2 shows the configuration of the cell body from several view points. As shown in the left panel of Figure 2.2, the body is composed of annular rings. Each of the rings is constructed with a discrete set of immersed boundary points and elastic links. As shown in the middle and right panels of Figure 2.2, neighboring annular rings are interconnected with additional elastic links that serve to maintain the rigidity of the cell body. The number of immersed boundary points on the inner and outer rings of each annulus are taken to be the same in order to simplify the link structure. The

link structure is described in detail in Chapter 2.3.

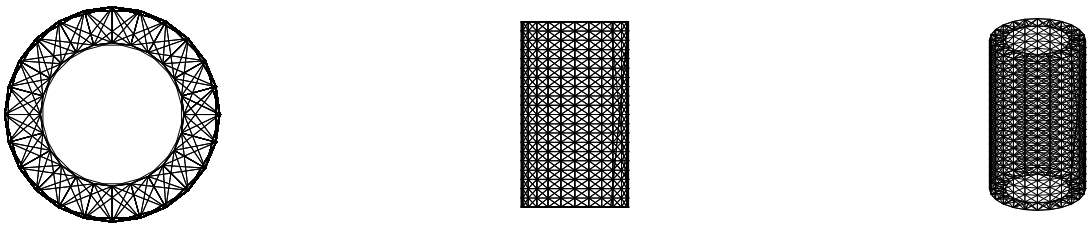

Figure 2.2: 3D view of the cell body from different view points.

The bacterial flagellum is modeled as left-handed helical filament and rotates in the counterclockwise (CCW) direction as viewed from tail when the cell swims forward. Figure 2.3 shows the top-down view of the flagellar forces and torque forces on the cell body. The flagellar amplitude and the cell body radius are the same so that the flagellum's main cylindrical helix is hidden behind the cell in Figure 2.3. The left panel on Figure 2.3 shows the cell body links and the left-handed filament coiling behind the cell body in the top-down view. In Figure 2.3 (right), we show the model cell with flagellar and torque forces. Figure 2.4 (left) shows a side-on view of the cell body and flagellar filament, and in Figure 2.4 (right), the flagellar forces on the filament. A series of frames from a numerical simulation that illustrated a single flagellar rotation from the top-down viewpoint is shown in Figure 2.5 and in Figure 2.6. The bars pointing out from the filament in Figure 2.6 represent the flagellar vector forces due to the rotation of the flagellum.

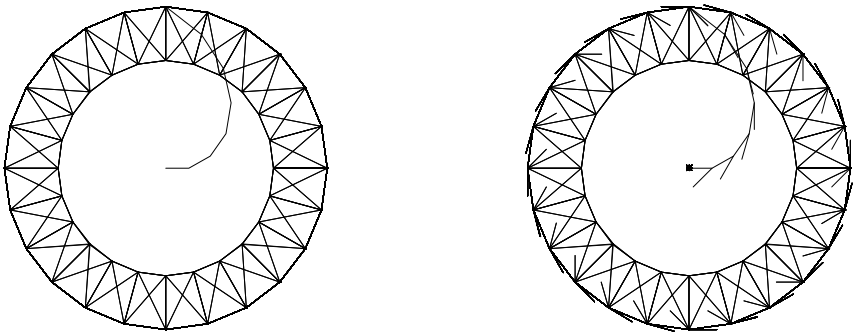

Figure 2.3: (left) Cell body links and flagellum. (right) Force illustration.

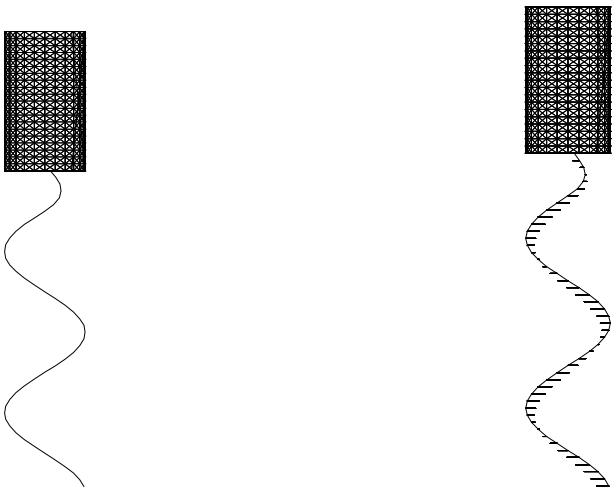

Figure 2.4: (left) Model cell and (right) flagellar forces .

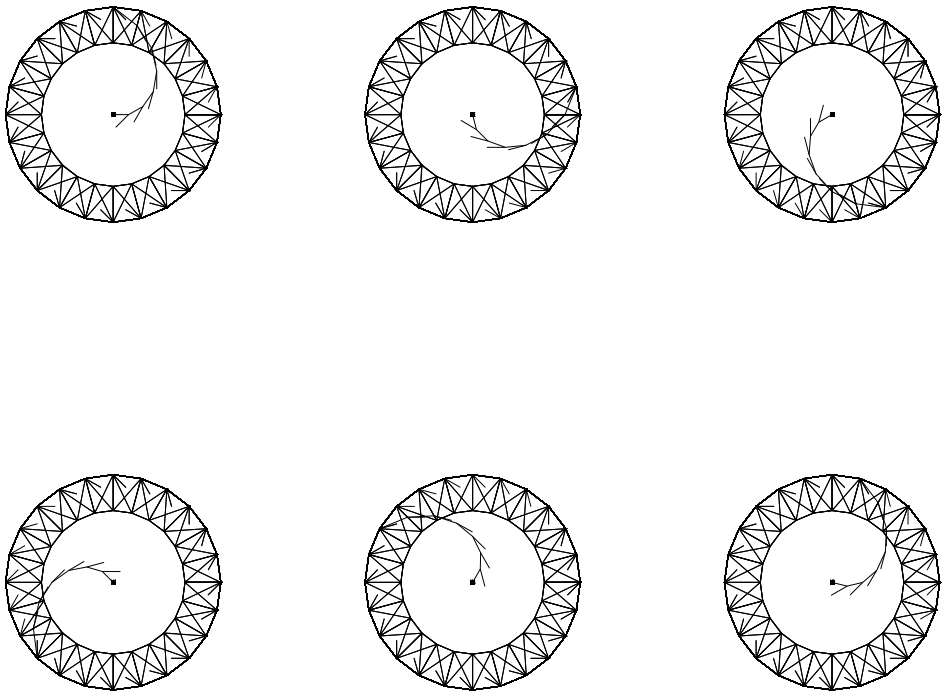

Figure 2.5: XY-view of one revolution of the flagellum with forces.

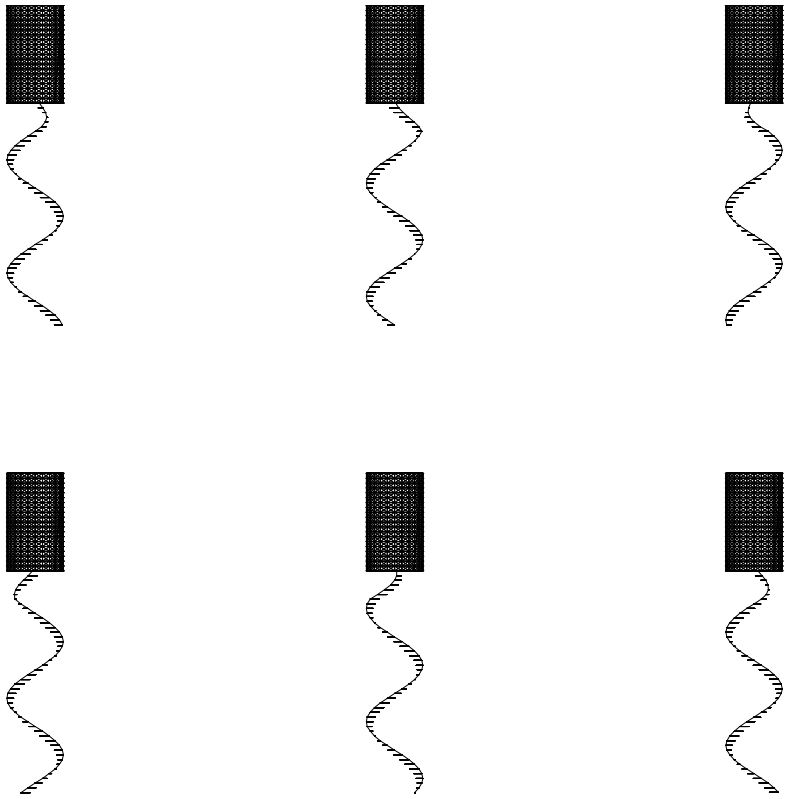

Figure 2.6: XZ-view of one revolution of flagellum with force vectors represented.

2.2 Flagellar Forces

In [102], Lighthill analyzed bacterial flagellar motion by considering the distribution of Stokeslets along a helical flagellum. A Stokeslet represents the flow generated by a concentrated force $\mathbf{f}$ acting at a point of fluid governed by the Stokes equations with the momentum equation:

$$-\nabla p + \mu \triangle \mathbf{u} + \mathbf{f}\delta(\mathbf{r}) = 0. \tag{2.2.1}$$

and the continuity equation:

$$\nabla \cdot \mathbf{u} = 0. \tag{2.2.2}$$

where $\mathbf{u}$ is the fluid velocity, p is pressure, $\mathbf{f}$ is a force vector and δ is the Dirac delta function. By taking the divergence of Equation (2.2.1) and using the continuity Equation (2.2.2), one can obtain the Poisson equation (2.2.3) in an unbounded domain.

$$\nabla^2 p = \nabla \cdot \mathbf{f}\delta(\mathbf{r}) \tag{2.2.3}$$

The Poisson equation can be solved for the pressure $p = \nabla \cdot (-\frac{\mathbf{f}}{4\pi r})$ which is a dipole field with $r = \|\mathbf{r}\|$ and $\mathbf{r}$ is the vector displacement from the point where the external force is applied. The associated velocity field $\mathbf{u}$ can be represented as

$$\mathbf{u} = \frac{r^2\mathbf{f} + (\mathbf{f} \cdot \mathbf{r})\mathbf{r}}{8\pi\mu r^3} \tag{2.2.4}$$

In Lighthill's analysis, the velocity field generated by a helical flagellum can be represented as distributions of Stokeslets and a chosen dipole in order to satisfied the no-slip boundary condition. Under the assumption that the ratio of the flagellar radius a to the flagellum length L is small [33], the flagellar velocity $\mathbf{w}$ can be represented

in terms of the flagellar force distribution $\mathbf{f}$ approximately as

$$\mathbf{w}(s_0) = \frac{\mathbf{f}_n(s_0)}{4\pi\mu} + \int_{r_0>\rho} \frac{r_0^2\mathbf{f} + (\mathbf{f}\cdot\mathbf{r}_0)\mathbf{r}_0}{8\pi\mu r_0^3} ds \tag{2.2.5}$$

where s is the distance along the centerline of the flagellum, $\mathbf{f}(s_0)$ is the flagellar velocity of a cross-section of the flagellum at $s = s_0$, and $\mathbf{r}_0$ is the position vector of the point s_0. $\mathbf{f}_n(s_0)$ is the vector normal to the centerline of the flagellum at $s = s_0$ by projecting the force $\mathbf{f}(s)$ on the plane normal to the center line and $\rho = \frac{1}{2}a\sqrt{e}$.

The rotation of a spiral with constant radius and constant pitch can be represented by the equations

$$x(s) = \alpha s, \quad y(s) = b\cos(\kappa s - \omega t), \quad z(s) = b\sin(\kappa s - \omega t)$$

where b, κ and ω are the radius, period and angular velocity at time t. The wavelength with respective to s is given by $\Lambda = \frac{2\pi}{\kappa}$ and the wavelength or pitch with respect to x is given by λ. Hence, $\alpha = \lambda/\Lambda < 1$ be defined as the contraction of the spiral. Then from the periodicity we get

$$x(s+\Lambda) = x(s) + \lambda, \quad y(s+\Lambda) = y(s), \quad z(s+\Lambda) = z(s)$$

If the wave travels along the spiral with a velocity c, then the wave velocity on the X-axis is given by $V = \alpha c$. The force $\mathbf{f}(s)$ per unit length along the centerline at $t = 0$ can be approximated by $\mathbf{f}(s) = (\hat{g}, \hat{h}\sin(\kappa s), -\hat{h}\cos(\kappa s))$ for some constants $\hat{g}$ and $\hat{h}$. Dillon, Fauci and Gaver [52] built a 2D flagellar bacterial swimming model by projecting Lighthill's spiral flagellar forces onto the 2D plane. We adopted this concept for the flagellar force in this 3D bacterium model and consider the flagellar force field on the cross-section of the flagellum distributed along the helix and rotating about the flagellar axis. The model flagellar force vectors, shown in Figure 2.7,

are the sum of a tangential and radial vector. In Figure 2.8 we show the radial flagellar force unit vectors, and in Figure 2.9, the tangential flagellar force unit vectors. The torque balance forces shown in Figure 2.10 are applied to the cell body and have the opposite orientation from the flagellar force tangential vectors. Detailed mathematical formulation of these forces and the torque balance equation will be given in Chapter 2.3.

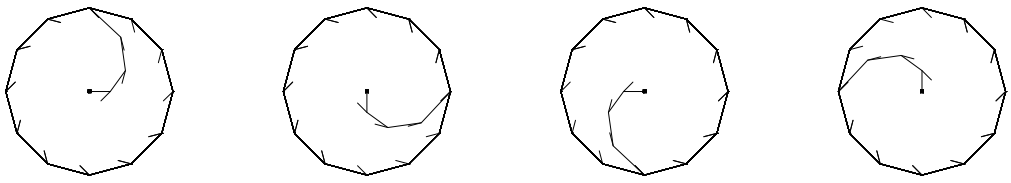

Figure 2.7: Flagellum with flagellar force vectors.

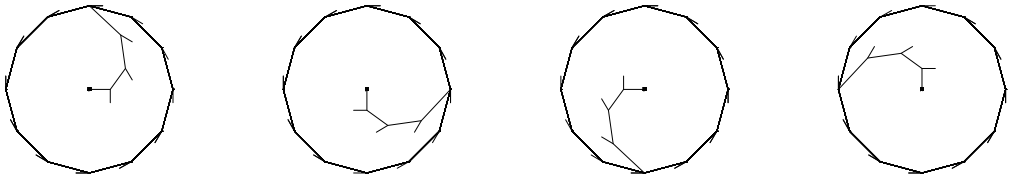

Figure 2.8: Flagellum with tangential force vectors.

We assume that the length of the rod-shaped cell body with radius r is twice its diameter and that the helical flagellum has two pitches. The length of each pitch, along the flagellar axis, is equal to one cell body length. Let r be the amplitude of the helix and L be the pitch length of the helix, then $L = 4r$. The model bacterial

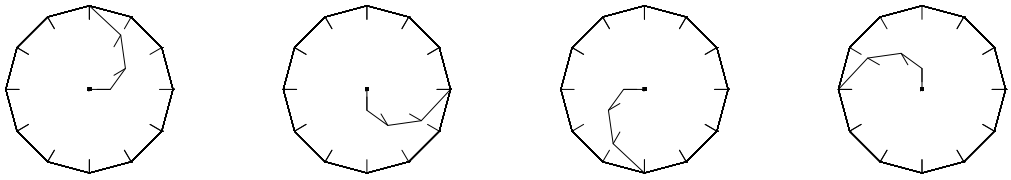

Figure 2.9: Flagellum with radial force vector.

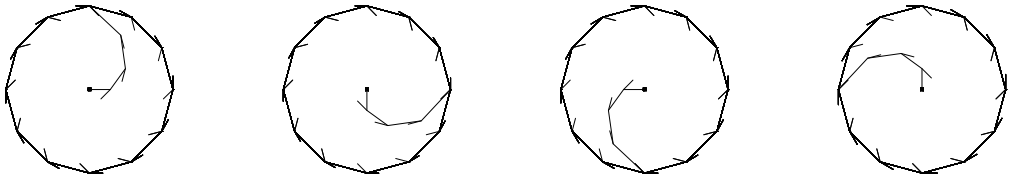

Figure 2.10: Flagellar and torque balance forces.

flagellum consists of two parts, (1) a helical filament with constant amplitude r and (2) a helical "hook" with a variable radius that tapers from r down to zero and connects the main part of the flagellum to the cell body at the centroid of the disk on the lower end of the bacterial body. The two components of the flagellum can be described mathematically by the equations in cylindrical coordinates for the cylindrical helical filament in component (1)

$$\begin{cases} z = \xi, & -2L \leq \xi \leq L_{hook}, \\ x = r\cos(\frac{-2\pi}{L}\xi), & \\ y = r\sin(\frac{-2\pi}{L}\xi), & \end{cases} \tag{2.2.6}$$

and the hook in component (2)

$$\begin{cases} z = \xi, & L_{hook} \leq \xi \leq 0 \\ x = -\frac{4r}{L}\xi \cos(\frac{-2\pi}{L}\xi), & \\ y = -\frac{4r}{L}\xi \sin(\frac{-2\pi}{L}\xi), & \end{cases} \tag{2.2.7}$$

where L_{hook} is the length of the hook. Since the amplitude of the main component of the flagellum is the same as the radius of the cell body, the flagellum lies directly below the cell body when viewed from the top, as in Figure 2.5, and is obscured by the outer ring of the cell body unless the cell body is tilted with respect to the Z-axis. However, we can clearly see the hook in the top down XY-view in Figures 2.7-2.10.

2.3 Mathematical Model and Numerical Algorithm

The mathematical model of the immersed boundary method can be described briefly by Equations (2.3.1)-(2.3.4).

$$\rho(\mathbf{u}_t + (\mathbf{u}\cdot\nabla)\mathbf{u}) = -\nabla p + \mu\triangle\mathbf{u} + \mathbf{F}(\mathbf{x},t) \tag{2.3.1}$$

$$\nabla\cdot\mathbf{u} = 0 \tag{2.3.2}$$

$$\mathbf{F}(\mathbf{x},t) = \int \mathbf{f}(\mathbf{s},t)\delta(\mathbf{x}-X(\mathbf{s},t))d\mathbf{s} \tag{2.3.3}$$

$$\frac{\partial X}{\partial t} = \mathbf{u}(X(\mathbf{s},t),t) = \int \mathbf{u}(\mathbf{x},t)\delta(\mathbf{x}-X(\mathbf{s},t))d\mathbf{x} \tag{2.3.4}$$

where $\mathbf{x}$ and $\mathbf{s}$ are the Eulerian and Lagrangian variables and $\delta(\mathbf{x})$ is the Dirac delta function. Equations (2.3.1) and (2.3.2) are the Navier-Stokes equations for an incompressible fluid. Here ρ is fluid density, μ is fluid viscosity, $\mathbf{u}$ is the fluid velocity, p denotes the pressure. The bacterial cell body and its flagellum are considered as an immersed boundary and denoted by $X(\mathbf{s},t)$ with an associated force density $\mathbf{f}(\mathbf{s},t)$ representing the elastic forces of the bacterial cell. $\mathbf{s}$ is a Lagrangian parameter. The Lagrangian forces generated by the bacterium $\mathbf{f}(\mathbf{s},t)$ are communicated to the Eulerian fluid domain in the calculation of $\mathbf{F}(\mathbf{x},t)$ by Equation (2.3.3). This force field $\mathbf{F}(\mathbf{x},t)$ drives the fluid motion in Equations (2.3.1). The bacterial structure $X(\mathbf{s},t)$ moves at the local fluid in Equation (2.3.4). The $\mathbf{F}(\mathbf{x},t)$ term in the Navier-Stokes equation (2.3.1) is the force density over the Eulerian computational domain taken as cube or a rectangular parallelepiped. This force density of the 3D bacterial model includes those forces due to the elasticity of the microbial cell wall, the swimming force field due to the flagellar hydrodynamics and the rotational torque force on the

cell body. These can be summarized by the following formula:

$$\mathbf{F}(\mathbf{x},t) = \mathbf{F}_{body} + \mathbf{F}_{rotate} + \mathbf{F}_{swim} \tag{2.3.5}$$

where $\mathbf{F}_{body}$ is the elastic force density due to the elasticity of the bacterial cell body, $\mathbf{F}_{swim}$ is the flagellar force, and $\mathbf{F}_{rotate}$ is the torque balance force that drives the counter rotation of the bacterial cell body. The various contributions to the Eulerian force field in Equation (2.3.6) are obtained from the Lagrangian force defined on the model bacterial cell

$$\mathbf{f}(\mathbf{s},t) = \mathbf{f}_{body} + \mathbf{f}_{rotate} + \mathbf{f}_{swim} \tag{2.3.6}$$

and communicated to the Eulerian fluid domain by Equation (2.3.3) where $\mathbf{f}_{body}$ is the elastic force due to the elasticity of the bacterial cell body, $\mathbf{f}_{swim}$ is the flagellar force, and $\mathbf{f}_{rotate}$ is the torque balance force which drives the counter rotation of the bacterial cell body. A detailed description of each term will given below.

In our 3D bacterial model, we discretize the cell body to obtain a set of immersed boundary points $\mathbf{X}_{i,j,k}(t)$ where $1 \leq i \leq N_P$, $1 \leq j \leq N_L$, $k = 1, 2$, N_P and N_L are the number of points on each annular ring and the number of annular rings on the body, $k = 1$ on the outer cylinder, $k = 2$ on the inner cylinder. There are three types of links:

- Horizontal links on the outer and inner rings. These are links between the immersed boundary points on the same ring $\mathbf{X}_{i,j,k}$ and $\mathbf{X}_{i\pm p,j,k}$ for $p = 1, 2, 3$
- Vertical links between adjacent layers. These are links between the immersed boundary points $\mathbf{X}_{i,j,k}$ and $\mathbf{X}_{i\pm p,j\pm 1,k}$ for $p = 0, 1, 2, 3, 4$
- Links between inner and outer rings on the same level or annulus. These are links between the immersed boundary points $\mathbf{X}_{i,j,k}$ and $\mathbf{X}_{i\pm p,j,k}$ for $p = 0, 1, 2$

The force contribution on the immersed boundary point $\mathbf{X}_q$ due to the elastic link with the immersed boundary point $\mathbf{X}_r$ is given by Hook's law for a linear elastic spring $\mathbf{f}_{qr} = S_{qr}\left(\parallel \mathbf{X}_r - \mathbf{X}_q \parallel - L_{qr}\right) \dfrac{\mathbf{X}_r - \mathbf{X}_q}{\parallel \mathbf{X}_r - \mathbf{X}_q \parallel}$ where S_{qr} and L_{qr} are the spring force constant and resting length of the link between the two immersed boundary points. The force on $\mathbf{X}_r$ is given by $\mathbf{f}_{rq} = -\mathbf{f}_{qr}$ The total force on the immersed boundary point $\mathbf{X}_q$ is the sum of forces $\mathbf{f}_q = \sum \mathbf{f}_{qr}$ where the sum is over all immersed boundary links to $\mathbf{X}_q$. Then, the total cell body force are found to be $\mathbf{f}_{body} = \{\mathbf{f}_q\}$. A discretized version of Equation (2.3.3) is used to interpolate the Lagrangian force $\mathbf{f}_q$ to the Eulerian grid force and obtain $\mathbf{F}_q$, hence $\mathbf{F}_{body} = \sum \mathbf{F}_q$.

Torque and Flagellar Forces In order to maintain conservation of momentum and angular momentum, the sum of all forces and of all torque forces produced by the model bacterial cell must sum to zero. This condition is automatically satisfied by the cell body forces because they are all represented as elastic links and $\sum \mathbf{f}_q = 0$. The flagellar forces and torque balance forces also sum to zero because they are applied axisymmetrically with respect to the bacterial cell axis. That is, an individual flagellar force vector has a complementary flagellar force vector on the opposite side of the flagellar helix and the sum of the forces is zero. A similar approach is used for the torque balance forces on the cell body. We also balance the torque generated by the flagellar forces with the torque produced by the torque balance forces.

- The torque balance forces $\mathbf{f}_{rotate}$ and $\mathbf{F}_{rotate}$:

  Let $\mathbf{N}$ is the unit axial vector aligned with the cell body axis, and $\mathbf{R}$ is the unit outward normal vector to the cylindrical body at $\mathbf{X}_{ij1}$. The magnitude of the torque force constant c_t is chosen to obtain torque balance with the torque forces induced by the rotation of the flagellum and will be defined in the torque

balance equation (2.3.12). The unit tangential force vector $\mathbf{f}_{ij}^t$ at the immersed boundary point $\mathbf{X}_{ij1}$ is found by the cross product of $\mathbf{N}$ and $\mathbf{R}$ as Equation (2.3.7):

$$\mathbf{f}_{ij}^t \equiv \frac{\mathbf{N} \times \mathbf{R}}{\| \mathbf{N} \times \mathbf{R} \|} \tag{2.3.7}$$

The total torque balance force $\mathbf{f}_{rotate}$ in Equation (2.3.6) at the cell's outer immersed boundary points $\mathbf{X}_{ij1}$ can be found as a vector field $\mathbf{f}_{rotate} = (c_t \mathbf{f}_{ij}^t)$, and the total torque balance force $\mathbf{F}_{rotate}$ in Equation (2.3.5) can be found as Equation (2.3.8):

$$\mathbf{F}_{rotate} = \Sigma_{j=1}^{j=N_L} \Sigma_{i=1}^{i=N_P} c_t \mathbf{f}_{ij}^t \delta(\mathbf{x} - \mathbf{X}_{ij1}) \tag{2.3.8}$$

- The swimming force $\mathbf{f}_{swim}$ and $\mathbf{F}_{swim}$:

  Let the unit flagellar force vector $\mathbf{f}_i^f$ at the immersed boundary point $\mathbf{X}_i^f$ of the flagellum is defined by Equation (2.3.9):

  $$\mathbf{f}_i^f \equiv \frac{\hat{\mathbf{f}}_i^f}{\| \hat{\mathbf{f}}_i^f \|} \tag{2.3.9}$$

  where the flagellar force, Equation (2.3.10), is defined as the sum of vectors $-\mathbf{R}$ and the unit tangential vector $-\mathbf{f}_{ij}^t$ found in Equation (2.3.7),

  $$\hat{\mathbf{f}}_i^f \equiv (-\mathbf{R}) + (-\mathbf{f}_{ij}^t) = (-\mathbf{R}) + (-\frac{\mathbf{N} \times \mathbf{R}}{\| \mathbf{N} \times \mathbf{R} \|}) \tag{2.3.10}$$

  Hence the total swimming force $\mathbf{f}_{swim}$ in Equation(2.3.6) can be found as a vector field $(c_f \mathbf{f}_i^f)$, hence the total swimming force $\mathbf{F}_{swim}$ in Equation (2.3.5) is given by Equation (2.3.11):

  $$\mathbf{F}_{swim} = \Sigma_{i=1}^{i=N_H N_P} c_f \mathbf{f}_i^f \delta(\mathbf{x} - \mathbf{X}_i^f) \tag{2.3.11}$$

  Here $\mathbf{X}_i^f$ is the immersed boundary point on the flagellum where $1 \leq i \leq N_H N_P$ with N_H is the number of pitches on the filament.

Torque Balance The torque generated by the rotation of the flagellum and the body must be balanced under the conservation of angular momentum. The magnitude of the torque generating forces on the body must balance the torque produced from the flagellar force. The torque balance equation (2.3.12) is given as follows:

$$\sum_{i=1}^{\frac{N_P}{4}}(r_i\mathbf{u}_r \times c_f\mathbf{u}_{f_\perp}) + \sum_{i=1+\frac{N_P}{4}}^{N_H \cdot N_P}(r\alpha\mathbf{u}_r \times c_f\mathbf{u}_{f_\perp}) = -N_L \cdot N_P(r\mathbf{u}_r \times c_t\mathbf{u}_t) \tag{2.3.12}$$

The first term on the left-hand side of the equation represents the torque generated by the flagellar hook. The second term on the left is the torque produced by the main flagellar component with constant amplitude αr where α is the ratio of the amplitude of the cylindrical helix to the radius r of cell body. The term on the right hand side of the equation is the torque driving the body rotation. The parameters for equation (2.3.12) are summarized in Table 2.1. After simplification we obtain an expression for the body force constant c_t as a function of the flagellar force constant c_f.

$$c_t = c_f(\frac{N_H - \frac{1}{8}}{N_L})\alpha\cos\theta \tag{2.3.13}$$

r	is the radius of the cell body.
N_P	is the number of points on each ring.
N_L	represents the layers of rings on the cell body.
N_H	is the number of pitches of the flagellum.
α	is the ratio of the amplitude of the flagellum to the radius of the cell body, when $\alpha = 1$ means the amplitude equal radius, take $0 \leq \alpha \leq 1$.
r_i	is the distance from the point on the hook part to the axis of the helix. $r_i = \frac{i \cdot \alpha \cdot r}{(1+\frac{N_P}{4})}$
$\mathbf{u}_r$	is the unit outward (radius) normal vector of the cell body.
$\mathbf{u}_t$	is the unit tangential vector of the cell body.
$\mathbf{u}_f$	is the unit flagellar force vector.
θ	is the angle between the unit tangential vector $-u_t$ and the unit flagellar force vector u_f.
$\mathbf{u}_{f_\perp}$	$\mathbf{u}_{f_\perp} = \cos\theta \|\mathbf{u}_f\|(-\mathbf{u}_t) = \cos\theta(-\mathbf{u}_t)$ is the orthogonal component of the unit flagellar force vector $\mathbf{u}_f$ which generates the torque, i.e $\mathbf{u}_{f_\perp} = \mathbf{u}_f \cos(\frac{\pi}{4})$.
c_f	is the flagellar force parameter.
c_t	is the torque balance force parameter.

Table 2.1: Parameters used in the torque balance equation.

Numerical Solution of the Model Equations The numerical method for solving the model equations (2.3.1)-(2.3.4) is based on Peskin's immersed boundary method. The fluid domain is discretized using a uniform 3D rectangular grid. The fluid variables $\mathbf{u}^n$, p^n, and $\mathbf{F}^n$ are defined at time t^n at these grid points. Similarly, as described above, the cell body, and flagellum are discretized to obtain immersed boundary points $\mathbf{X}_{i,j,k}$ for the cell body and $\mathbf{X}_i^f$ for the flagellum. Once the force density $\mathbf{F}$ is determined we can solve the Navier Stokes equations (2.3.1) and (2.3.2) with periodic boundary conditions using efficient Fast Fourier Transform (FFT) methods. Here we use a method that is similar to one used by Peskin and McQueen [125, 127, 117, 118]. This method is also described in Dillon and Othmer [56]. Equations (2.3.1) and (2.3.2) are discretized using finite differences. In the discretized equation we use a semi-implicit method in which the fluid velocities on the right hand side of (2.3.1) and the pressure p in Equation (2.3.1) are represented at time t^{n+1}. We use a forward difference scheme for the time derivative and an upwind scheme for the nonlinear momentum term $(\mathbf{u} \cdot \nabla)\mathbf{u}$. The fluid velocities in the momentum term are represented at time t^n as is the force field $\mathbf{F}$. The resulting system of algebraic equations is solved using FFT methods. The approximate 3D Dirac Delta function $\delta_h(\mathbf{x})$ in (2.3.3) and (2.3.4) is the product of three continuous functions, that is $\delta_h(\mathbf{x}) = d(x)d(y)d(z)$ where h is the mesh width and $d(r)$ is shown in Equation (2.3.14).

$$d(r) = \begin{cases} \frac{1}{4h}(1 + \cos(\frac{\pi r}{2h}) & , \|r\| < 2h \\ 0 & , \|r\| \geq 2h \end{cases} \tag{2.3.14}$$

This is a standard form for the delta function and was introduced by Peskin 1977 [123]. The compact support of this approximate delta function lends itself to efficient computation as the forces from each immersed boundary point are interpolated to a

small number of nearby grid points. Detailed descriptions of the immersed boundary method can be found in [124, 61, 52, 53].

The algorithm of the immersed boundary method is summarized as follows. At time t^n we have the fluid velocities $\mathbf{u}^n$ and current configuration of the bacterial cell body $\mathbf{X}^n$. In order to find the fluid velocities and configuration of the cell at time t^{n+1}, we:

1. Find the force densities $\mathbf{f}_{body}$ and $\mathbf{f}_{rotate}$ from the location of the cell's immersed boundary points $\mathbf{X}^n$ and elastic link structure.

2. Determine the location of the flagellar immersed boundary points $\mathbf{X}_f$. We assume that the flagellar reference frame moves with the cell body. We calculate the location and orientation of the flagellar reference frame from $\mathbf{X}^n$, determine the updated flagellar configuration $\mathbf{X}_f$ at the new rotation angle θ^n.

3. Calculate the flagellar force $\mathbf{f}_{swim}$ from the updated flagellar configuration $\mathbf{X}_f$.

4. Spread the force densities $\mathbf{f}_{body}$, $\mathbf{f}_{rotate}$, and $\mathbf{f}_{swim}$ using the approximate delta function to obtain the Eulerian force distribution $\mathbf{F}^{n+1}$ in Equation (2.3.3)

5. Solve the Navier Stokes equation (2.3.1) and (2.3.2) for the fluid velocity $\mathbf{u}^{n+1}$.

6. Advect the cell's immersed boundary points at the local fluid velocity using $\mathbf{u}^{n+1}$ in Equation (2.3.4) to obtain $\mathbf{X}^{n+1}$

Chapter 3

Numerical Simulations of Bacterial Swimming

In this chapter, we present numerical results for the 3D bacterial swimming model. The results for a single model cell include a numerical convergence study shown in Chapter 3.1, the behavior of a single cell swimming forwards in Chapter 3.2, a single cell swimming forwards and backwards in Chapter 3.3. In Chapter 3.4 we show numerical results for the interaction or two or more swimming bacteria. The hydrodynamic interaction between multiple bacterial cell is investigated in Chapter 3.5. Since the simulations are fully three-dimensional, we show bacterial swimming results from several viewpoints in order to visualize the model results.

In this study, the fluid temperature, fluid density and viscosity are considered as constants. The organism is assumed to be massless and neutrally buoyant. The computational domain is a rectangular parallelepiped with period boundary conditions for the fluid velocities. We use fluid markers to visualize the fluid flow of the simulations. These fluid markers are advected in the fluid velocity field at each time step during the course of the simulations and have no influence on the simulation results. One set of fluid markers is introduced around the cell body for the purpose of visualizing the

fluid flow near the bacteria. A second set of fluid markers is placed initially at each grid point in the fluid domain for the purpose of visualizing the overall fluid flow.

We show physical parameters, such as the values of the fluid viscosity, fluid density, fluid grid size and computational time step in Table 3.1.

Parameter	Symbol	Data
Density	ρ	$1g/cm^3$
Viscosity	μ	0.01 $gcm^{-1}s^{-1}$ (1cP)
Grid size	h	0.625 μm
Time step	Δt	2.4×10^{-7} sec

Table 3.1: Fluid and computational parameters.

Since the size of the computational domain varies, the dimensions will be reported with the discussion of each simulation. Table 3.2 shows the physical parameters for the bacterial model.

3D model information	Data	Unit
Bacterial boundary points	12	point
Bacterial body layers	11	layers
Bacterial diameter	1.25	μm
Bacterial body length	2.29	μm
Bacterial body thickness	0.21	μm
Bacterial body rotational frequency	10-15	rps
Body stiffness S_0	2.4×10^{-1}	dynes/μm
Flagellar amplitude	0.625	μm
Flagellar pitch (wave length)	2.3958	μm
Number of pitches	2	
Flagellar length	9.33	μm
Flagellar force c_f	1.0×10^{-3} (or indicated)	pN
Flagellar rotational frequency	200	rps
Swimming speed	10-25	μm/sec

Table 3.2: Physical parameters for the bacterial model.

3.1 Swimming Trajectory and Convergence Study

Centroid Trajectory Purcell [131, 132], considered bacteria with a characteristic size of 1∼2 μm in length and a swimming velocity of 10∼90 μm/sec in the low Reynolds number regime. He argued that reciprocal motions could not be used for motility for low Reynolds number swimming since symmetric motions would produce negligible net motion. Moreover, Purcell showed that the rotating helical flagellum used by flagellated bacteria would efficiently propel a swimming microorganism. A typical bacterial flagellum consists of a cylindrical helical filament and a helical hook that connects the cylindrical helix to the bacterial motor at the cell body. The geometry of our 3D model bacterial flagellum mimics the form of the wild-type bacterial flagellum.

The tangential forces applied to the cell body produce counter rotation and provide torque balance with the flagellum [21]. Keller and Rubinow [88, 89] studied the path of a flagellated bacterium and argued that its trajectory would form a helix with small radius. Berg and Brown [14, 11] found that swimming bacteria meandered in each run. In Figure 3.1(right) we show the centroid trajectories of our model cell.

Figure 3.1(left) shows the trajectory of a model cell with total run time of 0.05 seconds. The trajectory forms a left-handed helix when viewed from below. In Figure 3.1(right), the centroid trajectory is shown for a total swimming time of 1.0833 seconds. Aside from the differences in running time, the two simulations are identical. There is a 1:22 difference in the spatial scales shown in the two figures. In this simulation, the computational domain is $10 \times 10 \times 40 \mu\text{m}^3$ with a $16 \times 16 \times 64$ computational grid. The bacterial swimming velocity is 17.182 μm/sec.

Numerical Convergence Study The computational domain for the numerical

Figure 3.1: The helical trajectory of the model swimming bacterium.

convergence study is a cube with edges of length 10 μm. We employed a set of N^3 computational grid with N=16, 32, 64, and 128. We used a fixed time step of $\Delta t = 0.875 \times 10^{-8}$ for each of the simulations. The time step was chosen small enough so that the simulations remained stable even on the finest grid. The velocity fields were compared at time $t = 1.75 \times 10^{-6}$ seconds which corresponds to 200 time steps. The computation on the finest grid required two hours of CPU time running on a single processor on the AMD cluster at the Center for Computational Science at Tulane University. The bacterial cell size is shown in Table 3.2. We used a fixed number of cell body and flagellar immersed boundary points and a fixed value for the flagellar and torque force constants c_f and c_t on each grid.

Let $u_{128} = u_{exact} + ch^p$, where h is the grid size of the finest scheme. The velocity approximations are $u_{128} = u_{exact} + ch^p$, $u_{64} = u_{exact} + c(2h)^p$, $u_{32} = u_{exact} + c(4h)^p$ and

$u_{16} = u_{exact} + c(8h)^p$ where c is a constant. We compute the ratios k_0 and k_1 given by

$$k_0 = \frac{A}{B} = \frac{\| u_{128} - u_{64} \|}{\| u_{128} - u_{32} \|} = \frac{\| 1 - 2^p \|}{\| 1 - 4^p \|}, \quad k_1 = \frac{AA}{BB} = \frac{\| u_{64} - u_{32} \|}{\| u_{64} - u_{16} \|} = \frac{\| 1 - 2^p \|}{\| 1 - 4^p \|}$$

Therefore, the convergence rate estimates p_0 and p_1 are given by $p_0 = \frac{\ln(\frac{1-k_0}{k_0})}{\ln(2)}$ and $p_1 = \frac{\ln(\frac{1-k_1}{k_1})}{\ln(2)}$.

In Table 3.3 we show convergence results for the centroid velocity and rotational velocity of the cell body. In Table 3.4 we show convergence results in several vector norms for the fluid velocity field over the entire computational domain. The velocity field on each grid is obtained from the solution of the Navier-Stokes equations. The error between velocities on the various grids is taken at each point of the domain on the coarsest grid.

Grids	Centroid velocity.	Rotational velocity.
128	1.129×10^{-4}	$6.999\times10^{+1}$
64	1.152×10^{-4}	$5.903\times10^{+1}$
32	1.231×10^{-4}	$4.064\times10^{+1}$
16	1.324×10^{-4}	$1.526\times10^{+1}$
A=$\| u_{128} - u_{64} \|$	2.3×10^{-6}	$1.096\times10^{+1}$
B=$\| u_{128} - u_{32} \|$	1.02×10^{-5}	$2.935\times10^{+1}$
Ratio k_0=A/B	2.305×10^{-1}	3.734×10^{-1}
Power=p_0	1.739	0.747
AA=$\| u_{64} - u_{32} \|$	7.9×10^{-6}	$1.839\times10^{+1}$
BB=$\| u_{64} - u_{16} \|$	1.72×10^{-5}	$4.377\times10^{+1}$
Ratio k_1=AA/BB	4.576×10^{-1}	4.20×10^{-1}
Power=p_1	0.235	0.465

Table 3.3: Convergence study of the body centroid and rotational velocity.

In Table 3.3, we see that the apparent convergent rate improves on the finer grids. For the centroid velocities, we obtain $p_0 \approx 1.7$ which is consistent with second order convergence. For the rotational velocities, we obtain $p_0 \approx 0.74$ which is consistent

Fluid vel.	L_1-norm	L_2-norm	L_∞-norm
A=$\parallel u_{128} - u_{64} \parallel$	5.410×10^{-4}	5.355×10^{-4}	5.35496×10^{-4}
B=$\parallel u_{128} - u_{32} \parallel$	2.271×10^{-3}	1.665×10^{-3}	1.504×10^{-3}
Ratio=A/B	0.238	0.322	0.356
Power=p_0	1.677	1.077	0.855
AA=$\parallel u_{64} - u_{32} \parallel$	2.311×10^{-3}	1.580×10^{-3}	1.351×10^{-3}
BB=$\parallel u_{64} - u_{16} \parallel$	5.437×10^{-3}	3.635×10^{-3}	2.947×10^{-3}
Ratio=AA/BB	0.425	0.435	0.458
Power=p_1	0.436	0.380	0.241

Table 3.4: Convergence study of fluid velocity.

with first order convergence. The values for p_1 computed on the coarser grid show much slower convergence rates. In Table 3.4, we see a convergence rate for the fluid velocity. The value $p_0 \approx 1.7$ in the L_1 norm, $p_0 \approx 1.1$ in the L_2 norm and $p_0 \approx 0.85$ in the L_∞ norm. These are consistent with second order convergence in the L_1 norm, and first order convergence in the L_2 and L_∞ norms. Smaller, but positive convergence rates p_1 are found on the coarser set of grids.

3.2 Numerical Simulations: Single Cell

In this section, we present numerical results for a single model bacterial cell. The physical parameters of the model are described in Table 3.2 for each simulation unless otherwise indicated. The computational domain size is $10 \times 10 \times 20$ μm^3 with a $16 \times 16 \times 32$ computational grid. The fluid dynamics are represented by sets of fluid markers over the entire domain and in the region surrounding the cell. The cell swimming velocity depends strongly on the flagellar swimming force constant c_f as indicated in each simulation table. The swimming speed is usually between 10-25 μm/sec. The XZ- and XY-viewing windows have the origin at the bottom- left corner. The YZ-viewing window has the origin at the bottom-right corner.

3.2.1 Forward Swimming: Short Time Behavior

In this section, we show simulation results of a model bacterial cell swimming forward in a $10\times10\times20\mu\text{m}^3$ domain with a $16\times16\times32$ computational grid with a flagellar force constant $c_f = 0.8 \times 10^{-3}$ pN. In Figure 3.2 we show snapshots of the simulation. The time interval between each frame is 0.1083 seconds. The calculated average swimming velocity of the bacterial cell is 13.523μm/sec with a total run time of 0.5417 seconds. Figure 3.3, 3.4 show snapshots from the same simulation in the XZ- and XY-viewing window.

Simulation information	Data	Unit
Computational domain	$10 \times 10 \times 20$	μm^3
Flagellar force c_f	0.8×10^{-3}	pN
Swimming speed	13.523	μm/sec.
Body rotational frequency	7.21	rps
Frames interval	0.10833	sec
Total swimming time	0.5417	sec

Table 3.5: Parameters for forward swimming.

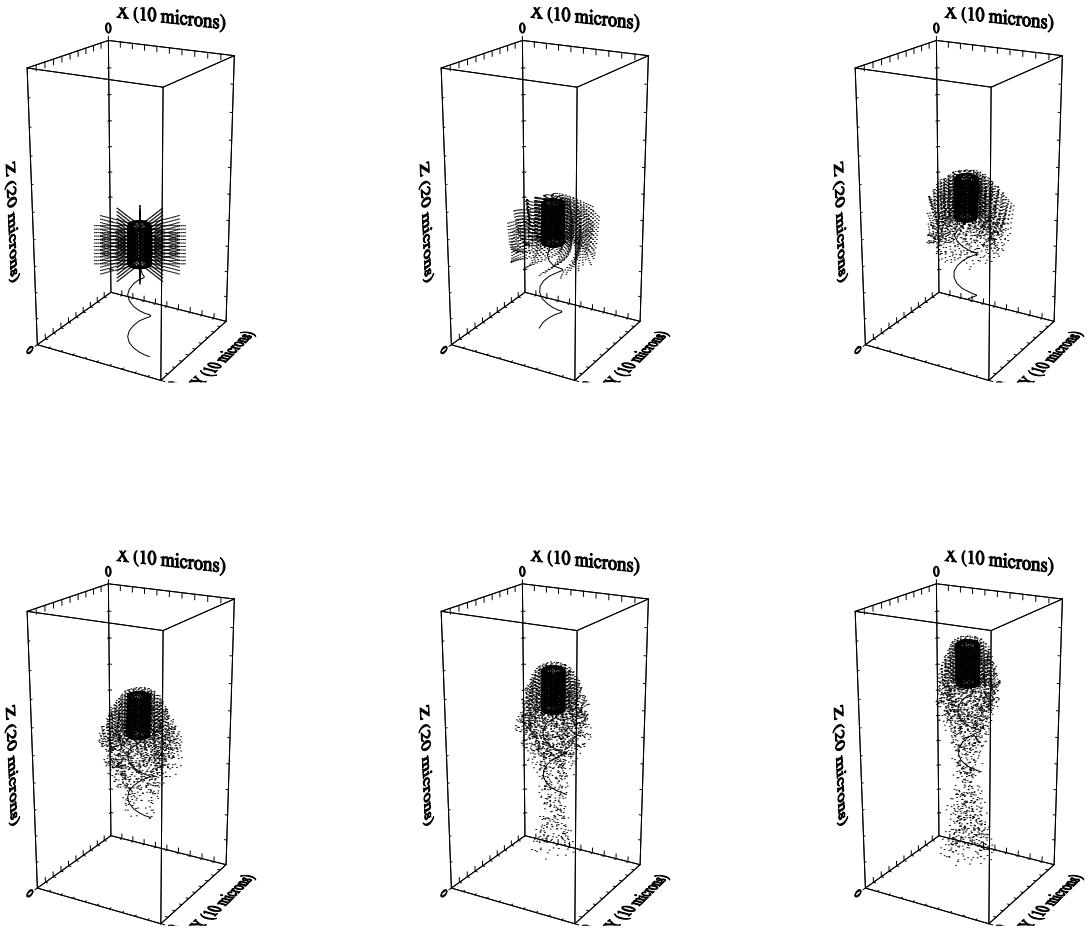

Figure 3.2: 3D view of model bacterium swimming forward.

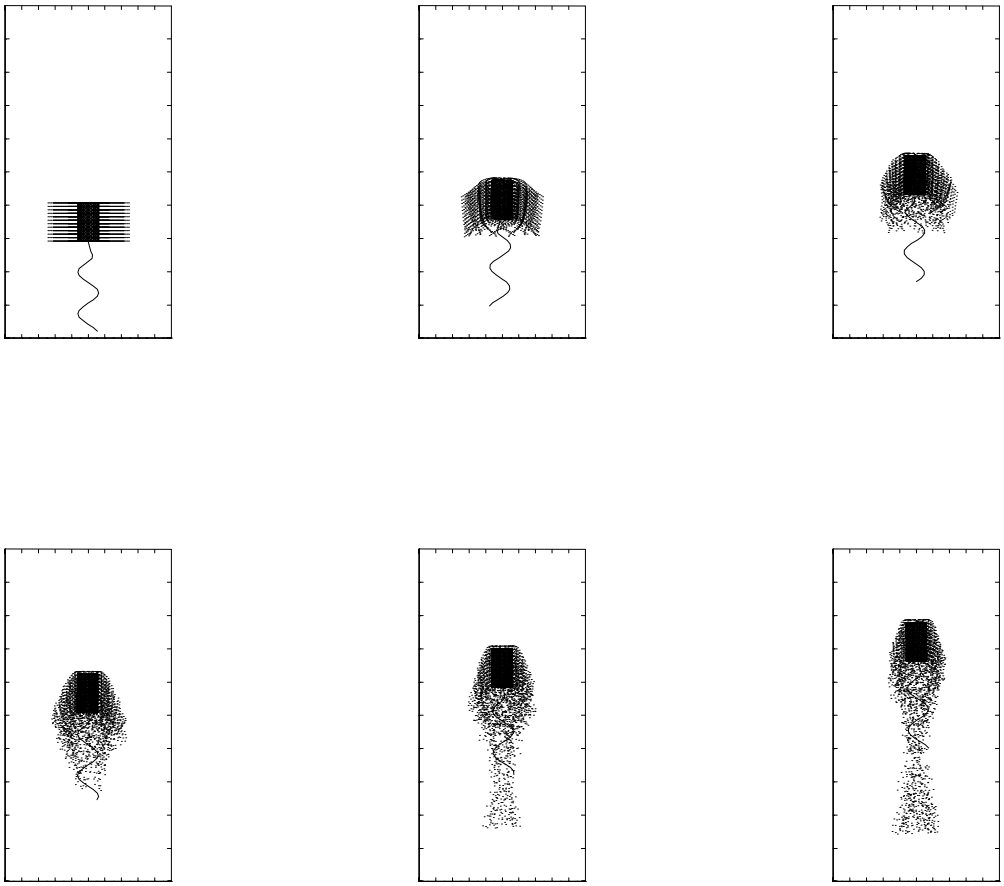

Figure 3.3: XZ-view of the model cell swimming forward.

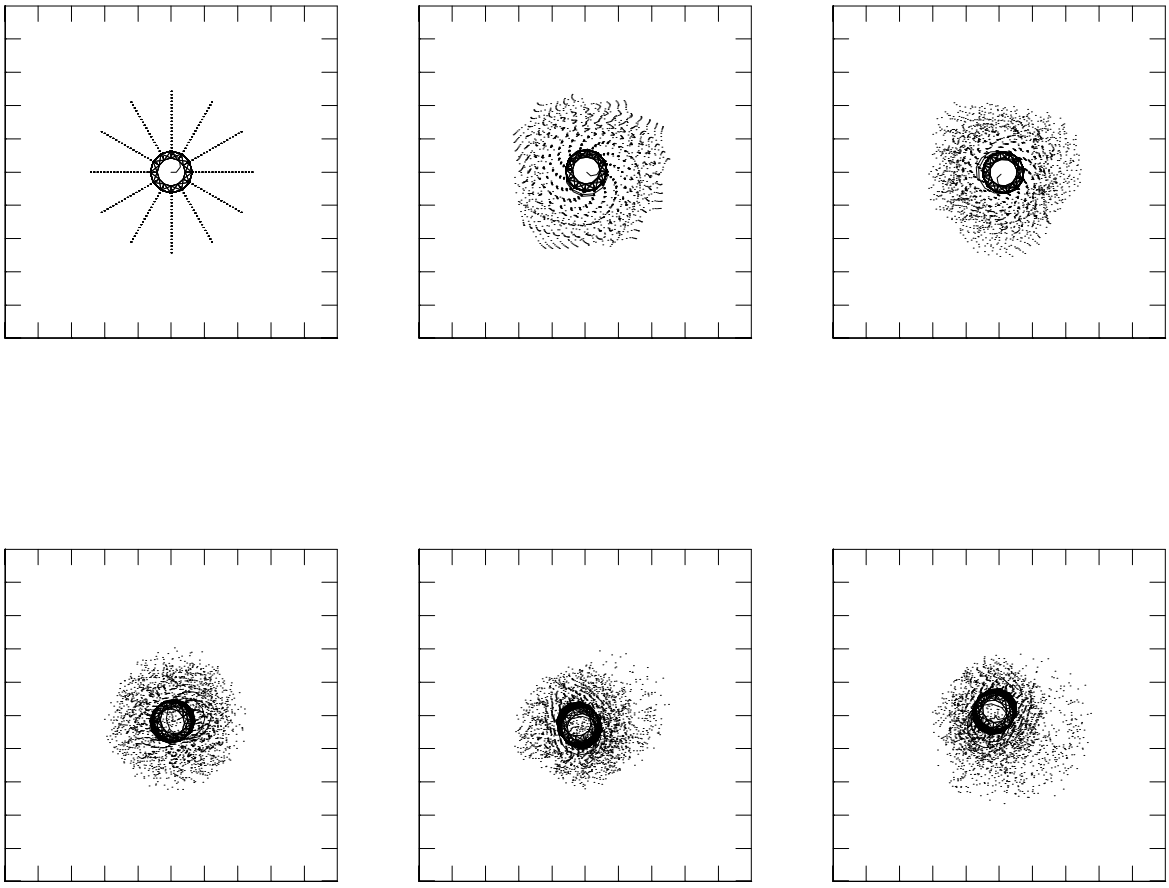

Figure 3.4: XY-view of the model cell swimming forward with fluid markers.

3.2.2 Swimming Forward: Long Time Behavior

In this section we show simulation results for a single swimming model cell over a longer duration. According to Berg in his book, *Random Walks in Biology* [11], the trajectory of a wild-type bacterium E. coli strain AW405 has the characteristics of a random walk composed of alternating run and tumble modes. A typical run mode has a duration of about 1 second. In Figure 3.5, we show simulation results for a model simulation with an overall run time of 1.0833 seconds. This is performed on a computational domain of $10 \times 10 \times 40$ μm^3 and a $16 \times 16 \times 64$ computational grid. In this simulation the flagellar force parameter $c_f = 1.0 \times 10^{-3}$ pN. The time interval between frames is 0.2167 seconds. The average swimming speed is 16.61 μm/sec. The series of snapshots shown in Figure 3.6 illustrate the fluid dynamics in the fluid domain. A central layer of fluid in the computational domain has been shown as the bacterium swims upwards in the XZ-view. The series of snapshots in Figure 3.7 show the simulation in the YZ-view along with fluid markers on the central layer of the computational domain. The series of snapshots in Figure 3.8 illustrate the fluid dynamics around the cell body while the bacterium swims up. The series of snapshots in Figure 3.9 show the fluid dynamics around the cell body and in the domain.

Simulation information	Data	Unit
Computational domain	$10 \times 10 \times 40$	μm^3
Flagellar force c_f	1.0×10^{-3}	pN
Swimming speed	16.61	μm/sec.
Frames interval	0.2167	sec
Total swimming time	1.0833	sec

Table 3.6: Long time swimming simulation.

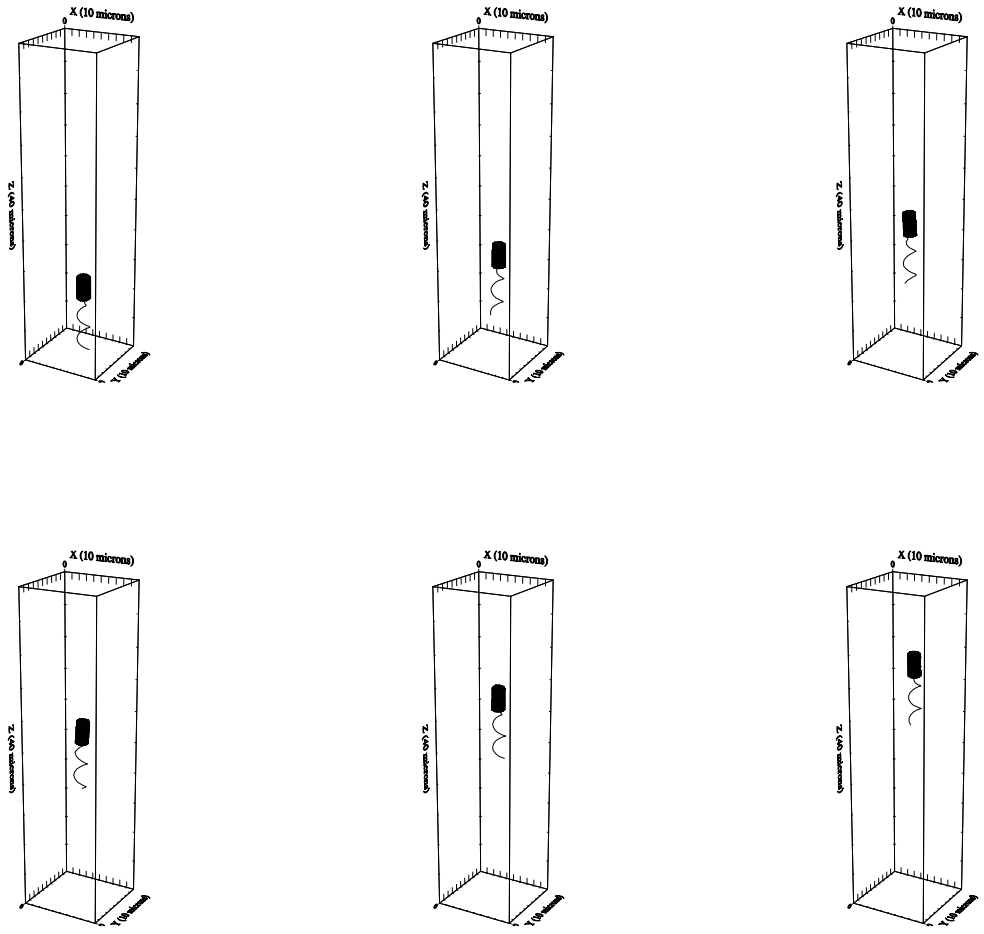

Figure 3.5: Bacterium swimming forward (long time).

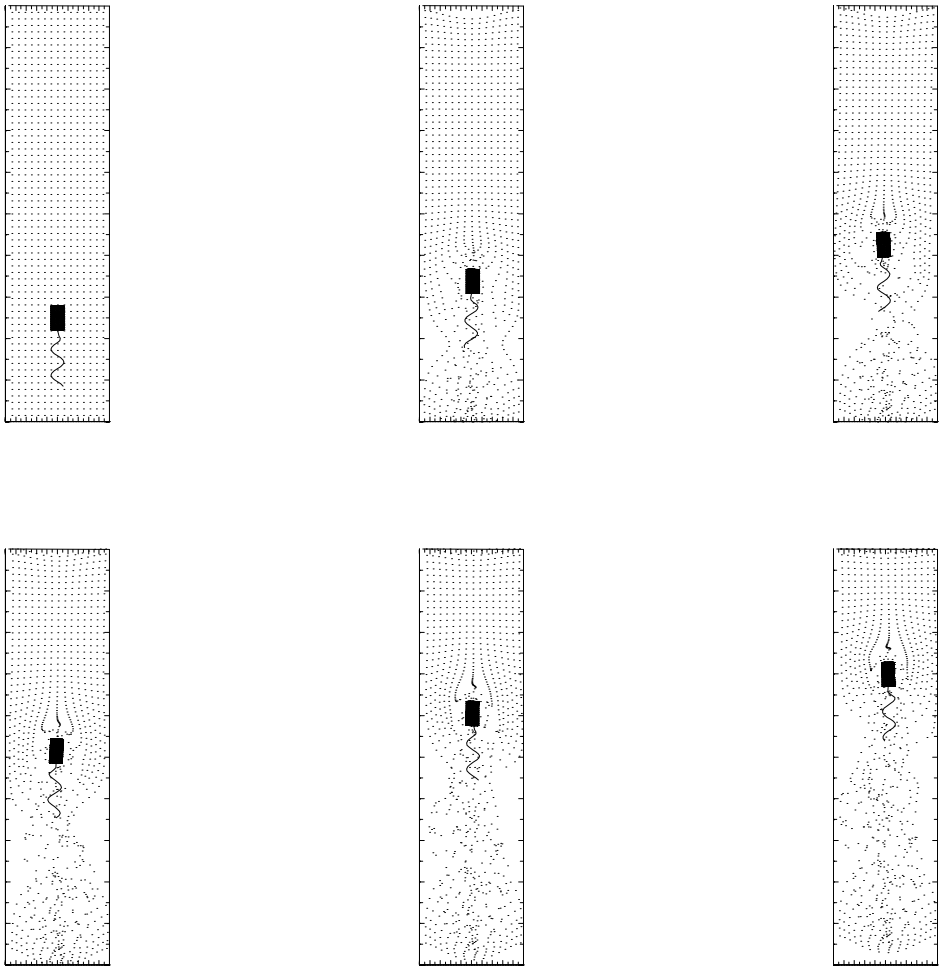

Figure 3.6: XZ-view of a bacterium swimming with one layer of fluid markers.

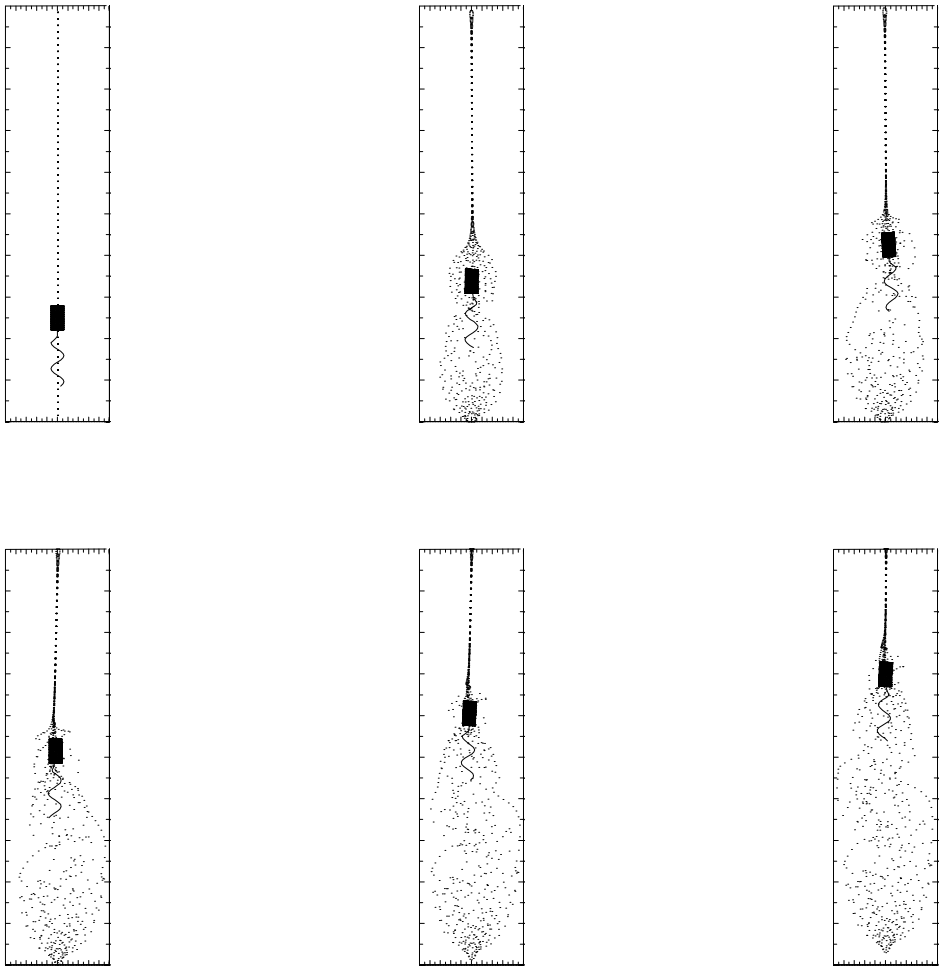

Figure 3.7: YZ-view of a bacterium swimming with one layer of fluid markers.

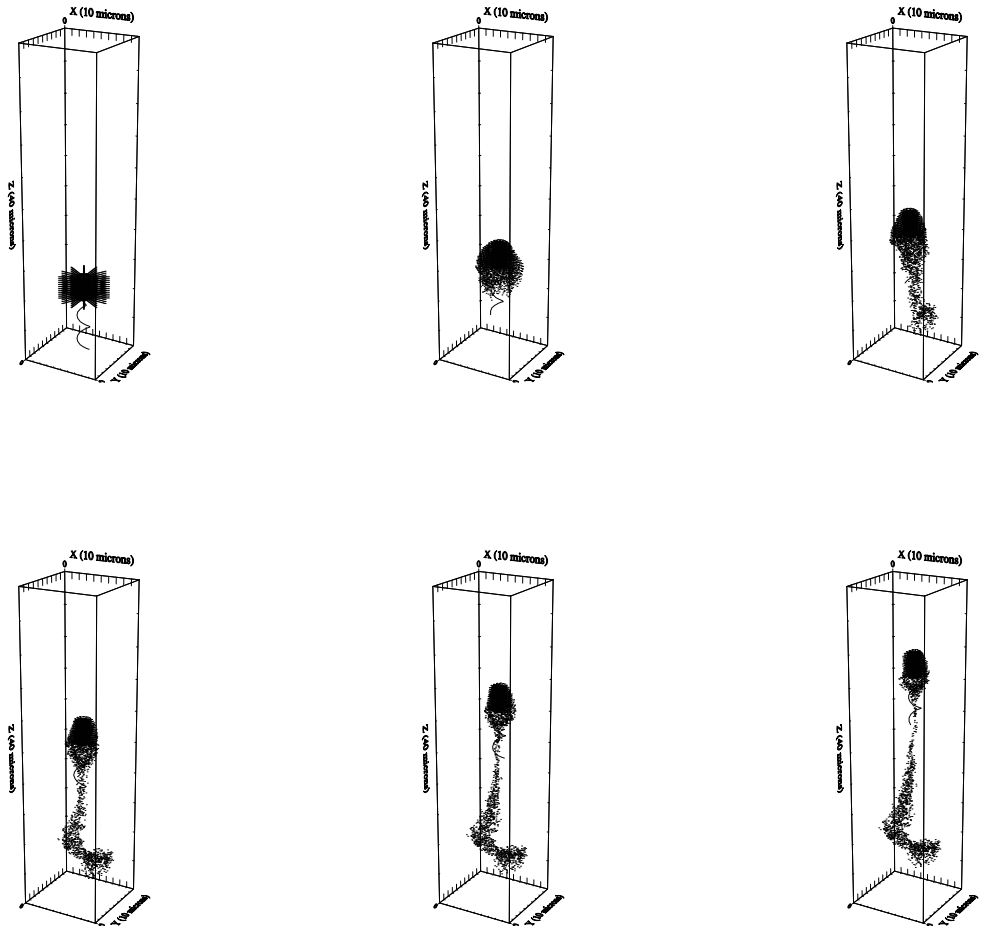

Figure 3.8: Fluid markers surrounding a swimming bacterium.

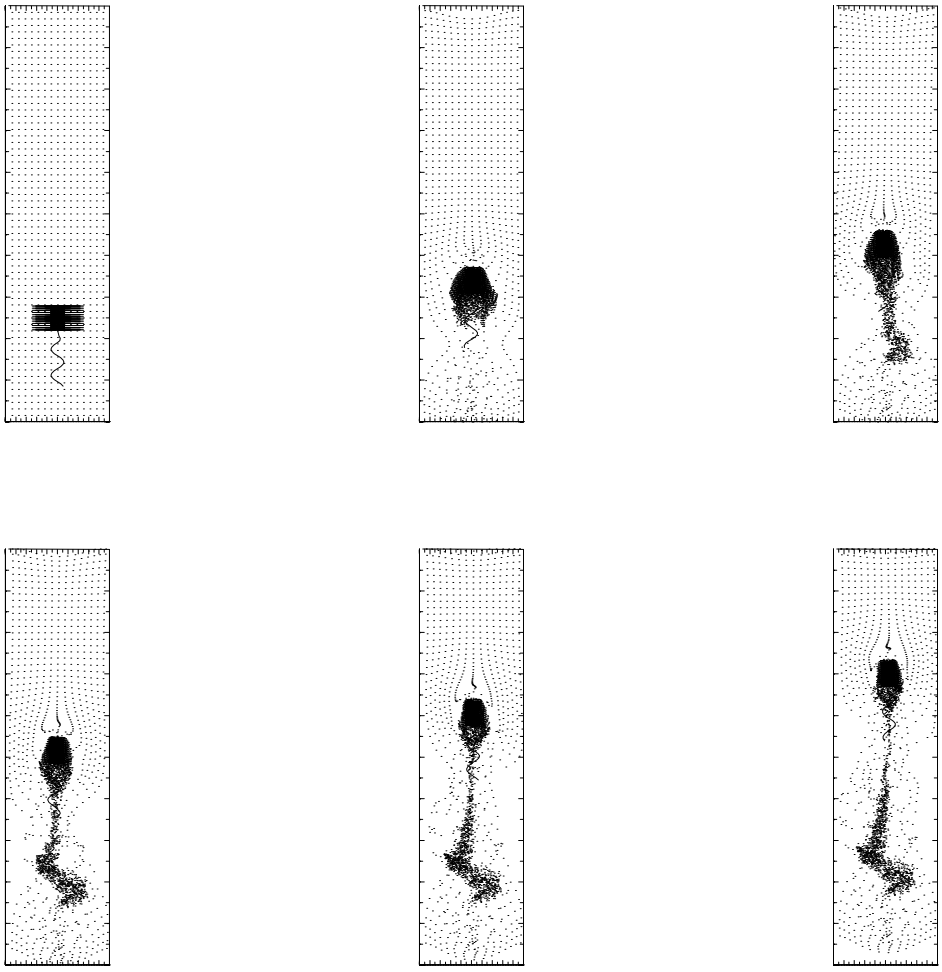

Figure 3.9: XZ-view of body with local and one layer of global fluid markers.

3.2.3 Swimming Forward: Modified Flagellar Force

In this section, we show preliminary results of the model cell swimming with an alternative flagellar force model. Here, the inward normal vector $\mathbf{R}$ in Equation (2.3.10) is omitted and replaced with a force vector in the axial direction. The modified force vector $\hat{\mathbf{f}}_i^f$ in Equation (2.3.10) is shown in the following equation:

$$\hat{\mathbf{f}}_i^f \equiv k_0\mathbf{N} + (-\mathbf{f}_{ij}^t) \tag{3.2.1}$$

where k_0 is a constant. Simulation details are provided in Table 3.7.

Simulation information	Data	Unit
Computational domain	$10 \times 10 \times 20$	μm^3
Axial vector parameter k_0	0.1	
Flagellar force c_f	0.8×10^{-3}	pN
Swimming speed	3.633	μm/sec.
Frames interval	0.542	sec
Total swimming time	1.0833	sec

Table 3.7: Simulation of the model cell with tangential and axial flagellar force.

The added axial force contribution is offset by axial force vectors in the negative Z direction on the cell body's lowest annular ring. The magnitude of the force on the cell body is chosen so that the resultant axial force sums to zero. This combination of flagellar forces, results in forward swimming. With the values of k_0 and c_f used here the average swimming speed is 3.633 μm/sec. Although this is slower than the swimming speeds shown in Chapter 3.2.1, we believe that faster swimming speeds can be obtained with a modification of the axial and tangential flagellar force constants. We show the simulation results in Figure 3.10-3.12.

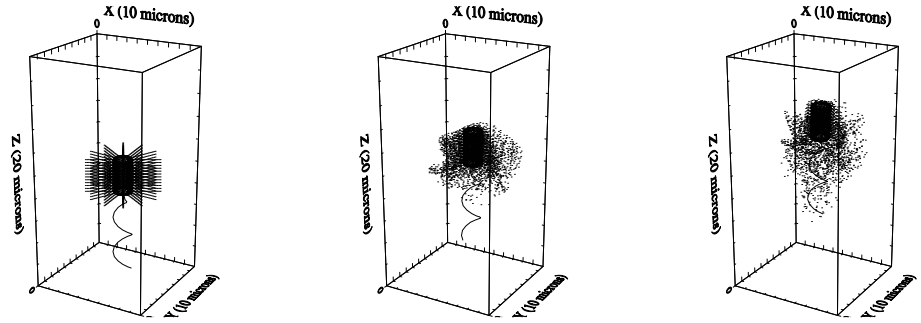

Figure 3.10: 3D view of a cell swimming with axial and tangential flagellar force.

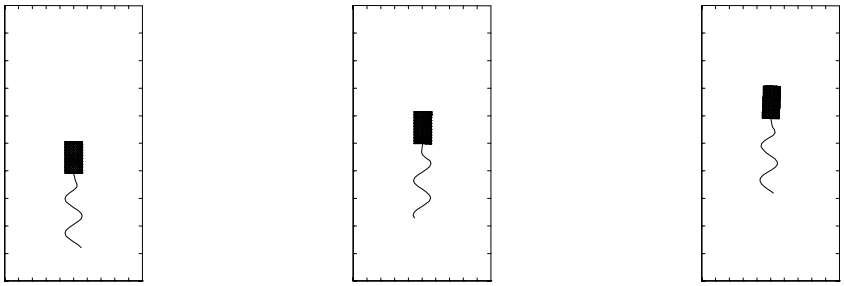

Figure 3.11: XZ-view of a cell with axial and tangential flagellar force.

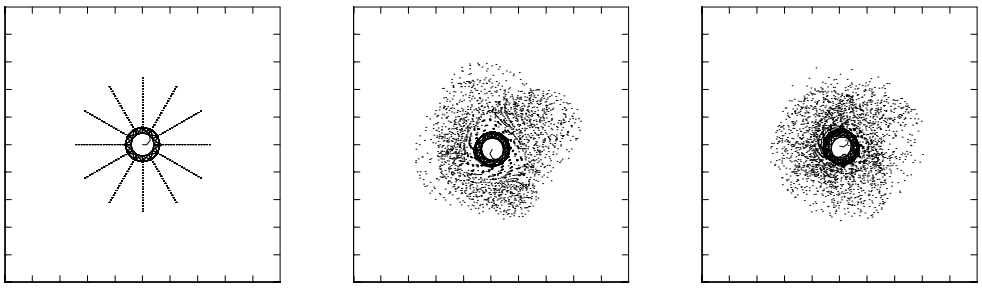

Figure 3.12: XY-view of a cell with axial and tangential flagellar force.

3.3 Reversal of Flagellar Rotation

The bacterial motor is capable of reversing it direction of rotation. Howard Berg noted that bacterial cells with a single polar flagella such as Vibrio metchnikovii, first found in a patient with cholecystitis, could swim steadily forward but could reverse direction and swim backwards in response to changes in the environment [6]. The lophotrichous bacteria, Chromatium okenii, swims backwards when the rotation direction of its flagellum is reversed. There is a considerable literature on the run and tumble motion of peritrichous bacteria, such as Escherichia coli and Salmonella typhimurium. These bacteria change swimming direction by a tumble motion when the flagellar bundles disassociate as a response to the reversal of rotational direction. When the swimming direction of peritrichous bacterium results in a decrease in chemoattractants, its bacterial motors are more likely to reverse. This changes the flagellar rotation from CCW to CW in one or more flagella. As a result, the flagellar bundle can unravel and the cell undergoes a tumble. Usually, the bacterial cell swims in a new direction after its flagellar bundle is reassembled. When the flagellar rotational direction switches from CCW to CW the flagellum can experience changes in handedness from left to right as well as changes in pitch, number of pitches, and amplitude of the cylindrical helix. Macnab and Koshland [111] found that Salmonella typhimurium flagella experienced such changes as well when the bacteria were stimulated by high intensity light or experienced changes in pH. This flagellar phase change has also been investigated by Shimada, Kamiya and Asakura [137].

The run and tumble model for chemotaxis may not be appropriate for monotrichous bacteria. With only a single flagellum, there is no “flagellar bundle”. Changes in rotational direction force changes in the handedness and flagellar phase change from

normal to coiled, semi-coiled, or curly. In Chapter 3.3.1 we reverse the rotational and swimming direction midway through the simulation. The reversal of rotational direction is also accompanied by a reversal in the cell body torque force, and change in flagellar handedness from left to right, but we keep the "normal" flagellar amplitude and pitch. In Chapter 3.3.2, we reverse the rotational direction midway through the simulation. Here, the helical configuration changes from left- to right-handed. In addition, the flagellar configuration changes from the "normal" to a "semi-coiled" configuration. In Chapter 3.3.3, the model cell swims forwards, then backwards, and then forwards. In the forward swimming direction, the flagellum has the "normal" left-handed configuration; in backward swimming, a right-handed "semi-coiled" configuration.

3.3.1 Forward and Backward Bacterial Swimming

In this section, we investigate the swimming behavior of the model cell in forward and backward swimming. In the first simulation results, we use the same flagellar amplitude, pitch length of pitches in both forward and backward swimming. In backward swimming the rotation of the flagellum is reversed, as is the handedness of the flagellar helix, and the direction of the flagellar and torque forces. The bacterial cell swims forward for the first half of the simulation and backwards for the second half. The forward and backward run times are 0.5415 seconds. A summary of the simulations details are shown in Table 3.8.

In order to understand the single bacterium swimming forward and backward motion by manipulating the flagellar forces and torque balanced forces, the following simulation is designed to keep the physical conditions of the flagellum such as amplitude, pitch length and number of pitches the same except the handedness and force direction. The forward and backward running time are each 0.5416 seconds. Table 3.8 summarizes the simulation information.

Simulation information	Data	Unit
Computational domain	$10 \times 10 \times 20$	μm^3
Flagellar force c_f	1.0×10^{-3}	pN
Frames interval	0.2167	sec
Total swimming time	1.0833	sec
Flagellar amplitude	1.0	radius
forward speed	17.70	μm/sec.
Swimming backward speed	17.12	μm/sec.

Table 3.8: Forward and backward swimming.

Simulation results are shown in Figures 3.13-3.15. The net swimming speeds in forward (17.7 μm/sec) and backward (17.12 μm/sec) swimming are very similar. In

both forward and backward swimming the trajectories are approximately straight.

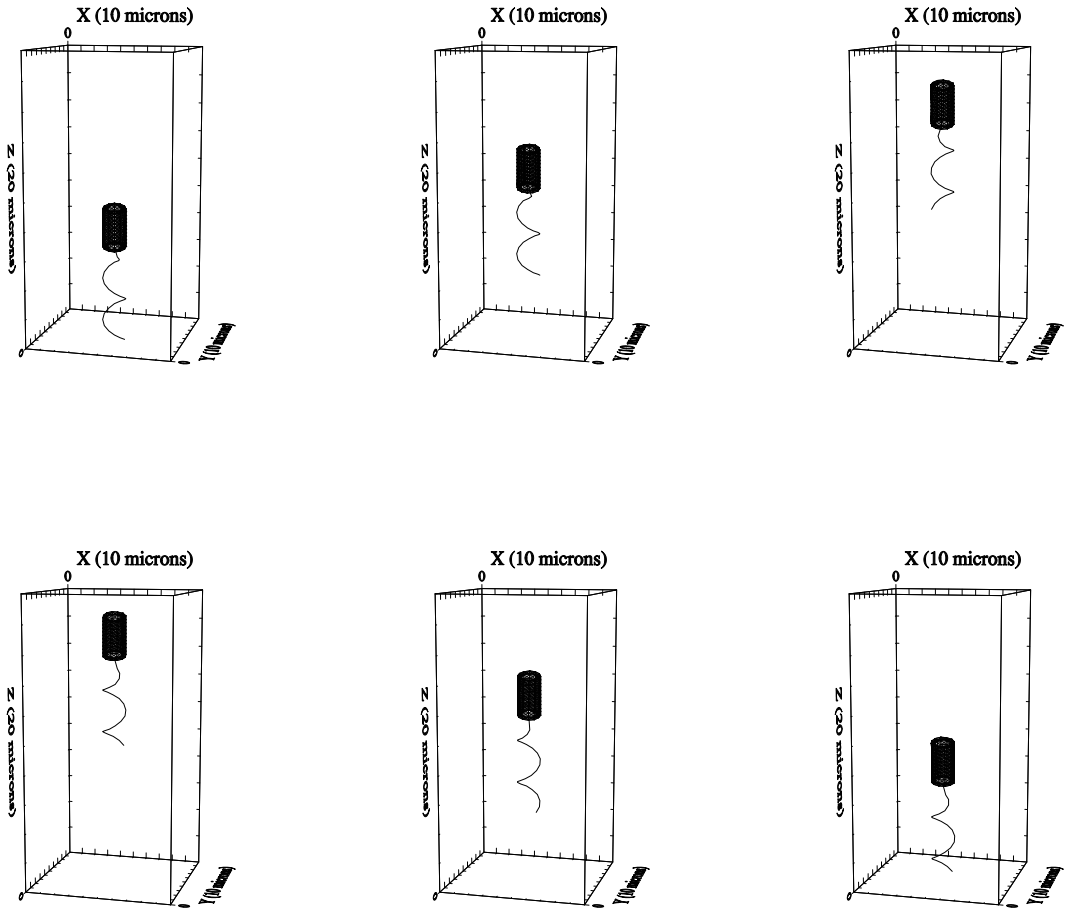

Figure 3.13: Forward and backward swimming with amplitude and pitch unchanged.

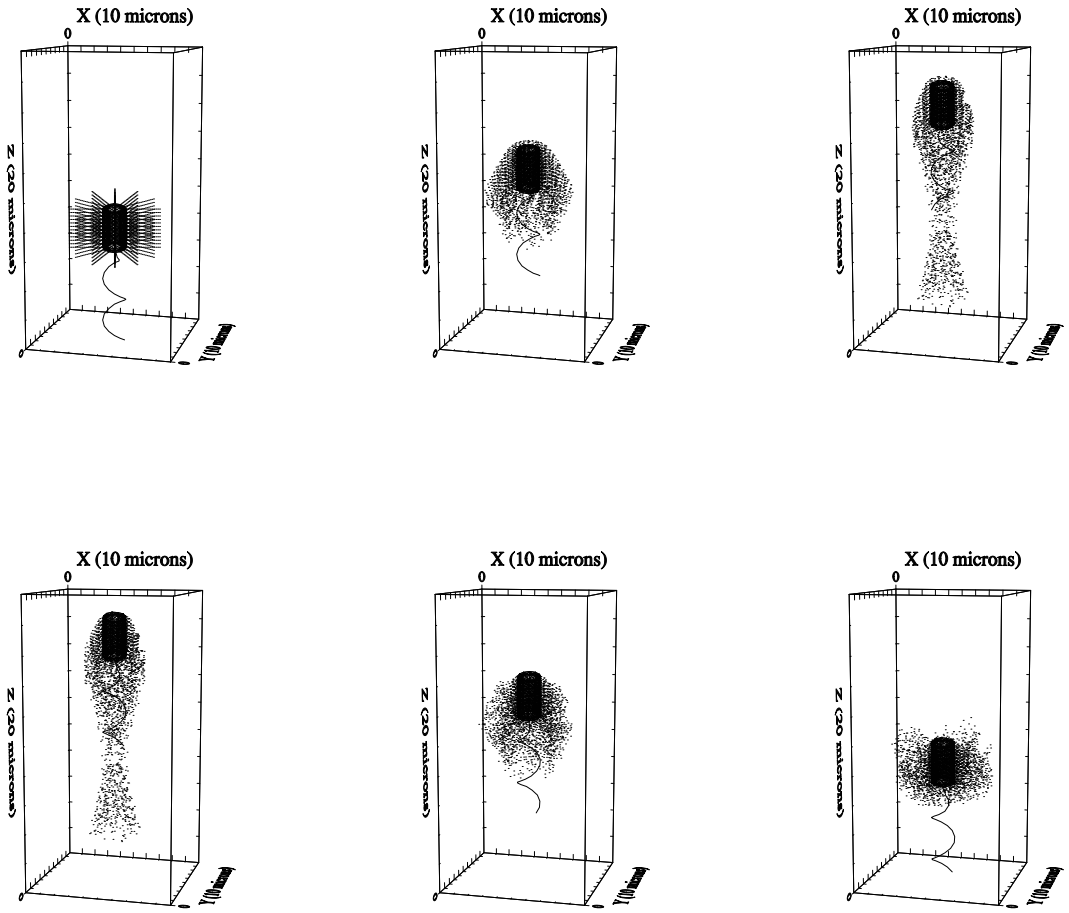

Figure 3.14: Forward and backward swimming with local fluid markers.

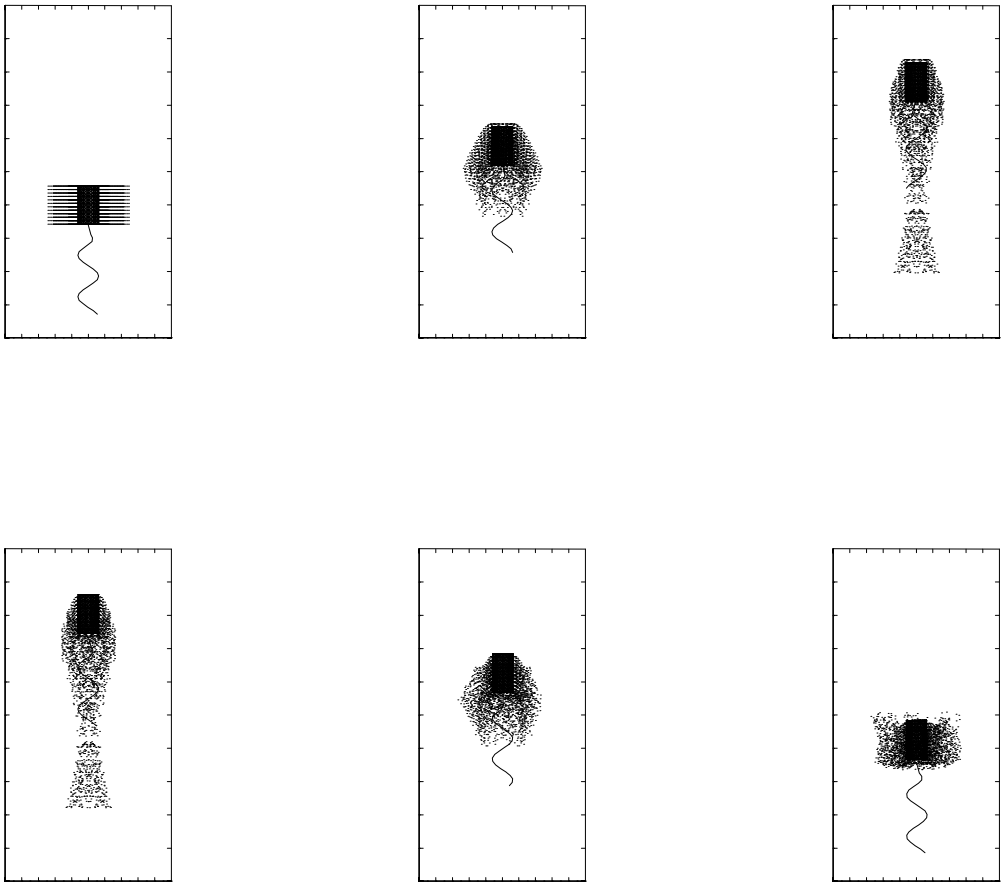

Figure 3.15: XZ-view of local fluid dynamics in forward and backward swimming.

3.3.2 Rotational Reversal with Changes in Flagellar Configuration

Shimada et al, Macnab and Koshland, Jones and Aizawa investigated the changes in flagellar configuration due to reversal of the rotational direction in Salmonella [137, 111, 86]. They found that the bacterial flagellum changed handedness from left to right and the flagellar configuration changed from normal to coiled, semi-coiled or curly. In the simulation results shown above in Chapter 3.3.1 the handedness was changed from left to right, but the amplitude, pitch, and number of pitches was held constant. In the following simulation shown in Figure 3.16-3.19, we change the handedness from left to right as well as the flagellar amplitude and pitch during CW rotation. A summary of the simulation details is shown in Table 3.9.

Simulation information	Data	Unit
Computational domain	$10 \times 10 \times 20$	μm^3
Flagellar force c_f	1.0×10^{-3}	pN
Frames interval (six frames)	0.2167	sec
Frames interval (three frames)	0.5416	sec
Total swimming time	1.0833	sec
Forward flagellar amplitude	0.5	radius
Forward pitch length	2	body long
Swimming forward speed	8.346	μm/sec.
Swimming forward flagellum arc-length	6.641	μm.
Backward flagellar amplitude	0.8	radius
Backward pitch length	1	body long
Swimming backward speed	14.903	μm/sec.
Swimming backward flagellum arc-length	6.607	μm.

Table 3.9: Forward and backward swimming with altered flagellar configuration.

In CCW rotation, we set the flagellar amplitude at one half the cell body radius and the pitch length at two cell body lengths. In CW rotation we increase the flagellar amplitude from 0.5 to 0.8 times the cell body radius and the total pitch

length is shortened to one body length. With this change in flagellar configuration, the flagellar arc length remaining effectively unchanged as it decreases by only 0.515%. We use two pitches in both CCW and CW rotation.

In this simulation the model bacterial cell swims forward with CCW flagellar rotation for 0.5417 seconds and backwards with CW flagellar rotation for 0.5417 seconds. The bacterial cell undergoes a change in direction when it begins to swim backward, and continues along an approximately linear trajectory. In addition, there is a speed change. With these changes in flagellar configuration, the cell swims backward approximately twice as fast as it swims forward. In the XZ- and YZ-views shown in Figure 3.17 and 3.18 we see that the forward swimming trajectory is approximately vertical, whereas the backward trajectory tilts toward the lower right corner. The XY-view shown in Figure 3.19 confirms that the model cell swims nearly straight up in forward motion but veers toward the corner in backward motion.

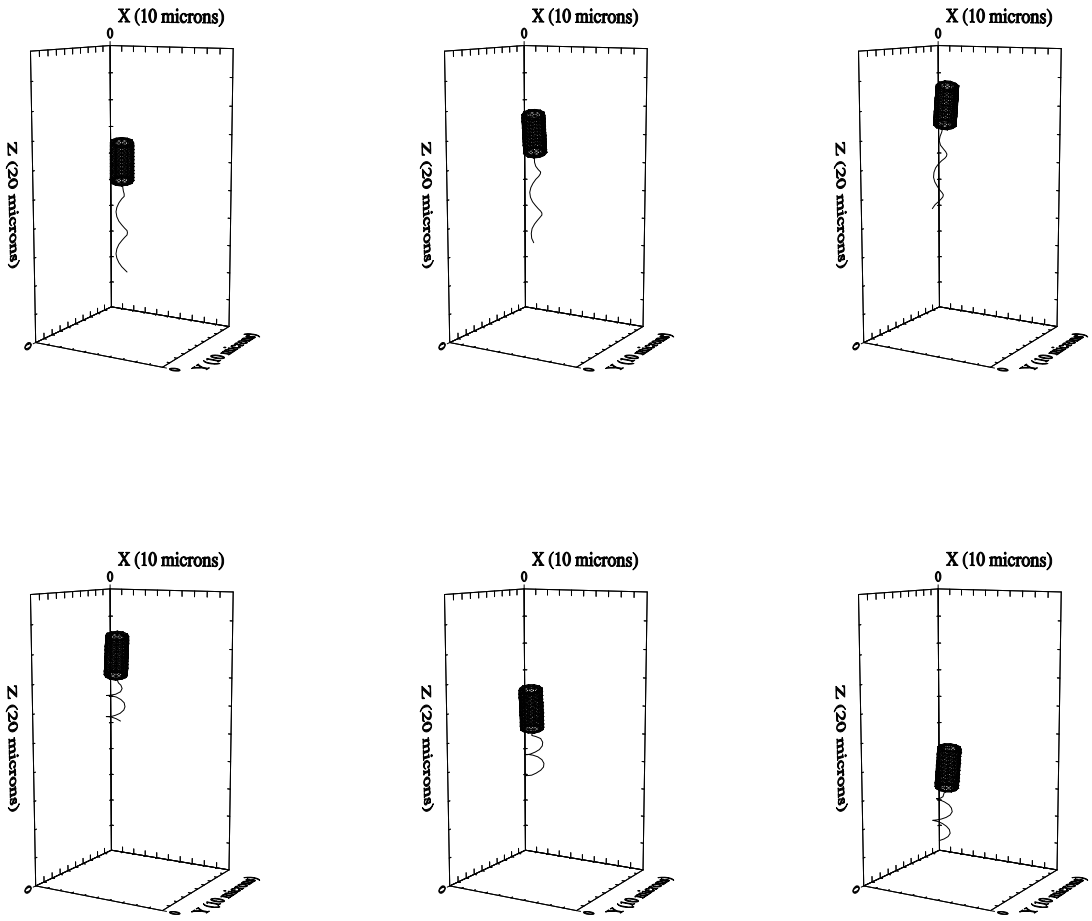

Figure 3.16: Forward and backward swimming with altered flagellar configuration.

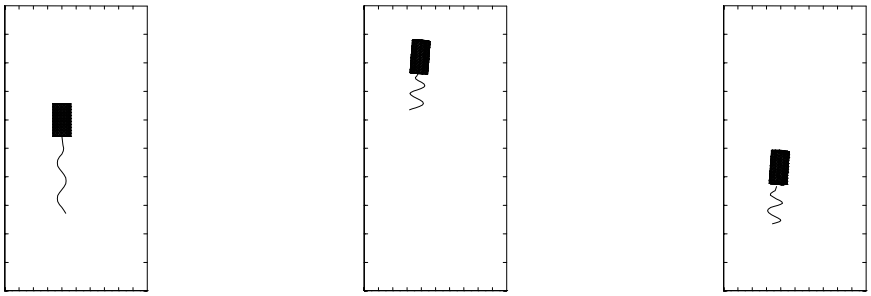

Figure 3.17: XZ-view with flagellar change from normal to semi-coiled.

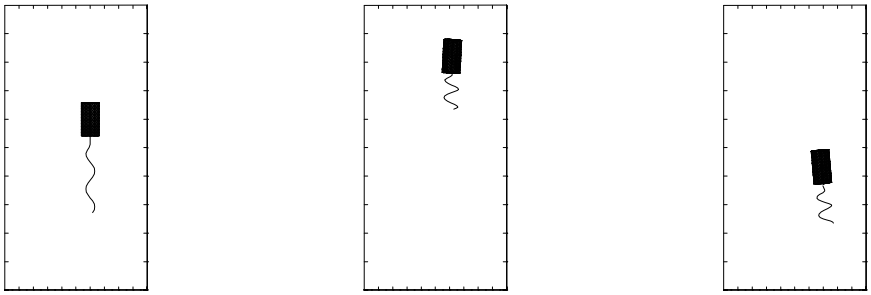

Figure 3.18: YZ-view with flagellar change from normal to semi-coiled.

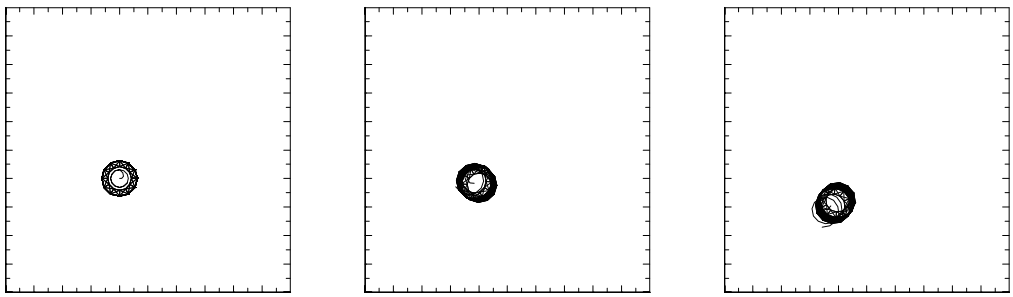

Figure 3.19: XY-view with flagellar change from normal to semi-coiled.

3.3.3 Alternate Swimming Motion by Reversal of Flagellar Rotation

In the following simulation we show simulation results for a model cell that swims alternatively forwards, backwards and forwards. We divide the total simulation run time into three equal periods. In the first and last periods, the model cell swims forward with a CCW flagellar rotation and a "normal" left-handed flagellar configuration. In the middle period, the model cell swims backwards with a CW flagellar rotation and a "semi-coiled" right-handed flagellar configuration [86]. Here the "normal" configuration is identical to that used in the previous simulation for forward swimming. The "semi-coiled" configuration is identical to that used in backward swimming. We summarize the simulation details in Table 3.10.

Simulation information	Data	Unit
Computational domain	$10 \times 10 \times 20$	μm^3
Flagellar force c_f	1.0×10^{-3}	pN
Total swimming time	1.625	sec
Frames interval(six frames)	0.325	sec
Frames interval(four frames)	0.542	sec
Forward flagellar amplitude	0.5	radius
Forward pitch length	2	body long
Swimming forward speed	8.346	μm/sec.
Backward flagellar amplitude	0.8	radius
Backward pitch length	1	body long
Swimming backward speed	14.903	μm/sec.
Forward flagellar amplitude	0.5	radius
Forward pitch length	2	body long
2nd forward speed	5.700	μm/sec.

Table 3.10: Alternate directions with pitch and amplitude changes.

The Figure 3.20 we show the simulation results with forward swimming in the upper panels, backward swimming in the middle panels and forward swimming in

the bottom panels. This simulation is identical to that shown above in Chapter 3.3.2 except for the additional segment in which the model cell returns to its initial forward swimming mode. We see in Figure 3.21 that the cell trajectory is again approximately vertical as the cell switches from backward to forward swimming.

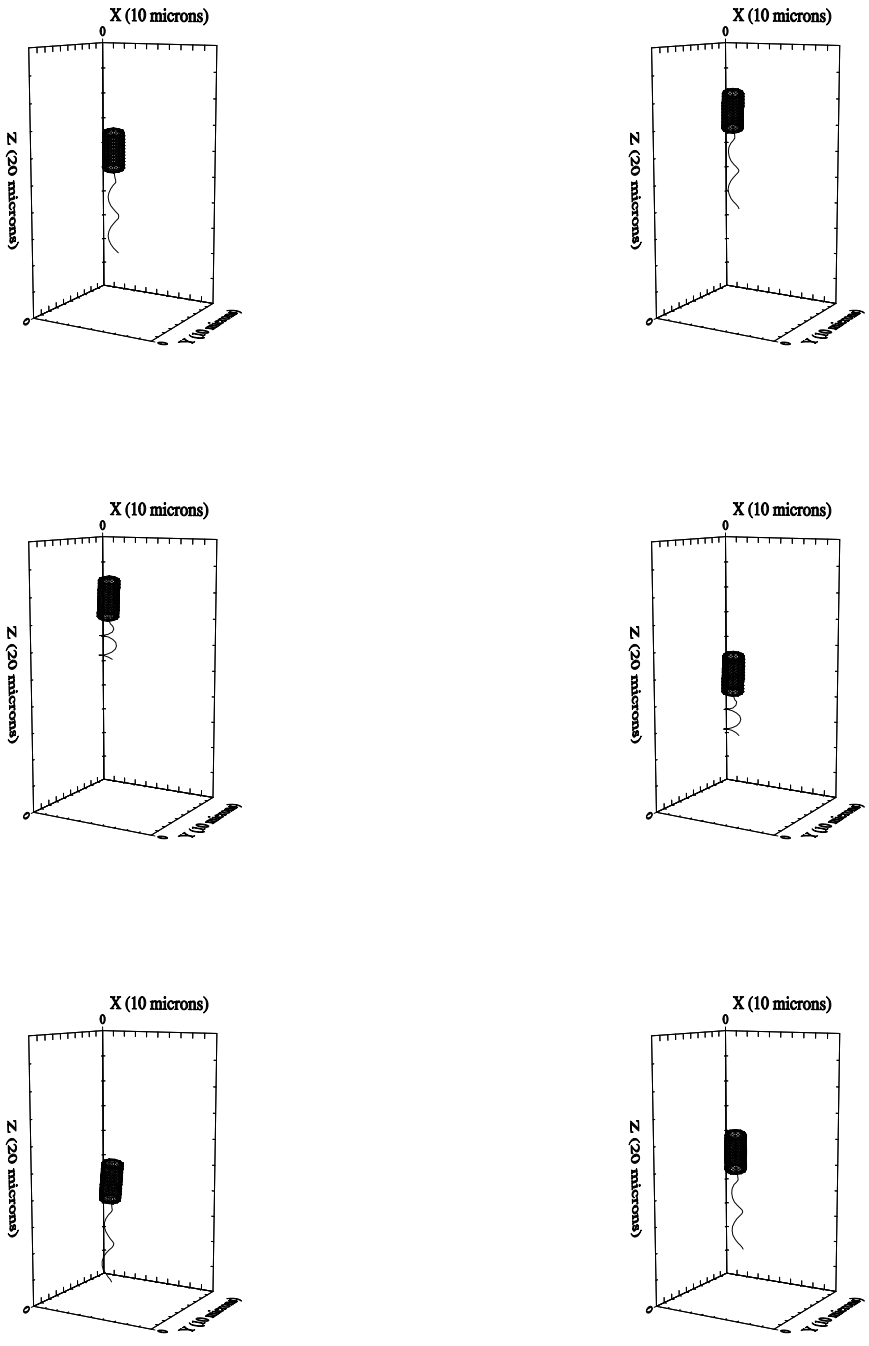

Figure 3.20: (top) Forward -(middle) Backward -(bottom) Forward movement.

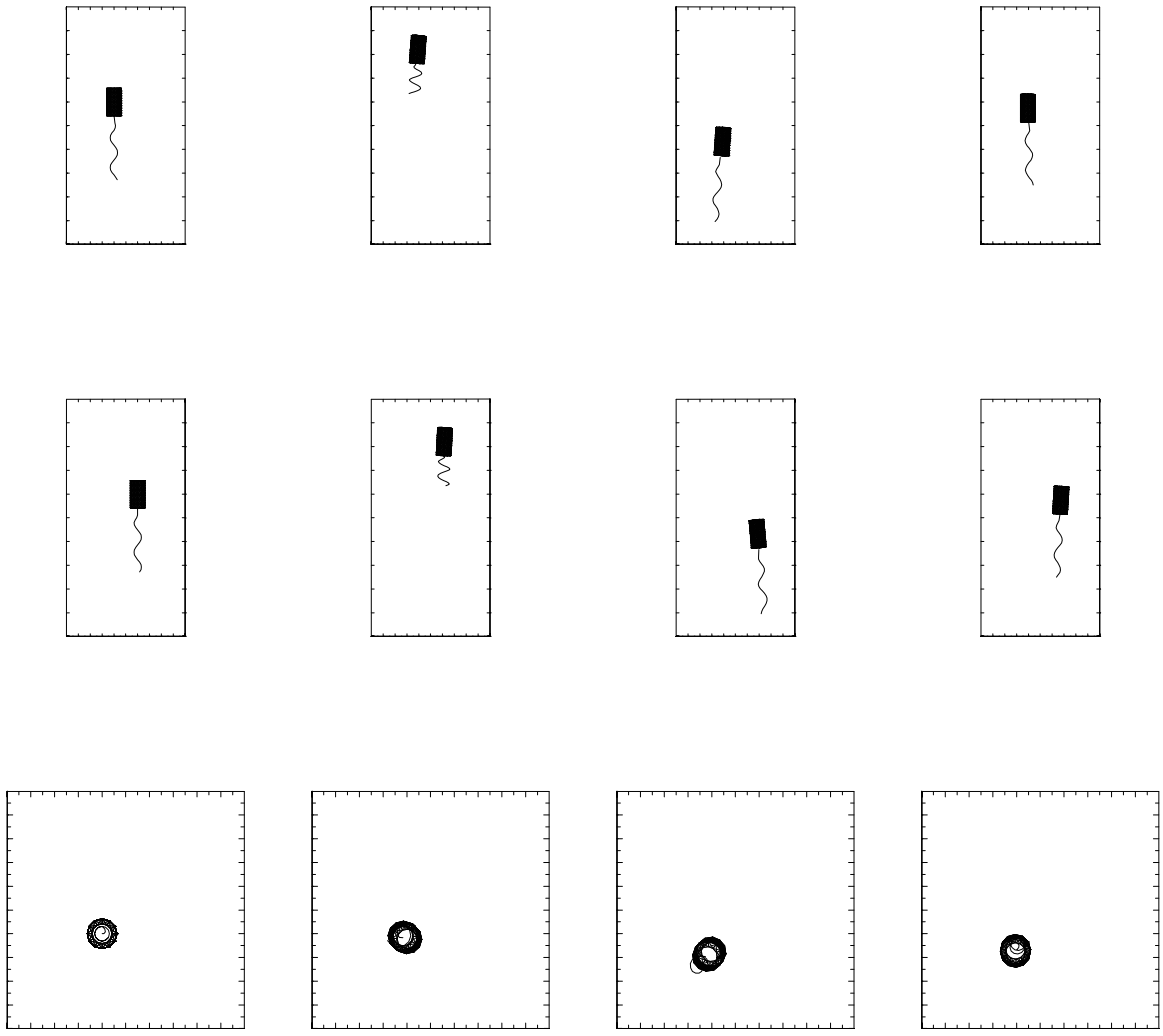

Figure 3.21: (top) XZ-view , (middle) YZ-view and (bottom) XY-view .

3.4 Interaction Between Two Model Cells

The interaction between two bacterial cells has been studied by Liu and Papadopoulos [103, 105], Dillon, Fauci, and Gaver [52] and, Ishikawa and Hota [85]. In this section, we investigate the hydrodynamic interaction of two model bacterial cells. The details of the hydrodynamic interaction between two model swimming cells depends on the initial orientations and locations of the model cells. In this study, we assume that the model cells are identical and swim with a CCW rotation in the forward direction. We restrict our study to special cases of initial cell orientation and location. In Chapter 3.4.1 we show simulations of cells swimming in the same direction in parallel with the Z-axis with an initial separation. In Chapter 3.4.2 and Chapter 3.4.3 we show simulations results of two cells oriented in the same direction with one swimming ahead of the other. In Chapter 3.4.4, we show simulation of two cells swimming in opposite direction. In these simulations, we see qualitative similarities with 2D simulations of bacterial motility presented in Dillon, Fauci, and Gaver [52]. In Chapter 3.4.5, we show simulation results of two cells swimming in opposite directions with a wide axial spacing. The hydrodynamic interaction between these cells is much less than in the case shown in Chapter 3.4.4. Hence, the swimming pattern is totally different.

In this chapter, the force term, Equation (2.3.6), for the multiple cells is replaced by Equation (3.4.1):

$$\mathbf{f}(\mathbf{s},t) = \sum_{nc}(\mathbf{f}_{body} + \mathbf{f}_{rotate} + \mathbf{f}_{swim}) \tag{3.4.1}$$

where nc is the number of bacterial cells.

3.4.1 Same Direction: Side-by-Side

We place two identical model cells adjacent to each other so that each cell's flagellar axis is initially aligned with the Z-axis. The initial cell centroid locations are in the same XY-plane separated by a distance of 2 μm which is approximately the cell body length. The initial configuration is shown in the upper left panels of Figures 3.22, Figures 3.24, and Figure 3.25 We summarize the simulation details in Table 3.11.

Simulation information	Data	Unit
Computational domain	$10 \times 10 \times 20$	μm^3
Flagellar force c_f	1.0×10^{-3}	pN
Bodies' axes (center) width	2	μm
Frames interval	0.087	sec
Total swimming time	0.4333	sec

Table 3.11: Two bacteria swimming side-by-side.

In the simulation results shown in Figure 3.22- Figures 3.25 we observe a synchronized swimming pattern. The trajectories of the two cells form a spiral and the cells rotate about each other. Figure 3.23 includes the fluid markers surrounding the cell bodies. Figure 3.24, includes the fluid markers initially placed at each point in the computational grid. In the XY-view shown in Figure 3.25 we see the rotation of the two model cells about a common axis. This simulation shows that when the axes of two model cells are aligned and very close to each other, the cells can swim as a synchronized cluster [119].

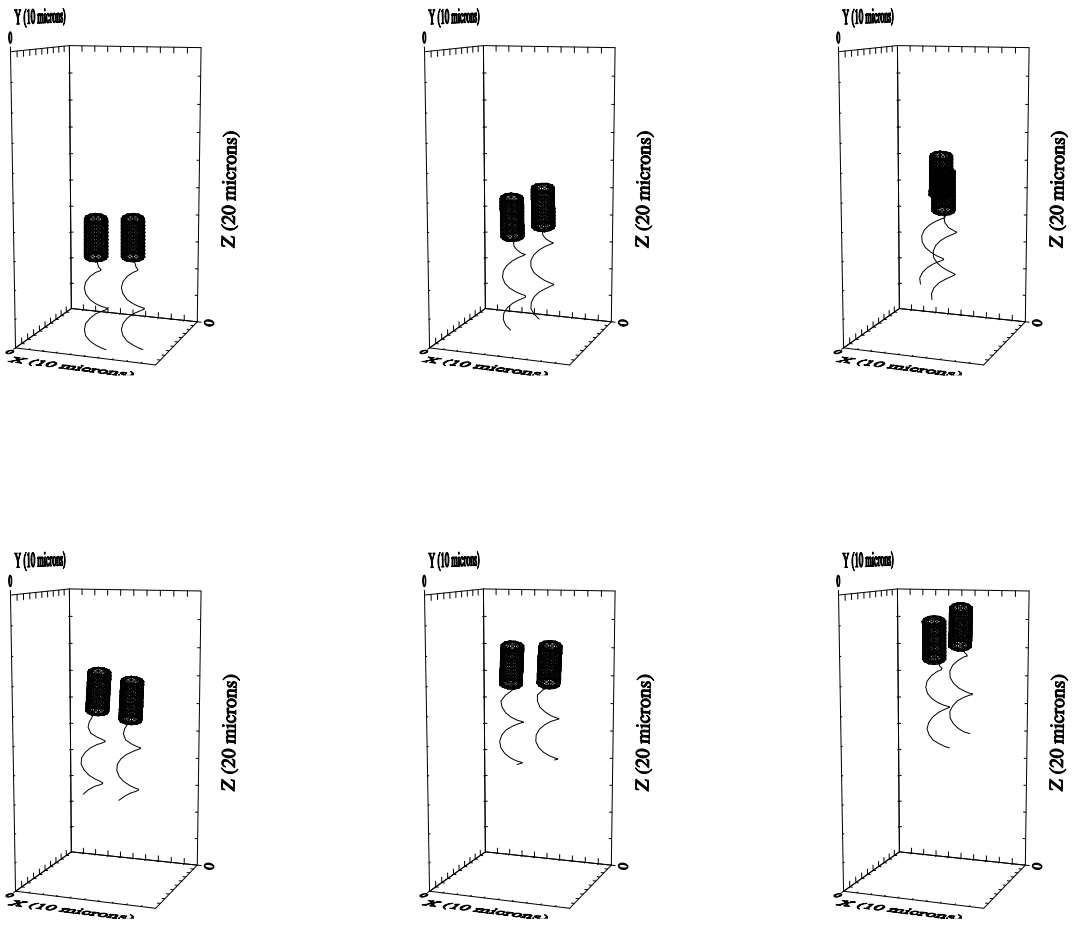

Figure 3.22: Two bacteria swimming forward synchronously.

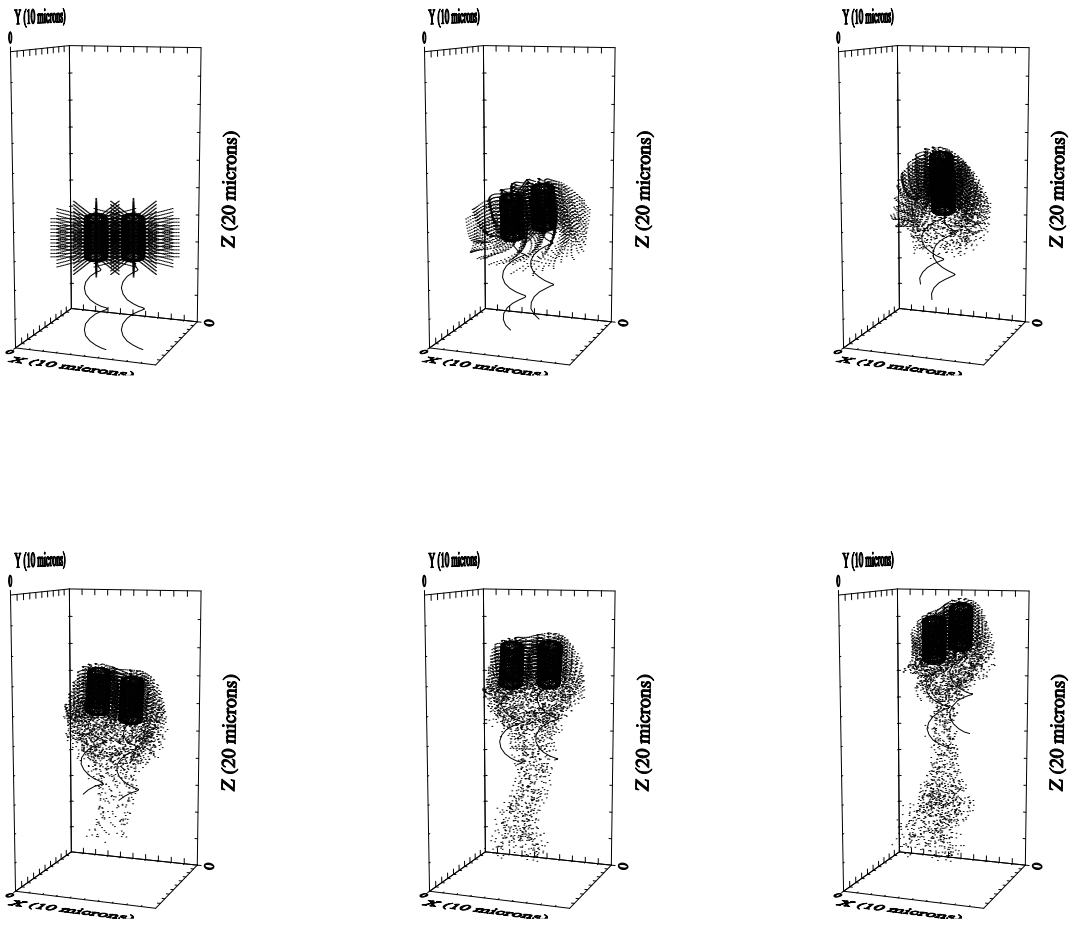

Figure 3.23: Two bacteria swimming forward with local fluid markers.

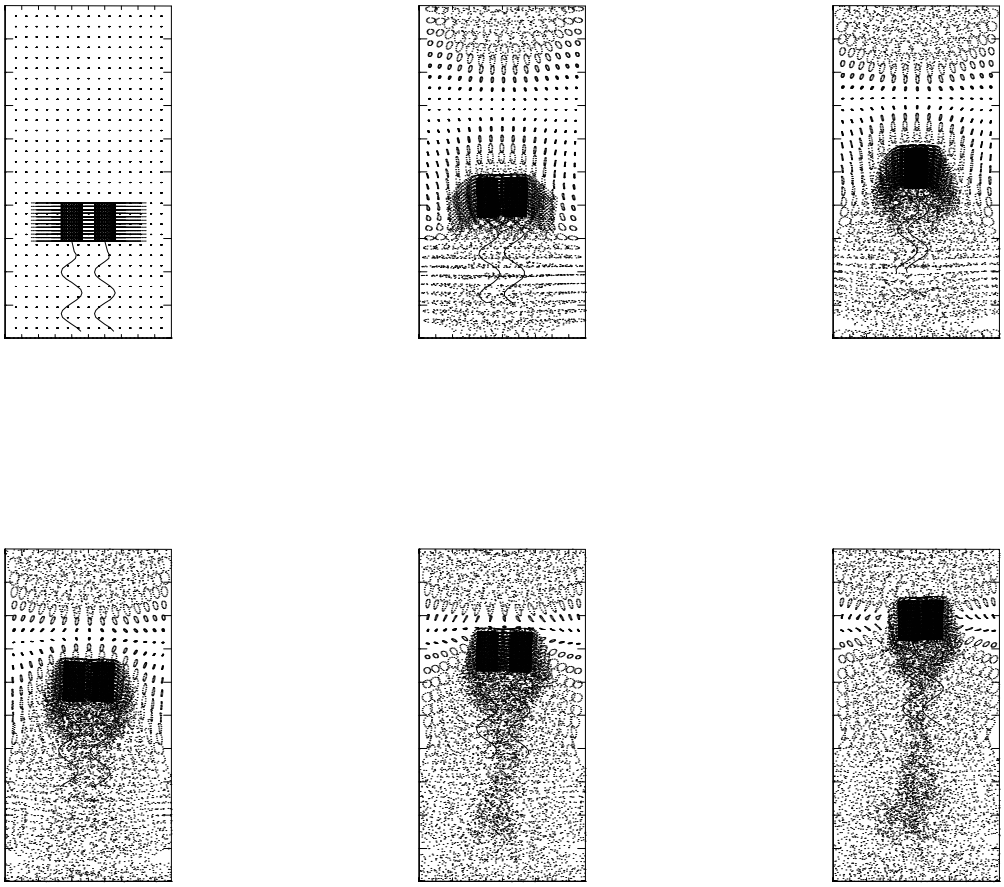

Figure 3.24: XZ-view of synchronously swimming with global fluid markers.

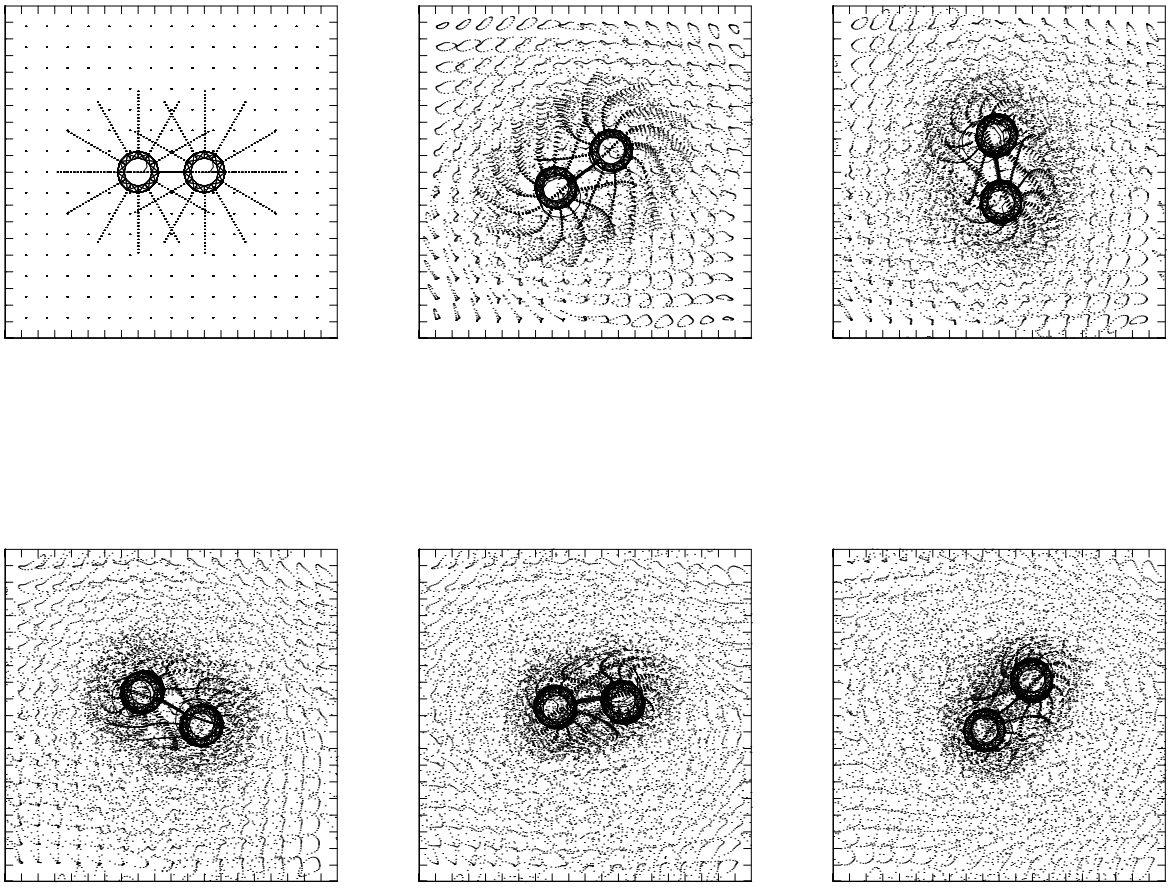

Figure 3.25: XY-view of synchronously swimming with global fluid markers.

3.4.2 Same Direction: Vertical Offset

In the simulation shown in Figures 3.26-3.27 the axes of the two cells are placed on parallel lines, oriented in the same direction but offset so that one cell is initially below the other. In this simulation we increase the rotational frequency in order to more readily observe the hydrodynamic interaction. A summary of the simulation details is shown in Table 3.12.

Simulation information	Data	Unit
Computational domain	$10 \times 10 \times 20$	μm^3
Flagellar rotational frequency	300	rps
Flagellar force c_f	0.4×10^{-4}	pN
Bodies' axes width	4	μm
Frames interval(six frames)	0.078	sec
Frames interval(three frames)	0.194	sec
Total swimming time	0.3888	sec

Table 3.12: Same direction with vertical offset.

The initial distance between the parallel cell axes is 4 μm with a 3 μm vertical offset between the upper and lower cell. The flagellar rotational frequency is increased to 300 rps from 200 rps used in the previous simulations. In addition, we reduce the flagellar force parameter c_f. Figure 3.26 includes the local fluid markers surrounding the cell bodies. We see that the fluid dynamics of the lower cell is disturbed by the flagellar rotation of the leading cell. This hydrodynamic interaction forces the lower cell to change swimming directions. The snapshots in the top row of Figure 3.27 shows the cells swimming upward with the rear one tilted away from its initial swimming direction. In the middle row of Figure 3.27 we see the XZ-view of the computational domain with local fluid markers. In the bottom row of Figure 3.27, we see an XY-view of the simulation. Here, the leading cells appears on the right. The formation of the fluid markers around the lower cell, shown on the left, show considerable deformation

in comparison with the pattern of the fluid markers of the leading cell. We can infer that the fluid velocities induced by the flagellar rotation of the leading cell has created a disturbance in the flow field surrounding the lower cell.

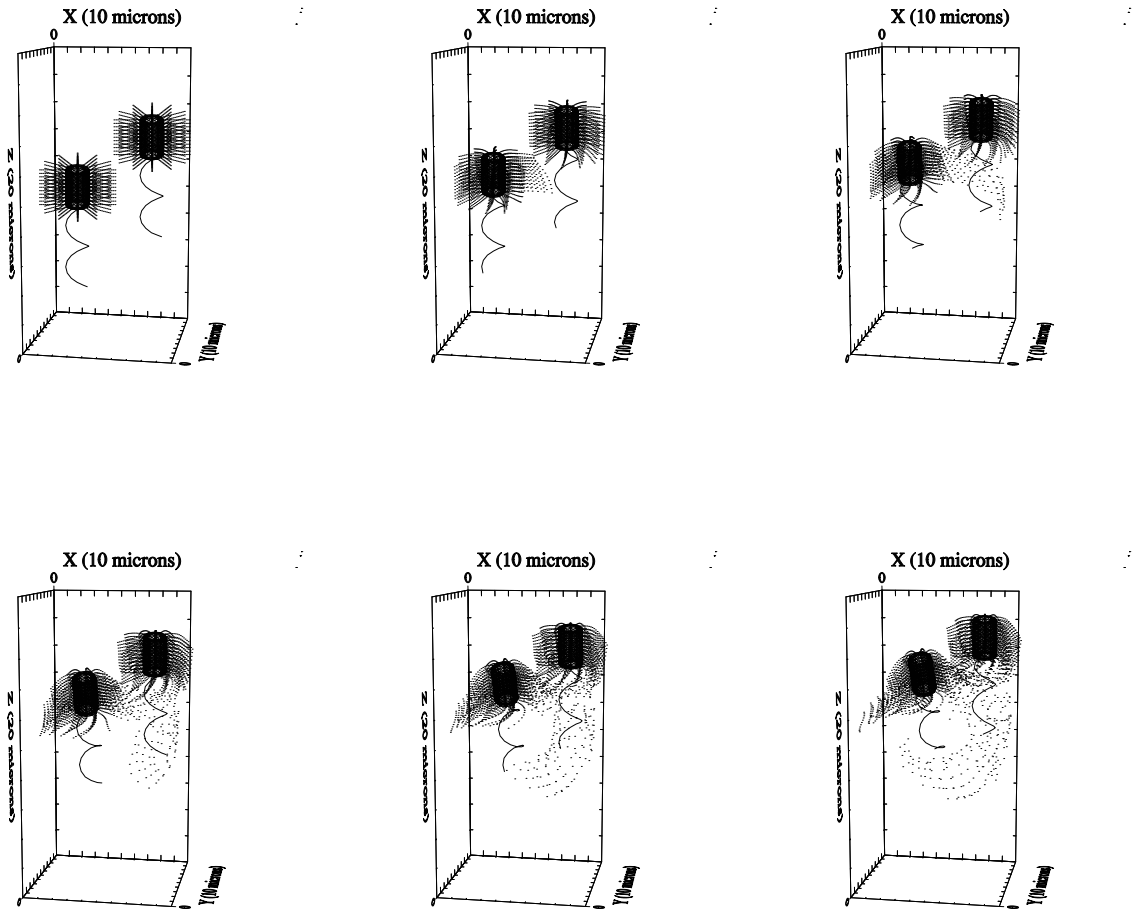

Figure 3.26: Two bacteria swimming with cell centered fluid markers.

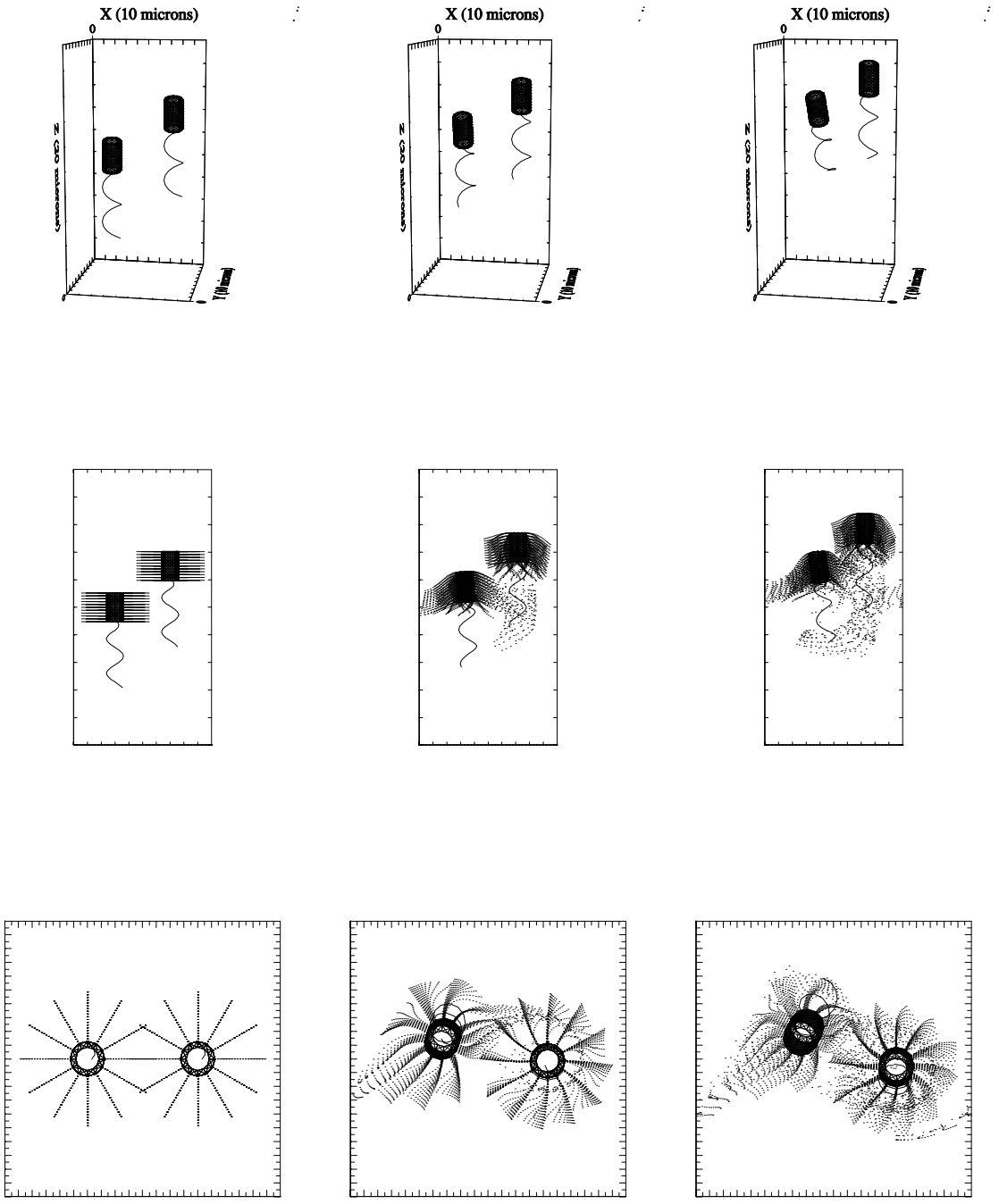

Figure 3.27: Two bacteria swimming one behind the other.

We show a similar simulation in Figure 3.28, with the flagellar rotational frequency reduced to taken as 200 rps with a total run time of 1.042 seconds. A summary of the simulation data is shown in Table 3.13.

Simulation information	Data	Unit
Computational domain	$10 \times 10 \times 20$	μm^3
Flagellar rotational frequency	200	rps
Flagellar force c_f	0.4×10^{-4}	pN
Bodies' axes width	4	μm
Frames interval	0.521	sec
Total swimming time	1.042	sec

Table 3.13: Two bacteria swimming one behind the other

In the top row of Figure 3.28 a 3D view of the swimming pattern for the two bacterial cells. The initial conditions are identical to those shown in the previous simulation. In the middle row of Figure 3.28 we shown an XZ-view of the simulation with the local fluid markers. In the bottom row of Figure 3.28, we show the XY-view with local fluid marker. The panel on the lower right gives the impression of an overlap or collision between the upper cell's flagellum with the lower cell's body. We have carefully examined this simulation from various angles and have determined that there is always separation between the neighboring flagellum and cell body.

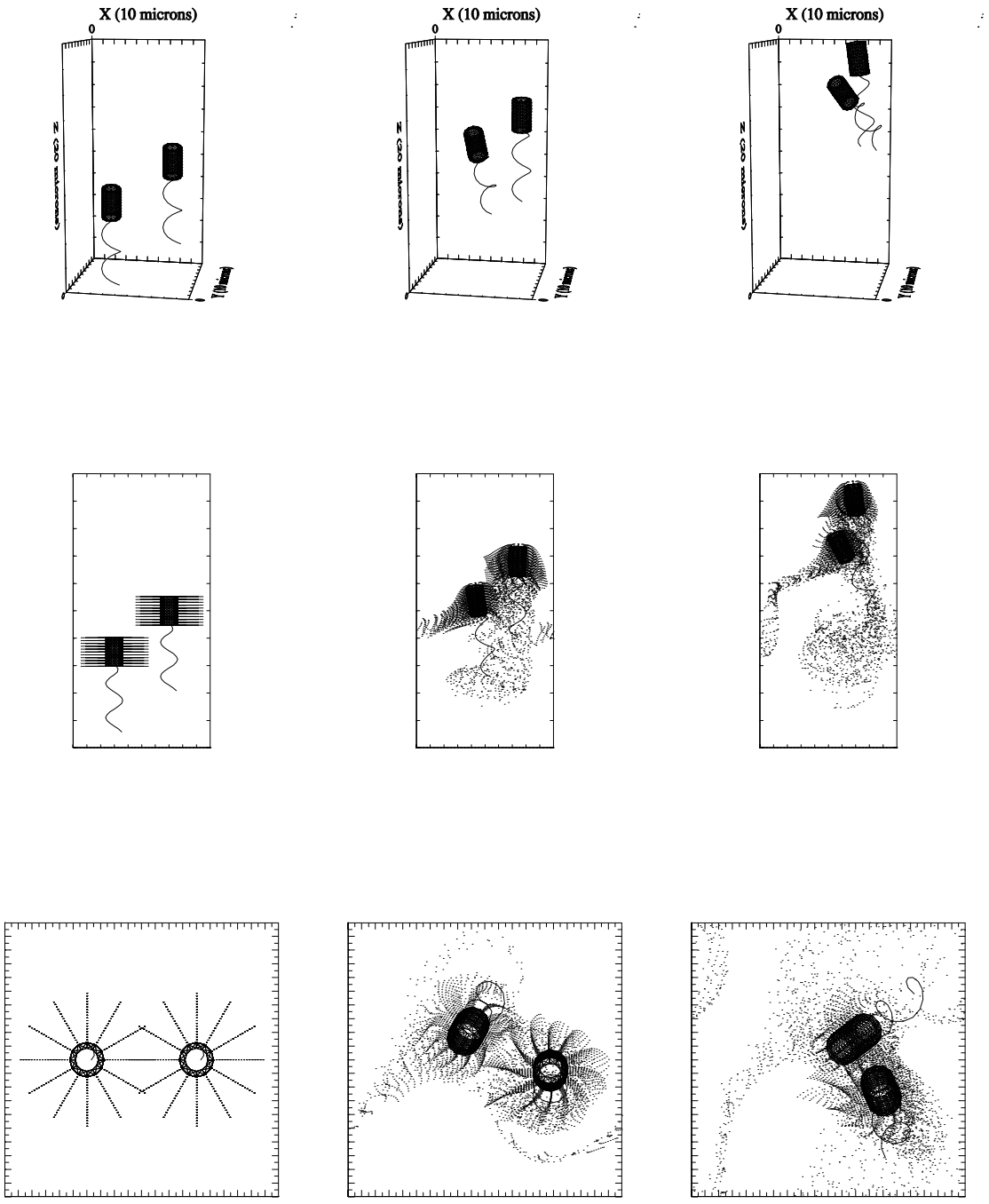

Figure 3.28: Two bacteria swimming one behind the other.

3.4.3 Same Direction with Vertical Offset, Part II

In Chapter 3.4.2 we found that the flow field induced by the flagellar rotation of the leading cell created a disturbance that altered the swimming trajectory of the trailing cell. In order to further investigate this hydrodynamic interaction, the following simulation was created. The computational domain doubled in size to $20 \times 20 \times 40 \mu\text{m}^3$ with a $32 \times 32 \times 64$ computational grid. As shown in Chapter 3.4.2, the axes of the two bacterial cells are initially parallel with a spacing of 4 μm and a vertical offset of 4 μm. Table 3.14 gives a summary of the simulation data.

Simulation information	Data	Unit
Computational domain	$20 \times 20 \times 40$	μm^3
Flagellar force c_f	1.0×10^{-3}	pN
Bodies' axes width	4	μm
Frames interval	0.108	sec
Total swimming time	0.325	sec

Table 3.14: Same direction with vertical offset (large domain).

In the simulation results shown in Figure 3.29-3.31 the lower cell swims around the trajectory of the leading cell in the direction of the leading cell's flagellar rotation but avoids intersection with the leading cell's flagellum. From the snapshots in Figure 3.29, we see that the swimming directions of both bacteria are influenced by the hydrodynamical interaction of the two cells. Figure 3.30 shows the simulation results in the XZ-view. Here we see the lower cell swimming from the left- to the right-side of the upper bacteria. The swimming trajectory of the leading cell changes gradually in the fourth frame in Figure 3.30. Figure 3.31 shows the XY-view of the domain, viewed from above. The swimming of the bacteria on the left is biased as it swims upwards and moves closer to the flagellum of the leading cell. However, swimming of the leading cell is also influenced by the presence of the lower cell. Its axis is tilted

toward the right. The apparent overlap seen in the third frame of Figure 3.31 is clarified in the third frame of Figure 3.32 where we see a definite separation between the two cells.

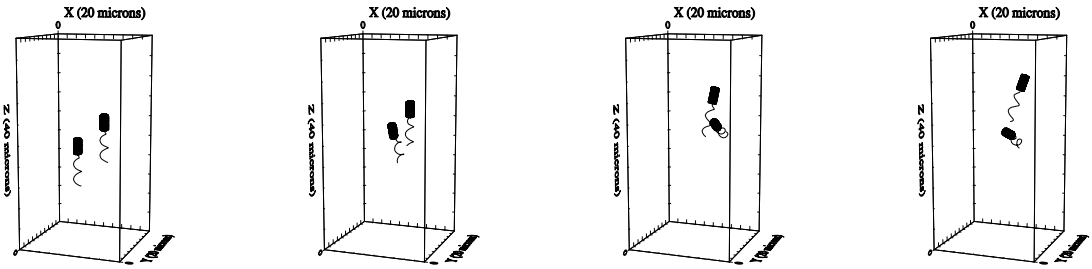

Figure 3.29: One bacteria in front, the other behind.

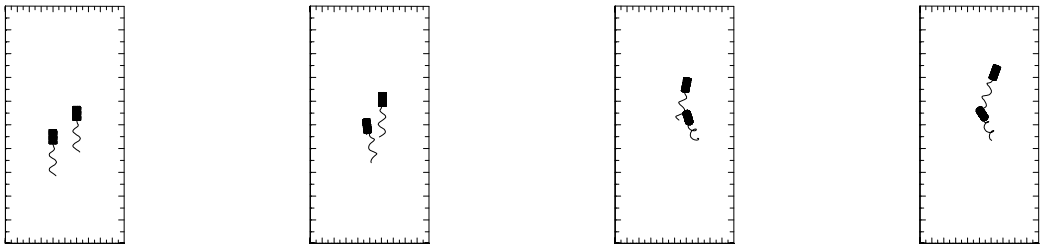

Figure 3.30: XZ-view of the interaction between two bacteria.

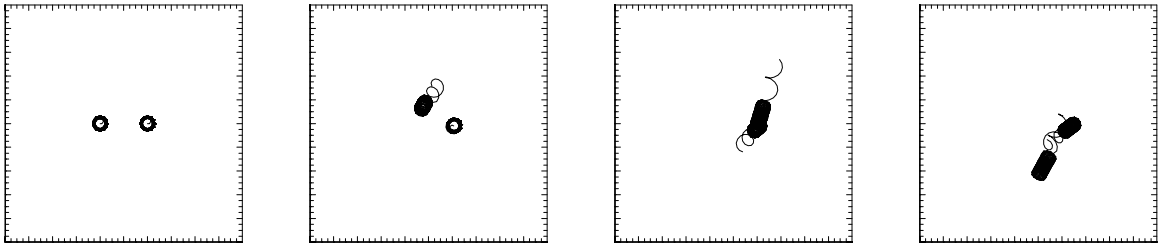

Figure 3.31: XY-view of the interaction between two bacteria.

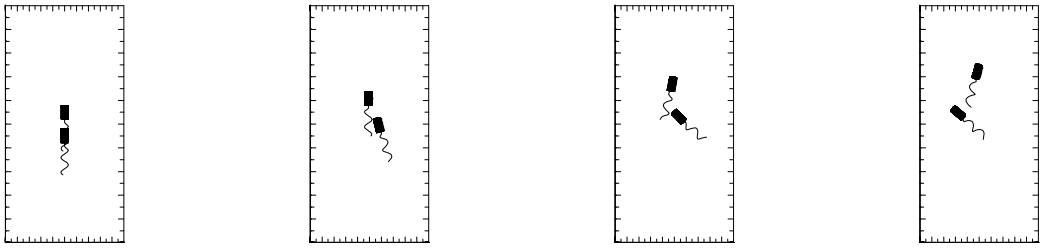

Figure 3.32: YZ-view of the interaction between two bacteria.

3.4.4 Opposite Directions with Vertical Offset: Narrow Spacing

In this section, we investigate the swimming patterns of two bacterial cells swimming in opposite directions in a $20 \times 20 \times 40 \mu\text{m}^3$ domain with a $32 \times 32 \times 64$ computational grid. The simulation details are summarized in the Table 3.15.

Simulation information	Data	Unit
Computational domain	$20 \times 20 \times 40$	μm^3
Flagellar force c_f	1.0×10^{-3}	pN
Bodies' axes width	4	μm
Frames interval	0.13	sec
Total swimming time	0.65	sec

Table 3.15: Swimming in opposite directions.

The initial axes of the two model cells are aligned in parallel on the same plane. The axes are separated by a distance of 4 μm. The cell centroids are separated in the vertical direction by 12 μm. Simulation results are shown in Figure 3.33. In the upper middle panel of Figure 3.33, the cell trajectories are approximately aligned with the Z-axis. In the upper right panel of Figure 3.33, the cell orientation begins to change. In the lower left and lower middle panels, we see the cells swim around each other. At the end of the simulation, shown in the lower right panel of Figure 3.33, we see that the cell swimming orientations show a near reversal from the initial orientations. Figure 3.35 shows the XZ-view of this simulation. Interestingly, in the YZ-view shown in Figure 3.37, we see that final orientation of the two model cells is reversed with respect to the Z-axis and that cells are swimming out of the original XZ plane.

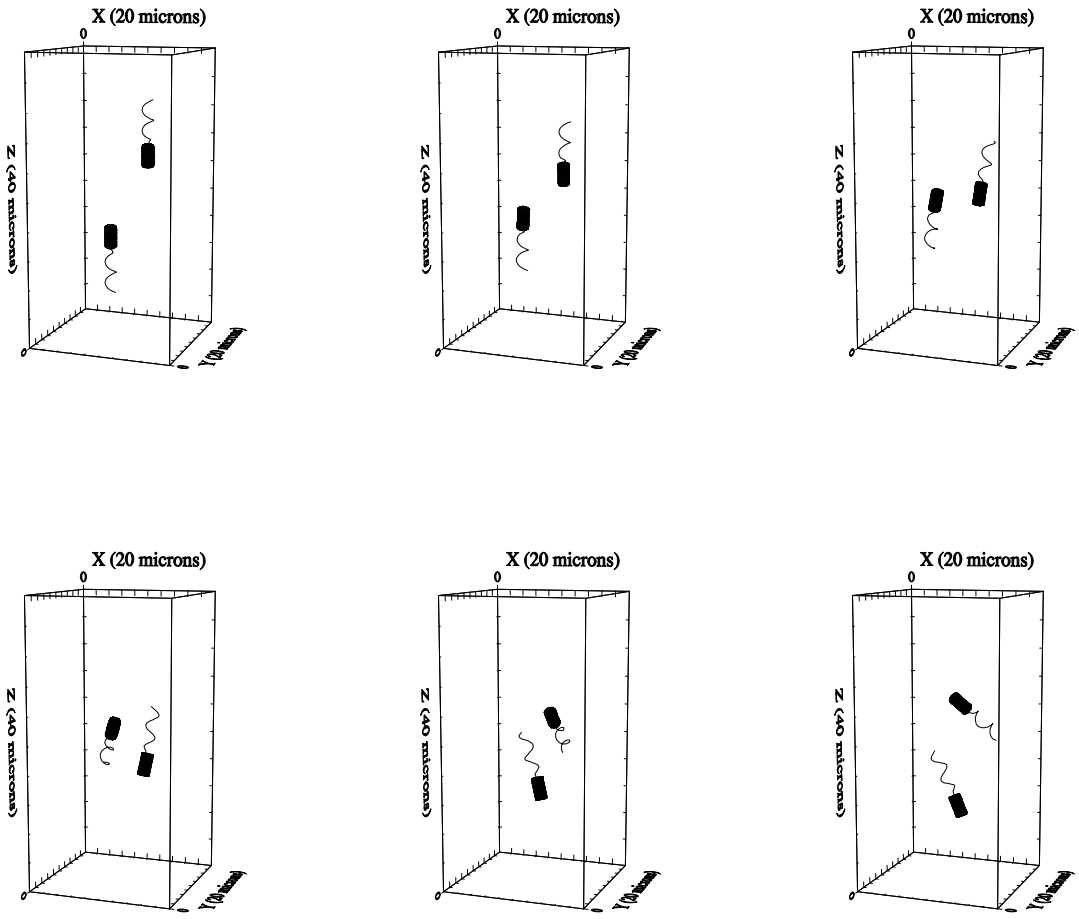

Figure 3.33: Two bacteria swimming in opposite direction.

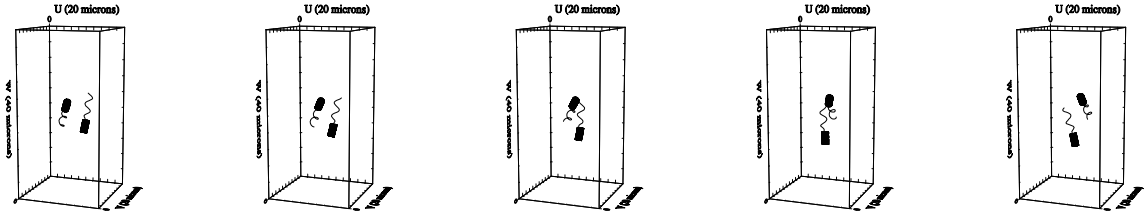

Figure 3.34: Snapshots between the 4th and 5th frames of Figure 3.33.

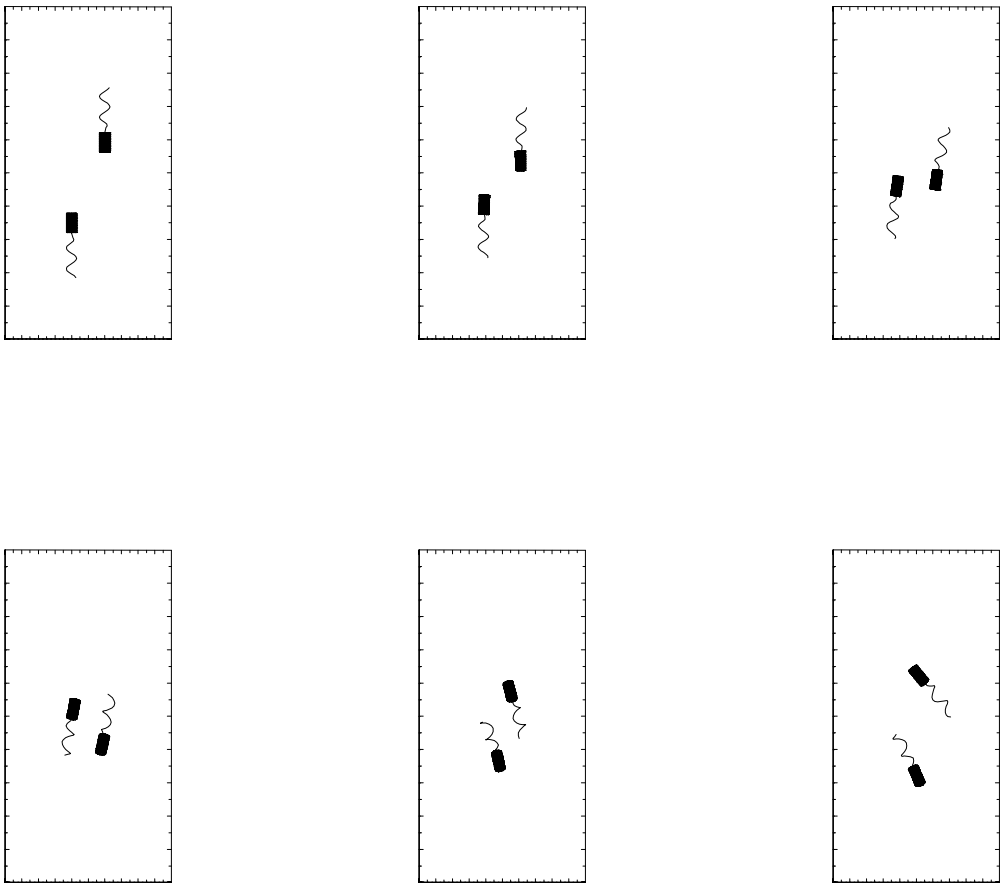

Figure 3.35: XZ-view of two bacteria swimming in opposite directions.

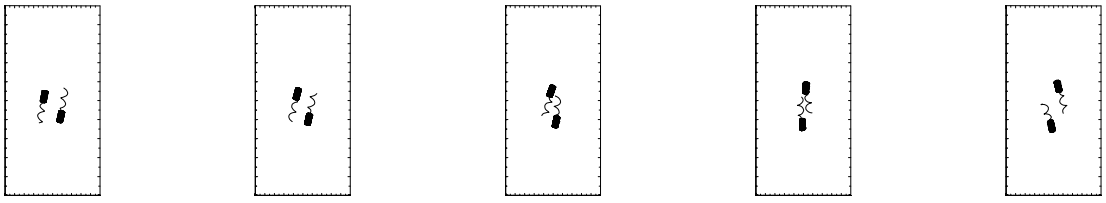

Figure 3.36: Snapshots between the 4th and 5th frames of Figure 3.35.

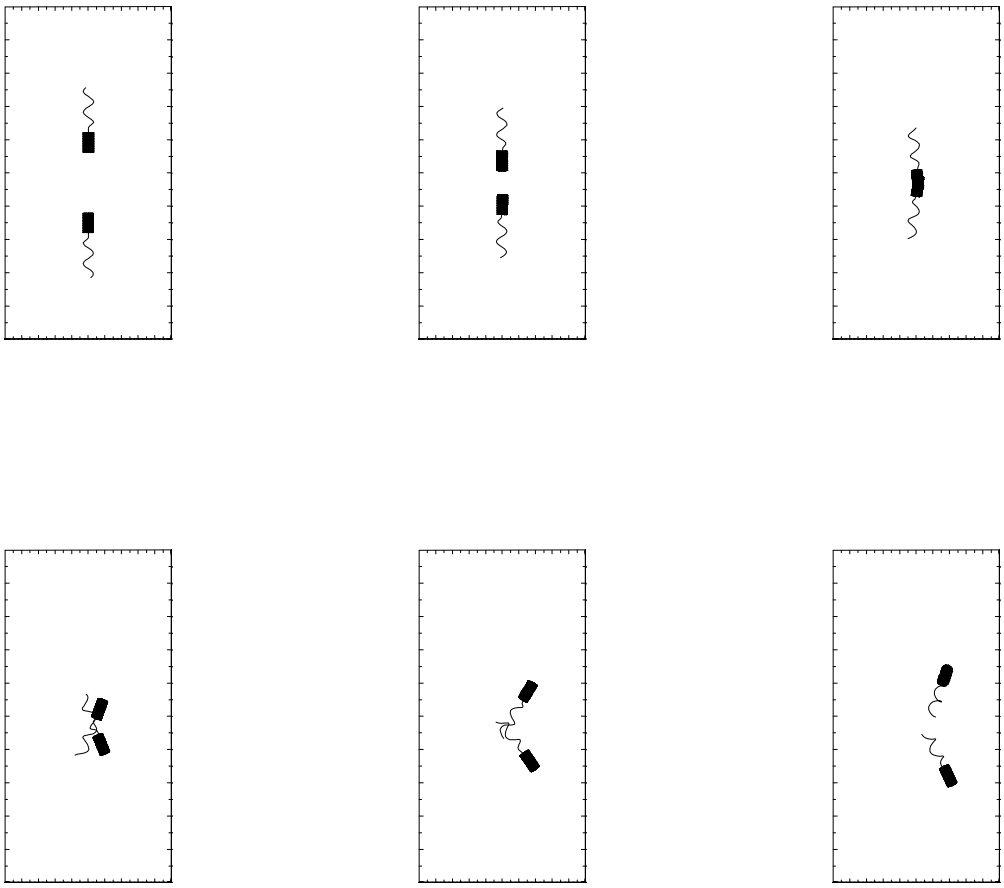

Figure 3.37: YZ-view of two bacteria swimming on the y=10 μm plane.

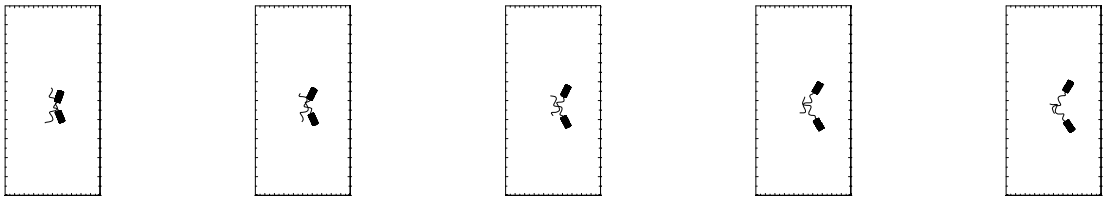

Figure 3.38: Snapshots between the 4th and 5th frames of Figure 3.37.

Next, two bacterial cells with opposite swimming directions are placed initially at the same height in a $20 \times 20 \times 40 \mu\text{m}^3$ domain with a $32 \times 32 \times 64$ computational grid. Simulation details are summarized in Table 3.16. A three-dimensional view of the simulation is shown in Figure 3.39. The cells begin to swim around each other at the beginning of the simulation. The rotation and switching of swimming axes is qualitatively similar to the simulation shown Chapter 3.4.4. The planar XZ-view is shown in Figure 3.40. In the YZ-view shown in Figure 3.41, we show that the cells are switching the swimming sides in XZ-view after the rotational interaction and that the cells are moving out of the original XZ-plane.

Simulation information	Data	Unit
Computational domain	$20 \times 20 \times 40$	μm^3
Flagellar force c_f	1.0×10^{-3}	pN
Bodies' axes width	4	μm
Frames interval	0.108	sec
Total swimming time	0.542	sec

Table 3.16: Two bacterial neighbors swimming in opposite directions.

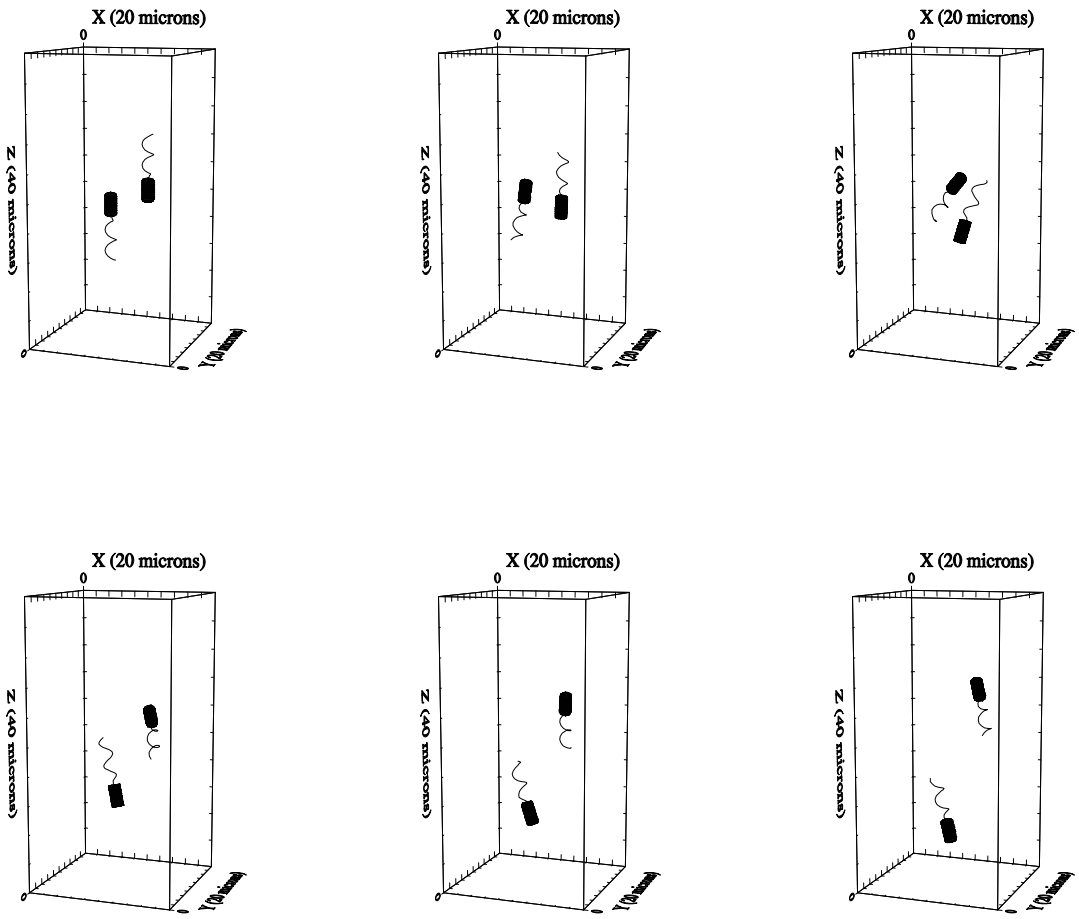

Figure 3.39: Two neighbor bacteria swimming in opposite directions.

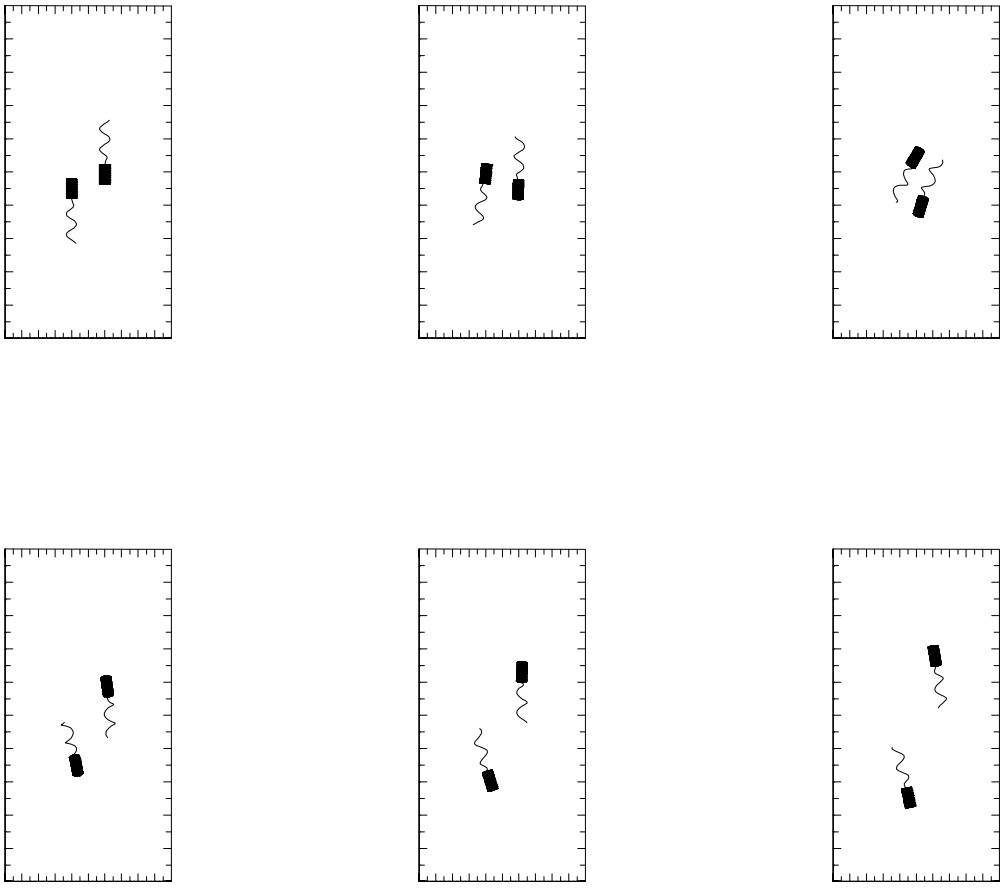

Figure 3.40: XZ-view of two neighbor bacteria swimming past each other.

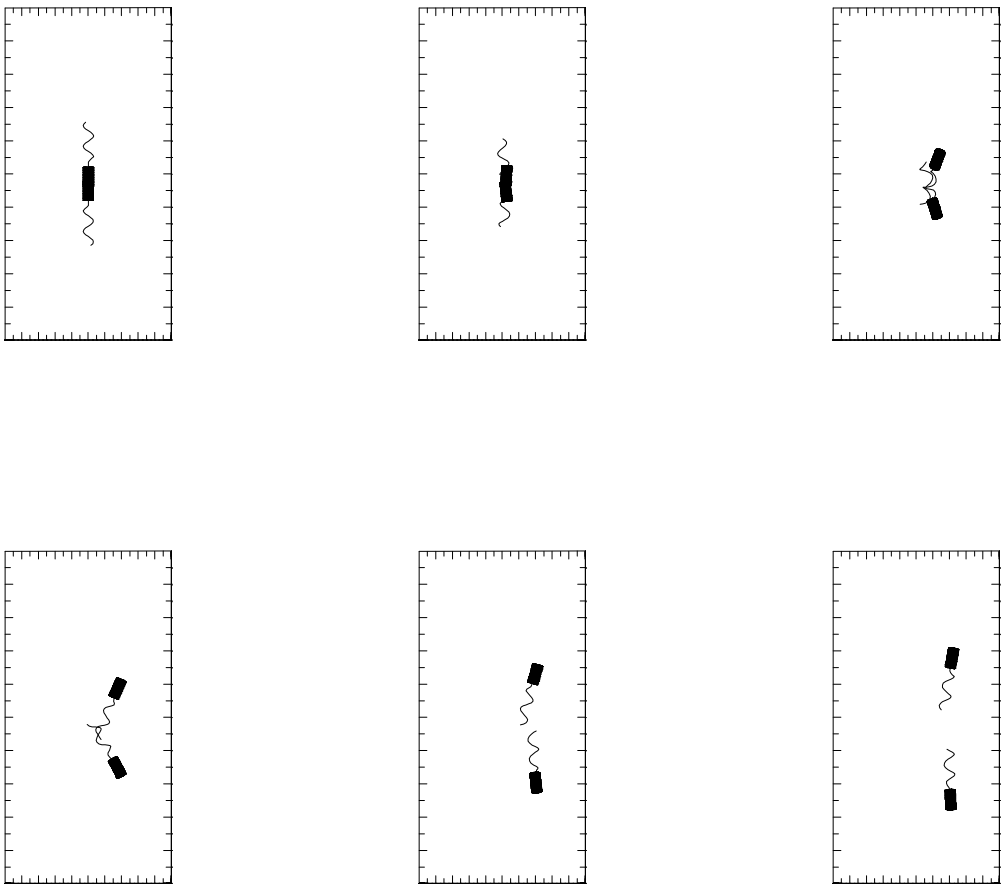

Figure 3.41: YZ-view of two neighbor bacteria swimming past each other.

3.4.5 Opposite Directions with Vertical Offset: Wide Spacing

In this section, we consider two bacterial cells swimming in opposite directions with an initial offset of 12 μm and an axial separation of 6 μm in a $20 \times 20 \times 40 \mu m^3$ domain with a $32 \times 32 \times 64$ computational grid.. This wider spacing between the axes of the two cells contrasts with the simulations results shown in Chapter 3.4.4. The simulation details are summarized in the Table 3.17.

Simulation information	Data	Unit
Computational domain	$20 \times 20 \times 40$	μm^3
Flagellar force c_f	1.0×10^{-3}	pN
Bodies' axes width	6	μm
Frames interval	0.314	sec
Total swimming time	0.628	sec

Table 3.17: Swimming in opposite directions with wider axial separation.

In the simulation results shown in Figure 3.44 (top) we see that the axial separation of the two cells narrows as the cells pass each other. However, the general swimming orientations remain similar to the initial orientations. In the YZ-view shown in Figure 3.44 (bottom), we see that the close range interaction of the two cells has resulted in a slight tilt of swimming direction with respect to the Z-axis and that the cells are swimming out of the XZ-plane.

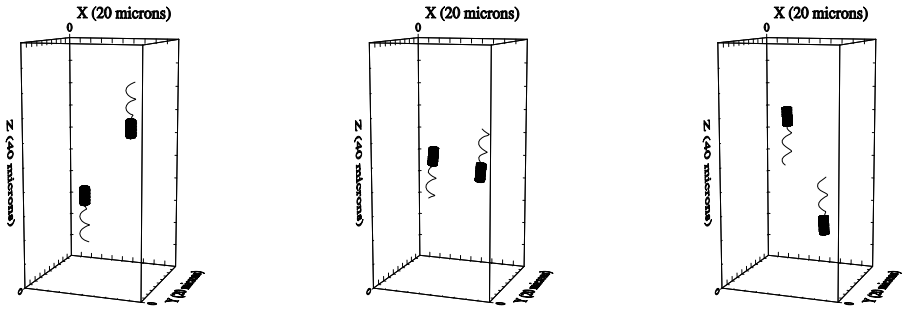

Figure 3.42: 3D view of two bacterial cells swimming with wide axial spacing.

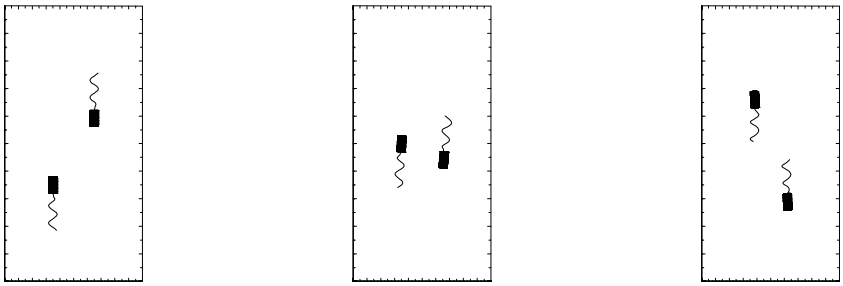

Figure 3.43: XZ-view of two bacterial cells swimming with wide axial spacing.

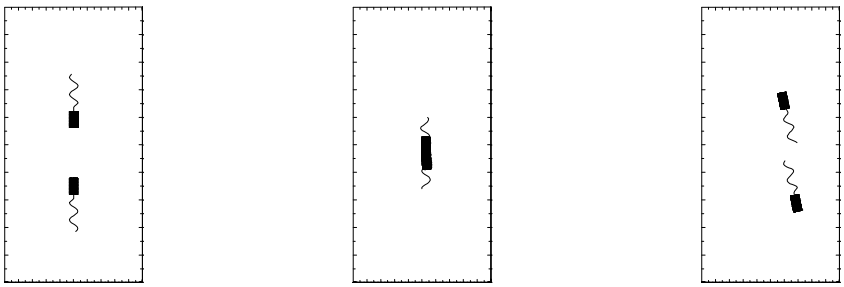

Figure 3.44: YZ-view of two bacterial cells swimming with wide axial spacing.

3.5 Hydrodynamic Interaction Between Multiple Bacterial Cells

In this section, we show a simulation with nine swimming bacterial cells. The addition of more bacterial cells in the fixed $20 \times 20 \times 40 \mu m^3$ domain with a $32 \times 32 \times 64$ computational grid requires very little additional CPU run time in comparison with simulations with one or two cells. The model cells in this simulation are the same size (1.25 μm in diameter and 2.5 μm in length) as in the previous simulations. The computational cost of our bacterial swimming model does depend on the computational grid size. A full study of bacterial bioconvection [84], pattern formation in biofilm [53, 54] or bacterial veil formation [145, 147, 37] would require significantly more model cells and a much larger computational grid. As a step toward a simplified bacterial model and the eventual study of the complex behavior of many swimming bacteria, we employ here a simplified model bacterial cell with only 6 immersed boundary points on each ring and 7 layers of annular rings. Table 3.18 provides summary of the simulation data.

Simulation information	Data	Unit
Computational domain	$20 \times 20 \times 40$	μm^3
Bacterial diameter	1.25	μm
Bacterial body length	2.5	μm
Bacterial boundary points	6	points
Bacterial boundary layers	6	layers
Time step	4.8×10^{-7}	sec
Flagellar force c_f	0.5×10^{-3}	pN
Frames interval	0.0167	sec
Total swimming time	1.00	sec

Table 3.18: Simulation data for nine bacterial swimming cells.

We show, in Figure 3.45, a 3D view of the simulation. The initial bacterial locations are shown in the upper left panel. Note that the bacteria are initially aligned with the Z axis. As the simulation progresses, we see a gradual realignment and randomization of bacterial orientation, although most of the cells are still swimming upwards at the end of the simulation.

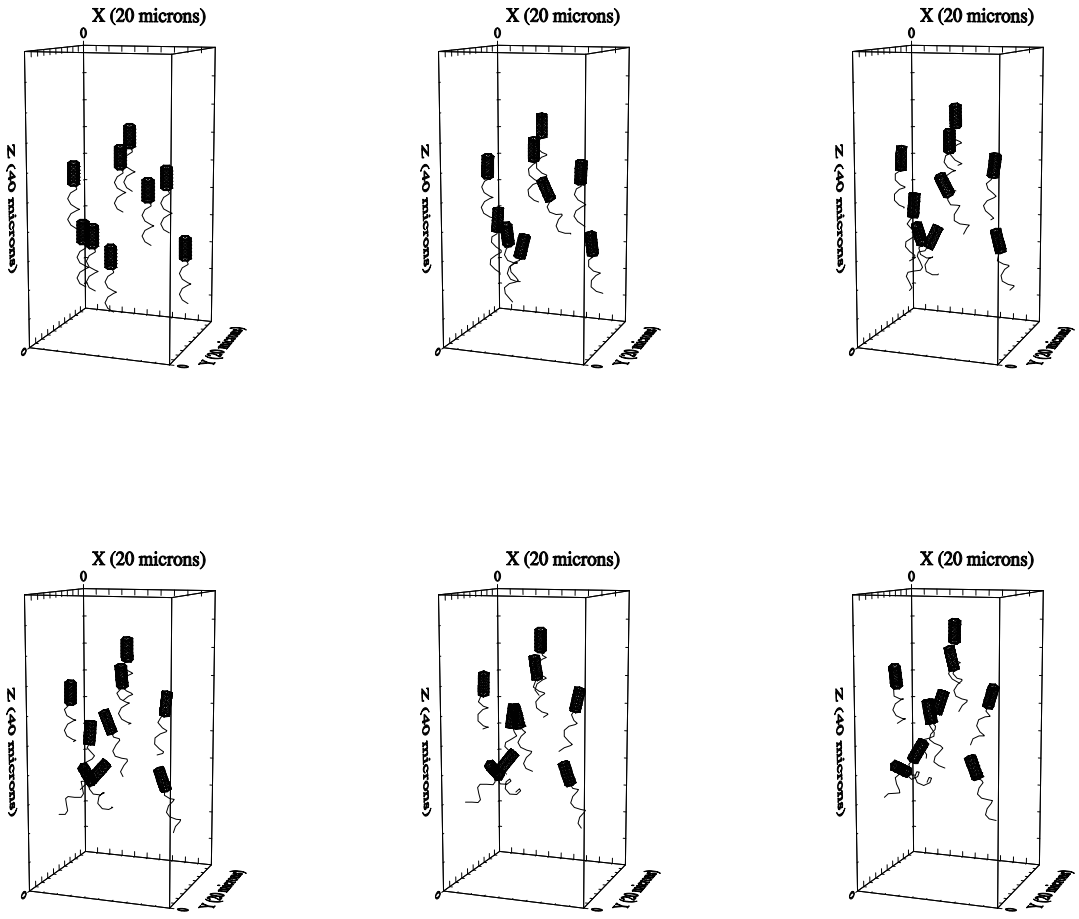

Figure 3.45: Nine bacteria swimming in the domain simultaneously.

Chapter 4

Bacterial Swimming Near Walls and Cylindrical Boundaries

In this chapter, we consider the hydrodynamic interaction of our model bacterial cell with walls and cylinders. We present simulations designed to investigate the model swimming behavior near a wall, or between two walls. In addition, we investigate the interaction between a model cell swimming within a cylindrical tube or between two cylinders.

The hydrodynamic interaction of a motile bacterial cell with structures such as planar walls and the behavior of a bacterial cell swimming in a channel or within and outside a cylinder has been addressed in several studies of bacterial hydrodynamics. Cox [41] investigated the behavior of a swimming slender body in the neighborhood of solids walls. Blake and Chwang [25] studied the fluid flow of some singularities near a stationary no-slip planar boundary. The importance of the "no slip boundary condition", Equation (2.3.4), at the wall was addressed in [23, 24, 25]. Ramia, Tullock and Phan-Thien [133] investigated the interaction of a monotrichous spherical bacteria cell with walls using the Stokes equations and a boundary element method. Frymier, Ford, Berg and Cummings [69] traced the trajectories of bacteria swimming

near a glass surface and found that bacterial swimming speeds were slower near the glass. The slower speeds were also predicted by Ramia et al. [133]. Goto and Magariyama, et al. [71, 114], also using a boundary element method, investigated the hydrodynamic interaction of a motile rod-shaped bacterial cell with stationary walls. Moreover, Berg and Turner [17] as well as Liu and Papadopoulos [103, 104, 105] studied bacterial swimming in capillary and micro-capillary chambers and observed the hydrodynamic interaction of swimming bacteria with other swimming bacterial cells. Liu and Papadopoulos also studied bacterial aggregation and the formation of bacterial clusters in the confinement of a narrow tube. Fauci and McDonald studied sperm motility in a channel with a 2D immersed boundary model [62].

We model planar walls and cylindrical tubes as immersed boundaries. These structures are considered as immersed elastic structures with large stiffness parameters. The structures are tethered to fixed points in the computational domain by elastic links with a large stiffness coefficient and a zero rest length. The simulations in Chapter 4 illustrate the hydrodynamic influence of a wall or cylinder on the swimming of the model cell. We show simulations of a model cell swimming near a wall, between two parallel walls, and within a cylindrical tube. We also present a simulation with one model cell swimming between two cylinders.

We represent the wall or cylinder as a regularly spaced mesh comprised of immersed boundary points $\mathbf{X}(t)$. Neighboring immersed boundary points are connected with elastic links so that the force $\mathbf{f}_{pq}$ at the immersed boundary point $\mathbf{X}_p$ at time t due to the elastic link with the neighboring immersed boundary point $\mathbf{X}_q$ is obtained from Hooke's Law:

$$\mathbf{f}_{pq} = S_1(\parallel \mathbf{X}_q - \mathbf{X}_p \parallel - L_{pq}) \frac{\mathbf{X}_q - \mathbf{X}_p}{\parallel \mathbf{X}_q - \mathbf{X}_p \parallel} \tag{4.0.1}$$

Here, S_1 is the wall or cylinder stiffness constant and L_{pq} is the resting length of the elastic link between these two immersed boundary points. The total force at $\mathbf{X}_p$ is defined by $\mathbf{f}_p = \sum_q \mathbf{f}_{pq}$, where the sum is over all neighbors q. And the total wall or cylinder force $\mathbf{f}_{wall}$ can be found as $\{\mathbf{f}_p\}$. The tether force at $\mathbf{X}_p$ at time t is given by $\hat{\mathbf{f}}_p = S_{tether} \parallel \mathbf{X}_p - \mathbf{X}_p^* \parallel \dfrac{\mathbf{X}_p^* - \mathbf{X}_p}{\parallel \mathbf{X}_p^* - \mathbf{X}_p \parallel}$ where $\mathbf{X}_p^*$ is the initial location of $\mathbf{X}_p$. Thus, each wall or cylinder immersed boundary point is tethered to a fixed point in the domain with a linear elastic spring with stiffness S_{tether} and a zero rest length. The total tether force $\mathbf{f}_{tether}$ can be found as $\{\hat{\mathbf{f}}_p\}$.

We spread the wall and tether force densities $\mathbf{f}_p$ and $\hat{\mathbf{f}}_p$ in step 4 of the algorithm shown in Chapter 2.3, to the Eulerian grid to obtain the Eulerian force $\mathbf{F}_{wall}$ and $\mathbf{F}_{tether}$. The total Eulerian force density $\mathbf{F}$ in Equation(2.3.1), $\mathbf{F} = \mathbf{F}_{body} + \mathbf{F}_{rotate} + \mathbf{F}_{swim} + \mathbf{F}_{wall} + \mathbf{F}_{tether}$.

In the following simulation, we represent the planar $10 \times 20 \mu\text{m}^2$ wall with a 32×64 grid of immersed boundary points. The wall is parallel to the YZ-plane in the computational domain of $10 \times 10 \times 20$ μm^3. The wall and tether stiffness parameters $S_1 = S_{tether} = 10^5$ dynes/μm.

4.1 Bacterial Swimming Near a Planar Wall

We model a planar wall, as shown in Figure 4.1, as a regular mesh of immersed boundary points connected by elastic links. The wall is initially embedded in the YZ-plane and runs from the top to the bottom of the domain. The immersed boundary points for the wall are tethered to fixed points in the domain and with elastic links with large stiffness coefficients and zero rest length. The influence of the wall is felt through the immersed boundary in the following way. Since the wall moves at the local fluid velocity (2.3.4), wall deformations and deflections create elastic forces which are communicated to the fluid via the Eulerian force term $\mathbf{F}(\mathbf{x}, t)$. Thus, the fluid velocity at the wall is effectively zero. The wall structure is added at very little additional computational cost in comparison with the cost associated with the solution of the Navier-Stokes equations. In Chapter 4.1.1, we show two contrasting simulations one with the immersed boundary wall, and a second with no immersed boundary wall. In the later case, the points of the wall become fluid markers that have no influence on the simulation. In Chapter 4.1.2, we enlarge the domain and increase the flagellar force parameters. These simulations show that the hydrodynamic influence of the wall reduces the swimming speed of the model cell and induces changes in swimming orientation.

4.1.1 Swimming Near a Wall: Short Time Behavior

Here we show two simulations in order to investigate the wall effect on swimming behavior. In the first simulation, we include the elasticity of the wall as well as the tethering forces. In the second, we set the S_1 and S_{tether} to zero so that the wall has no influence on the simulation. Since the immersed boundary points are advected at the local fluid velocity, the wall's immersed boundary points function as fluid markers. The initial spacing between the wall and the cell axis is 2.5 μm. We summarize the simulation details in the Table 4.1.

Simulation information	Data	Unit
Computational domain	$10 \times 10 \times 20$	μm^3
Flagellar force c_f	0.8×10^{-3}	pN
Frames interval	0.2600	sec
Total swimming time	0.52	sec
Swimming speed without wall influence	13.76	μm/sec.
Swimming speed with wall influence	11.94	μm/sec.

Table 4.1: Short time behavior.

We show the simulation results in Figures 4.1-4.3 with a "real" wall (top row) and a "fake" wall (bottom row). Figure 4.1 shows the 3D view of the bacterial cell swimming near the wall. The trajectory of the model cell swimming in proximity to the "fake" wall is approximately vertical as expected. We see that the effective no-slip boundary condition at the "real" wall changes the fluid dynamics and influences the swimming trajectory. In Figure 4.2 the "real" wall structure is marked by "*" (asterisks). In the bottom row, the "fake" wall is marked "+" (cross) markers. In Figure 4.3, the bacterial cell and wall are shown in the XZ-view. The initial orientation of the bacterial cell is aligned with the wall. In Figure 4.3, we see that the bacterial cell orientation changes and begins to swim away from the wall. As shown in Table 4.1,

the wall effectively reduces the swimming speed of the bacterial cell by 13.23%.

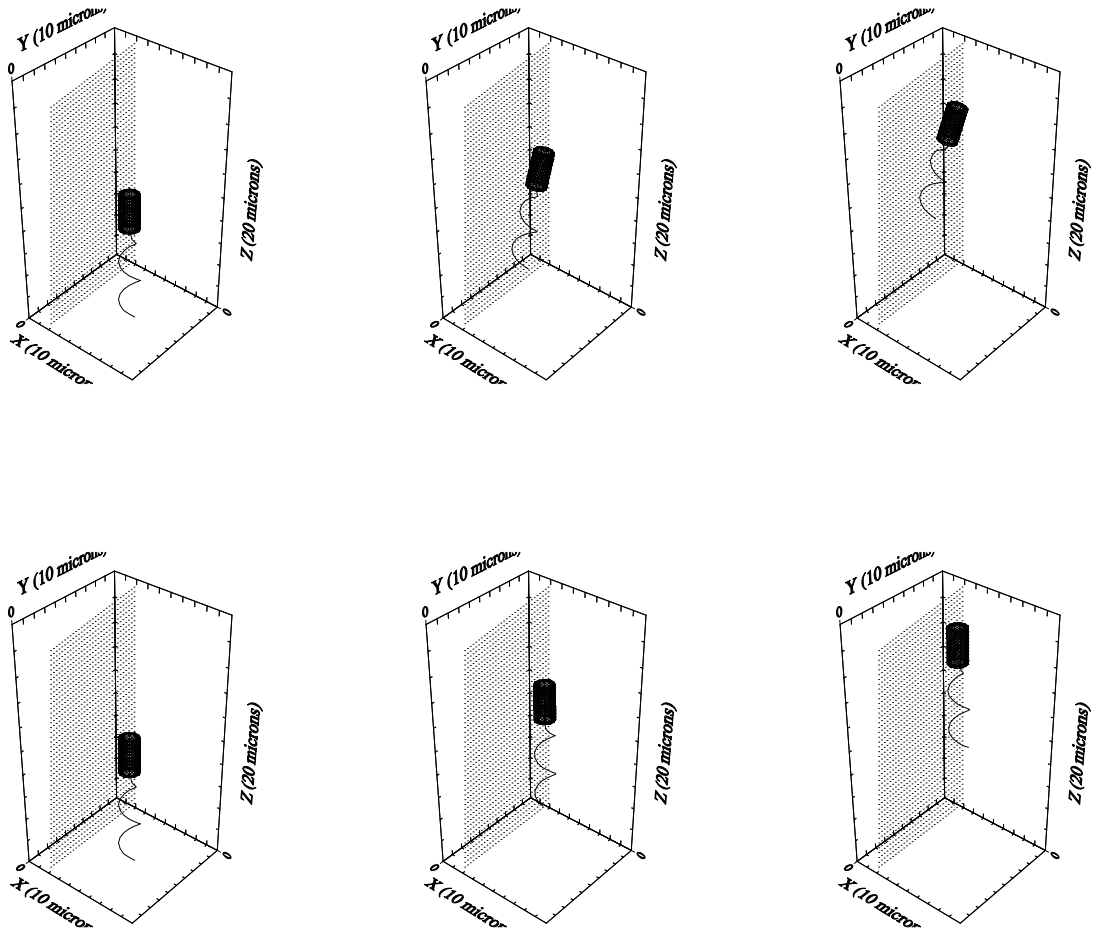

Figure 4.1: (top) With wall influence. (bottom) Fake wall.

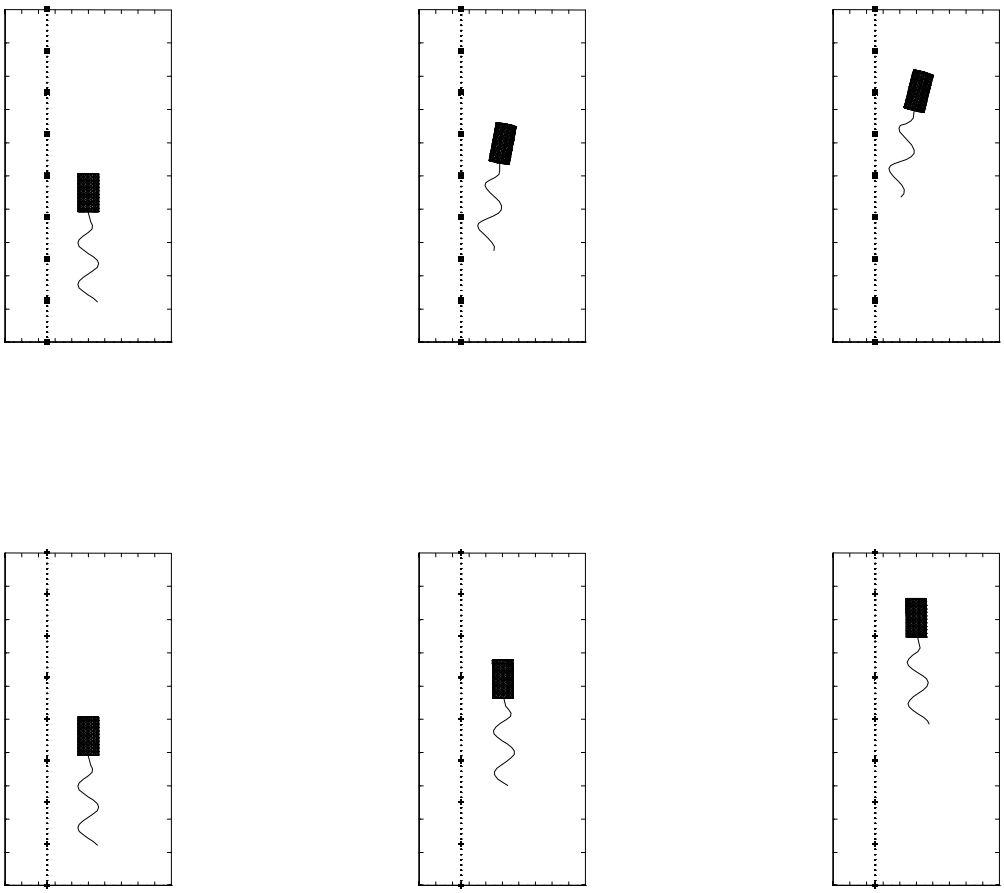

Figure 4.2: XZ-view of a bacterium swimming with and without wall influence.

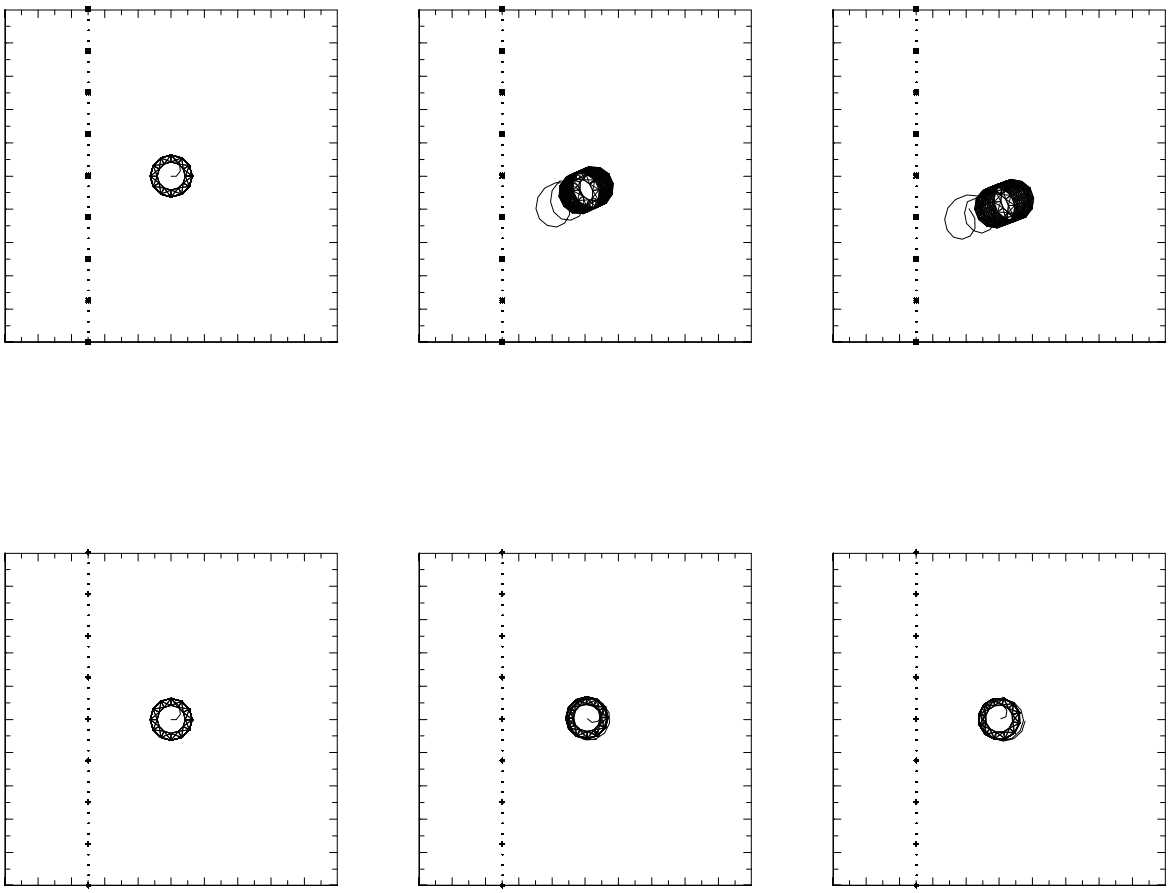

Figure 4.3: XY-view of a bacterium swimming with and without wall influence.

4.1.2 Swimming Pattern Near a Wall in a Large Domain

Here we increase the domain size from $10\times10\times20$ μm^3 on a $16\times16\times32$ computational grid to $20 \times 20 \times 40$ μm^3 on a $32 \times 32 \times 64$ computational grid to further elucidate the influence of the wall on the model cell trajectory. The initial spacing between the the wall and the cell axis is 3.125 μm. In this simulation, we increase the flagellar swimming force and swimming speed in order to visualize the cell-wall interaction in the enlarged domain within a reasonable computational time period. In Table 4.2, we summarize the simulation parameters.

Simulation information	Data	Unit
Computational domain	$20 \times 20 \times 40$	μm^3
Flagellar force c_f	1.2×10^{-3}	pN
Frames interval(three frames)	0.2083	sec
Frames interval(eight frames)	0.0833	sec
Total swimming time	0.4166	sec
Swimming speed with wall	20.66	μm/sec.
Swimming speed without wall	23.62	μm/sec.

Table 4.2: Long time behavior.

We see, in the top row of Figure 4.4, the model cell orientation rotate toward the viewer, and in the bottom row of Figure 4.4, rotate away from the wall. In Figure 4.5, we show a series of snapshots with a smaller time interval (0.0833 seconds) to illustrate the cell rotation above the YZ-plane (asterisks markers). The rotation and movement away from the wall are also seen in the XY-view shown in Figure 4.6. For comparison, results from an identical simulation with "fake" wall (not shown) show that the bacterial swimming speed is reduced by 12.53%.

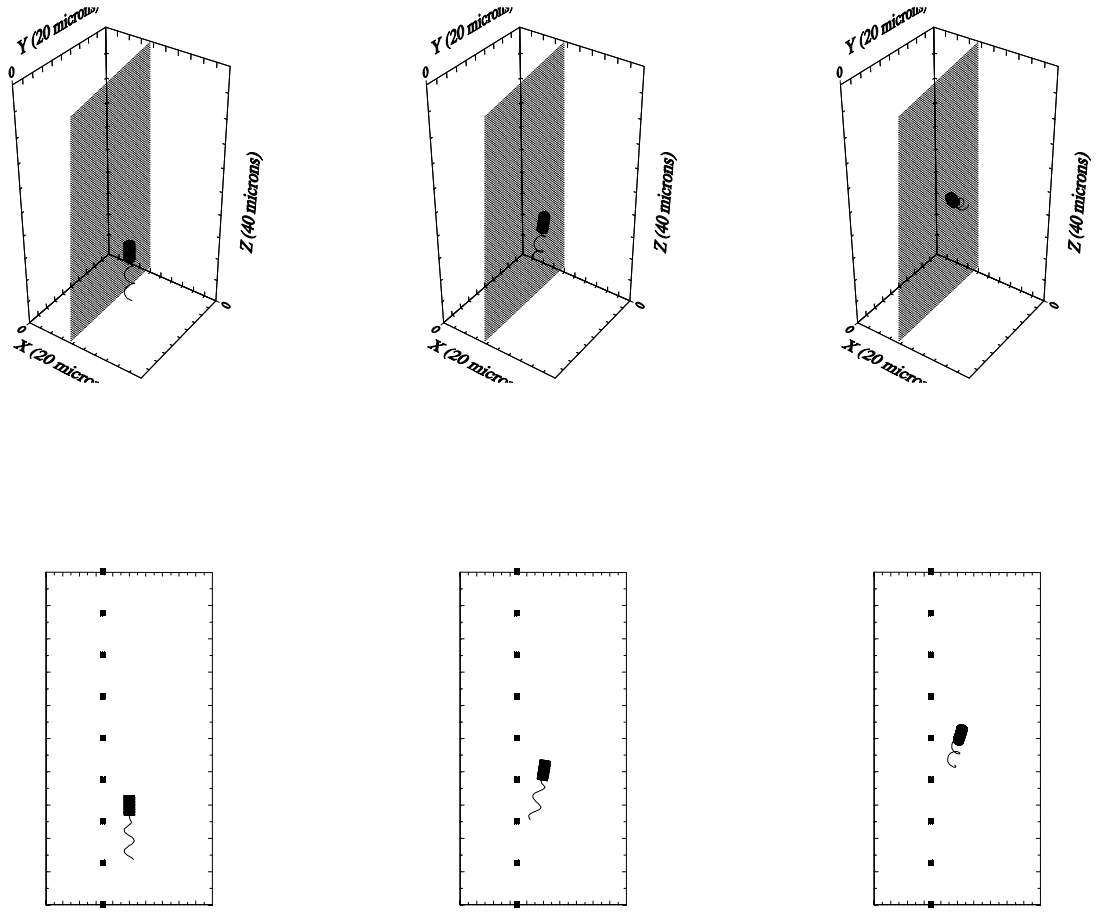

Figure 4.4: (top) 3D viewing box , (bottom) XZ-viewing window.

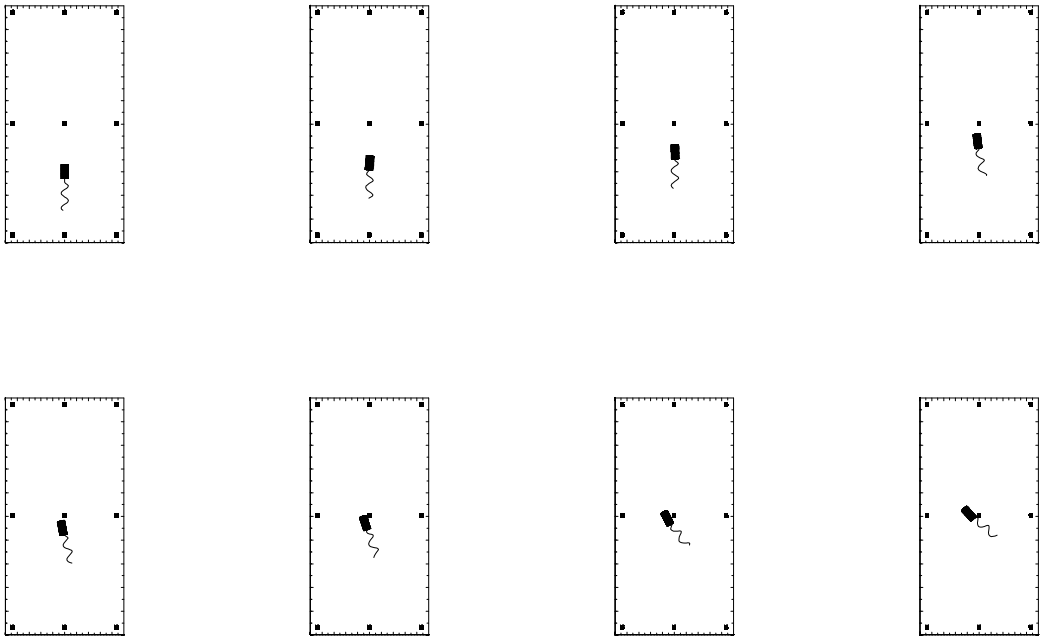

Figure 4.5: YZ-view of a bacterium swimming near a wall.

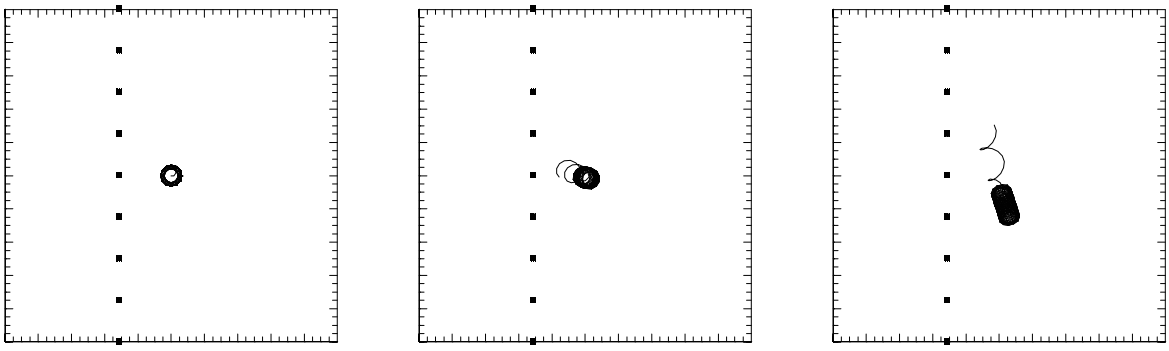

Figure 4.6: XY-view of a bacterium swimming near a wall.

4.2 Bacterial Swimming Between Parallel Walls

In the following pair of simulations, we show a single model bacterial cell swimming between two parallel walls. Each immersed boundary wall is identical and modeled as described above. The additional computational CPU time for an additional wall is negligible compared to the overall cost of the method. We show a simulation in Chapter 4.2.1 of a single cell swimming midway between the two walls, and in Chapter 4.2.2 of a single cell swimming nearer one of the walls. We summarize the details of the simulation in the simulation information for the two simulations are shown in Table 4.3.

Simulation information	Data	Unit
Computational domain	$10 \times 10 \times 20$	μm^3
Flagellar force c_f	0.8×10^{-3}	pN
Frames interval	0.433	sec
Total swimming time	0.867	sec
Swimming speed at midpoint	9.134	μm/sec.
Swimming speed near one wall	8.90	μm/sec.

Table 4.3: Swimming between parallel walls.

4.2.1 Behavior at the Midpoint

In this simulation, the initial location of the bacterial model cell is exactly between the parallel walls. The tethered walls are placed in parallel to the YZ-plane with a spacing of 7.5 μm in the $10 \times 10 \times 20$ μm^3 computational domain with a $16 \times 16 \times 32$ grid. The axis of the model cell is aligned the the Z-axis and parallel to the walls. We show a 3D view of the simulation results in the top row of Figure 4.7 in which the walls are represented as dots. We show the XZ-view of the simulation in the middle row of Figure 4.7 with both local and global fluid markers. The trajectory of the model cell is approximately vertical. Compared to the simulation described in Chapter 4.1.1 without influence, the swimming speed here is reduced by 33.62%. Compared to the simulations described in Chapter 4.1.1 with wall influence, the swimming speed is reduced by 23.5%

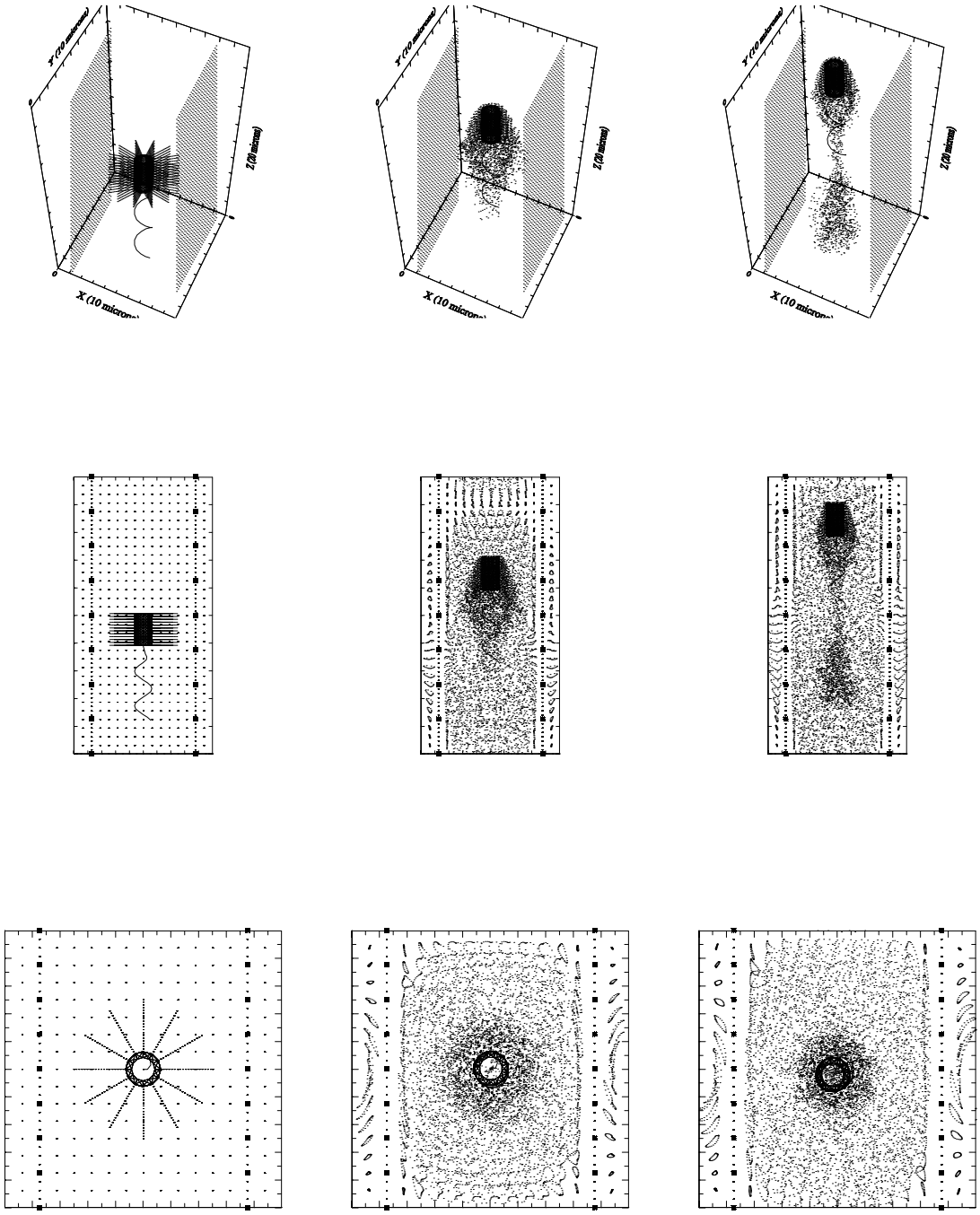

Figure 4.7: A bacterium swims midway between two walls.

4.2.2 Behavior Near One Wall

The following simulation shows that the position of the bacteria in the channel formed by two parallel walls can alter the swimming trajectory of the model bacterial cell due to the no-slip boundary condition at the wall. The walls are aligned with the YZ-plane with a spacing of 6.25 μm in a domain of with dimensions $10 \times 10 \times 20 \mu\text{m}^3$ with a $16 \times 16 \times 32$ computational grid. The spacing between the model bacterial cell wall and the wall on the left 1.875 μm. In Figure 4.8 (top row) we show the 3D view of the simulation. The row of dots on both sides of the bacterial cell represent the location of the immersed boundary walls. We see in the XZ-view shown in Figure 4.8 (middle row) and in the XY-view shown in Figure 4.8 (bottom row) that the model cell swims away from the wall on the left. The model cell swimming speed has been reduced by 2.56% compared with the simulation shown above in Chapter 4.2.1. Table 4.3 shows the simulation parameters.

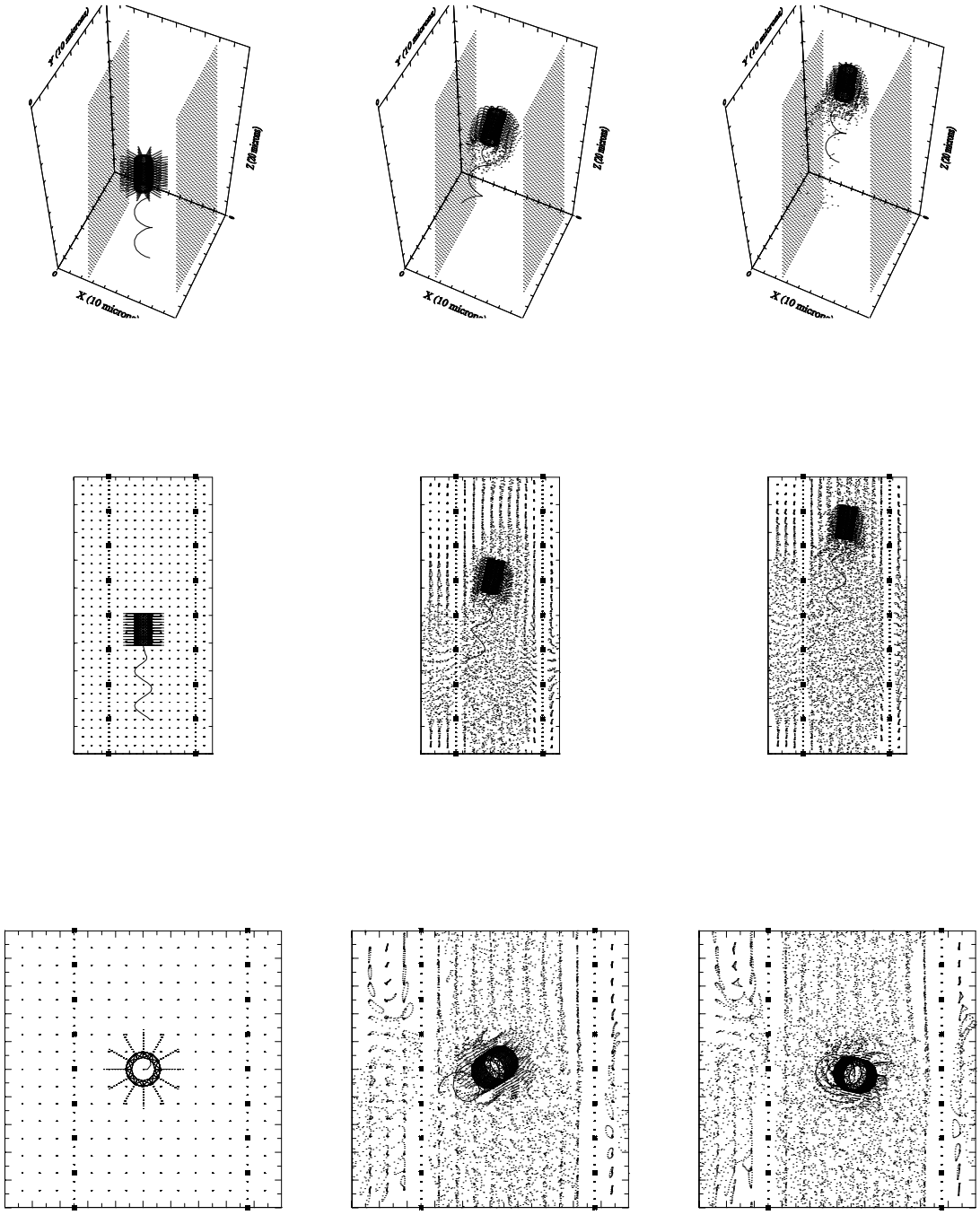

Figure 4.8: A bacterium swims near one of two walls.

4.3 Influence of Cylindrical Boundaries

Flagellated bacterial cells are found in many types of environments including the lung, intestinal and urinary tracts, as well as catheters [48, 136]. The interaction between an elastic cylindrical structure and fluid flow plays an important role in the study of hydrodynamics. Vesier and Yoganathan [148] have studied steady flow in a flexible cylinder in the high Reynolds number regime in order to elucidate the interaction of cardiovascular tissue and blood flow. Liu and Papadopoulos [103, 104] investigated bacterial swimming inside capillary cylinders with 3 to 50 μm diameters in order to study bacterial motility, chemotaxis and aggregation within a narrow tube.

In the following, we investigate model cell swimming within a cylindrical immersed boundary tube. The elastic structure of the cylinder is similar to the outer cylinder of the model bacterial cell (see Figure 2.2 for reference). The cylinder is constructed from a set of immersed boundary points which form a regular cylindrical grid. The cylinder's immersed boundary points are connected with elastic links with the same stiffness parameters as the bacterial cell body. As in the construction of the cell body, we include links between the neighboring immersed boundary points in the horizontal and vertical directions. Hence, the cylindrical wall can be considered as a thin cylindrical wall. The cylinder is also tethered to fixed points in the domain that coincide with the initial position of the cylinder's immersed boundary points. The stiffness of elastic springs on the cylinder is the same as the stiffness parameter S_0 of the bacterial body. As a result, the cylinder's immersed boundary points have a near zero velocity and remain close to their initial positions. The cylinder's elastic and tether forces contribute to the force density $\mathbf{F}$ in Equation (2.3.1) in the Navier Stokes equations. The height of the cylinder is designed to be 16.67 μm and the

stiffness constant of a cylinder is taken as $S_{tether} = 2.4 \times 10^{-1}$ dynes/μm.

In Chapter 4.3.1, we show simulation results of a model cell swimming within an untethered cylinder. In Chapter 4.3.2, we consider a model cell swimming within a tethered cylinder. In Chapter 4.3.3, we consider a model cell swimming within a cylindrical wall and placed near one side of the cylinder. In Chapter 4.3.4 through Chapter 4.3.6, the simulation domain is expanded to $20 \times 20 \times 20$ μm^3. We investigate model cell swimming in the larger domain with the cell swimming inside the cylinder in Chapter 4.3.4 and outside of the cylinder in Chapter 4.3.5. In Chapter 4.3.6, we conclude with a model cell swimming between two immersed boundary cylinders.

4.3.1 Swimming Inside a Cylinder: Untethered

We begin with a study of bacterial swimming within an untethered cylinder. The cylinder, with a diameter of 7.46 μm, is placed in a computational domain with dimensions of $10 \times 10 \times 20$ μm^3 and a $16 \times 16 \times 64$ computational grid. We describe the tube with 150 immersed boundary points on each 81 rings and set $S_{tether} = 0$. The simulation details are summarized in Table 3.5.

Simulation information	Data	Unit
Computational domain	$10 \times 10 \times 20$	μm^3
Diameter of the cylinder	7.46	μm
Flagellar force c_f	0.8×10^{-3}	pN
Frames interval	0.2600	sec
Total swimming time	0.52	sec
Swimming speed inside cylinder	4.54	μm/sec.

Table 4.4: Bacterial cell swimming inside an untethered cylinder.

We show simulation results in Figure 4.9. In Figure 4.9(top) we see that the cylindrical tube rotates in a clockwise direction when viewed from the top. Thus the tube is totally in the same direction as the model flagellum. In the XZ-view shown in Figure 4.9(middle) we can see that the cylinder moves vertically as the bacterial cell swims upwards. In the XY-view shown in Figure 4.9(bottom) we show the fluid markers inside and outside of the cylinder. The swimming speed of the bacterial cell is approximately 4.54 μm/s. For comparison, the bacterial swimming speed was approximately 13.523 μm/s in the simulation of free swimming shown Chapter 3.2.1.

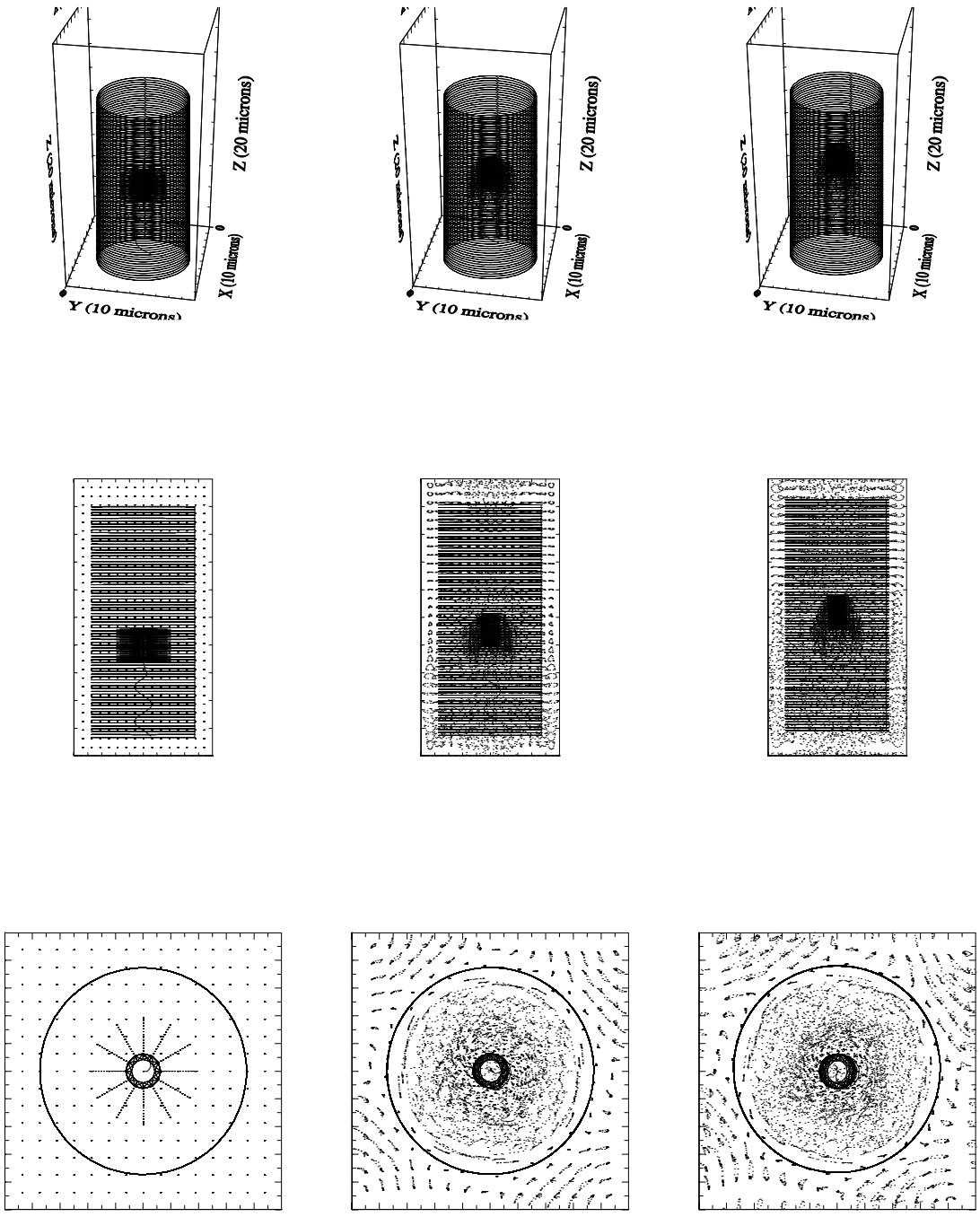

Figure 4.9: Swimming inside an untethered cylinder.

4.3.2 Swimming Inside a Cylinder: Tethered

In the following simulation, we introduce a single model bacterial cell into a tethered cylinder. The cylinder structure has elastic forces as well as tethered forces. The tube with height 16.67 μm has 150 immersed boundary points on each of the 81 rings. The simulation data is summarized in Table 4.5.

Simulation information	Data	Unit
Computational domain	$10 \times 10 \times 20$	μm^3
Diameter of the cylinder	7.46	μm
Flagellar force c_f	0.8×10^{-3}	pN
Frames interval	0.2600	sec
Total swimming time	0.52	sec
Swimming speed inside cylinder	3.002	μm/sec.

Table 4.5: Swimming inside a tethered cylinder.

This simulation is identical to that shown in Chapter 4.3.1, except that the cylinder here is tethered. The bacterial swimming speed in the tethered cylinder is approximately 3.0 μm/s which is a 33.88% reduction compared with the swimming speed in the untethered cylinder. The simulation results are shown in Figure 4.10. Note that the patterns of the fluid markers as shown in Figure 4.10 (bottom) appear quite different from the patterns seen above in Figure 4.9 (bottom).

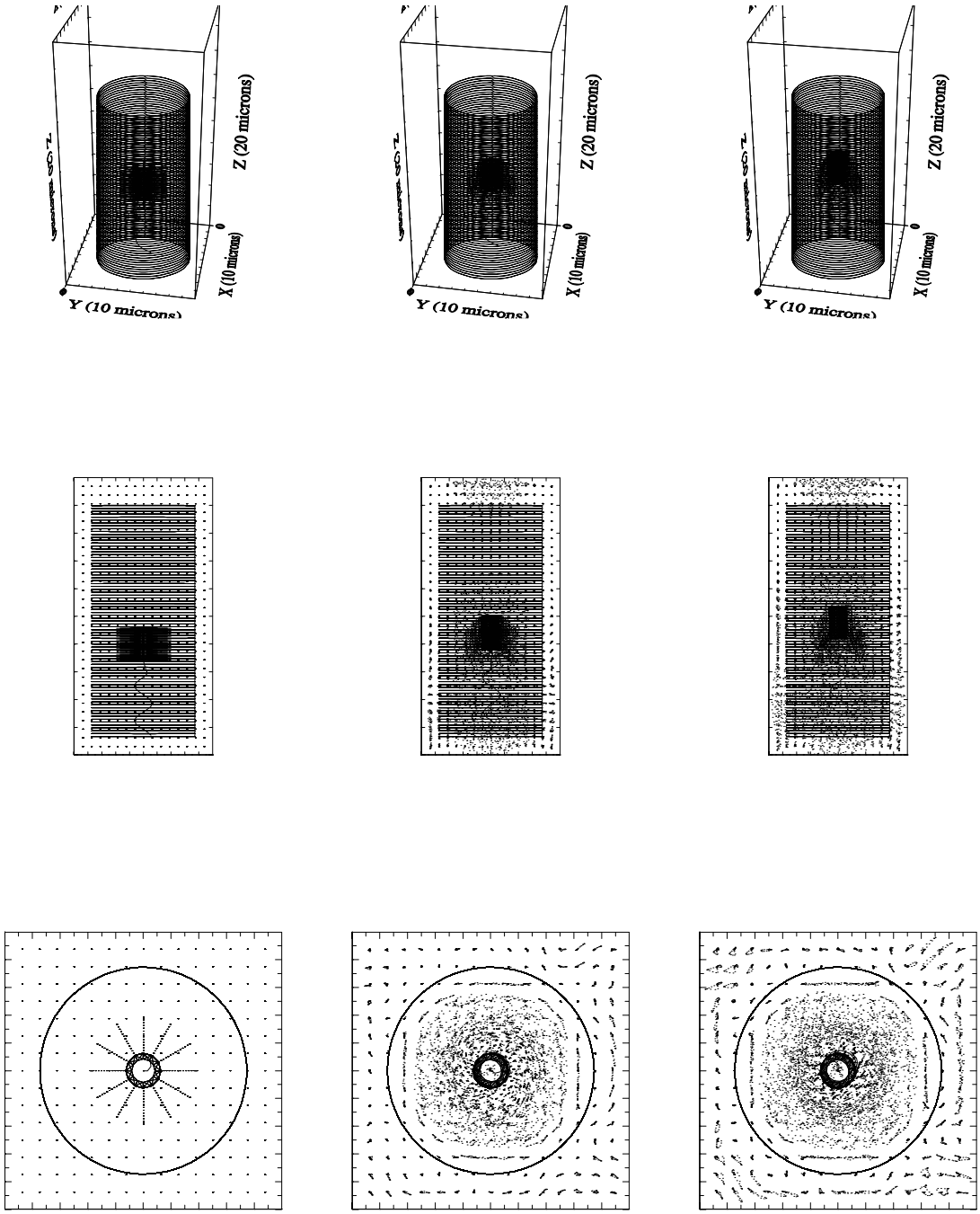

Figure 4.10: Swimming inside a tethered cylinder.

In the Figure 4.11, we show the results of a similar simulation with faster swimming speeds obtained by doubling the flagellar force constant. This allows us to observe a longer model cell trajectory with the same amount of computational CPU time. The total swimming time is 0.813 seconds. The model bacterial cell swimming speed is 7.73 μm/sec. We summarize the simulation information in Table 4.6.

Simulation information	Data	Unit
Computational domain	$10 \times 10 \times 20$	μm^3
Diameter of the cylinder	7.46	μm
Flagellar force c_f	1.6×10^{-3}	pN
Frames interval	0.271	sec
Total swimming time	0.813	sec
Swimming speed inside cylinder	7.73	μm/sec.

Table 4.6: Swimming inside a cylinder with flagellar force doubled.

In the top and middle rows of Figure 4.11, we see the model cell swims upwards in the first two frames, veers to the right in the third and turn back toward the left in the fourth. We show the XY-view from the top in the bottom row.

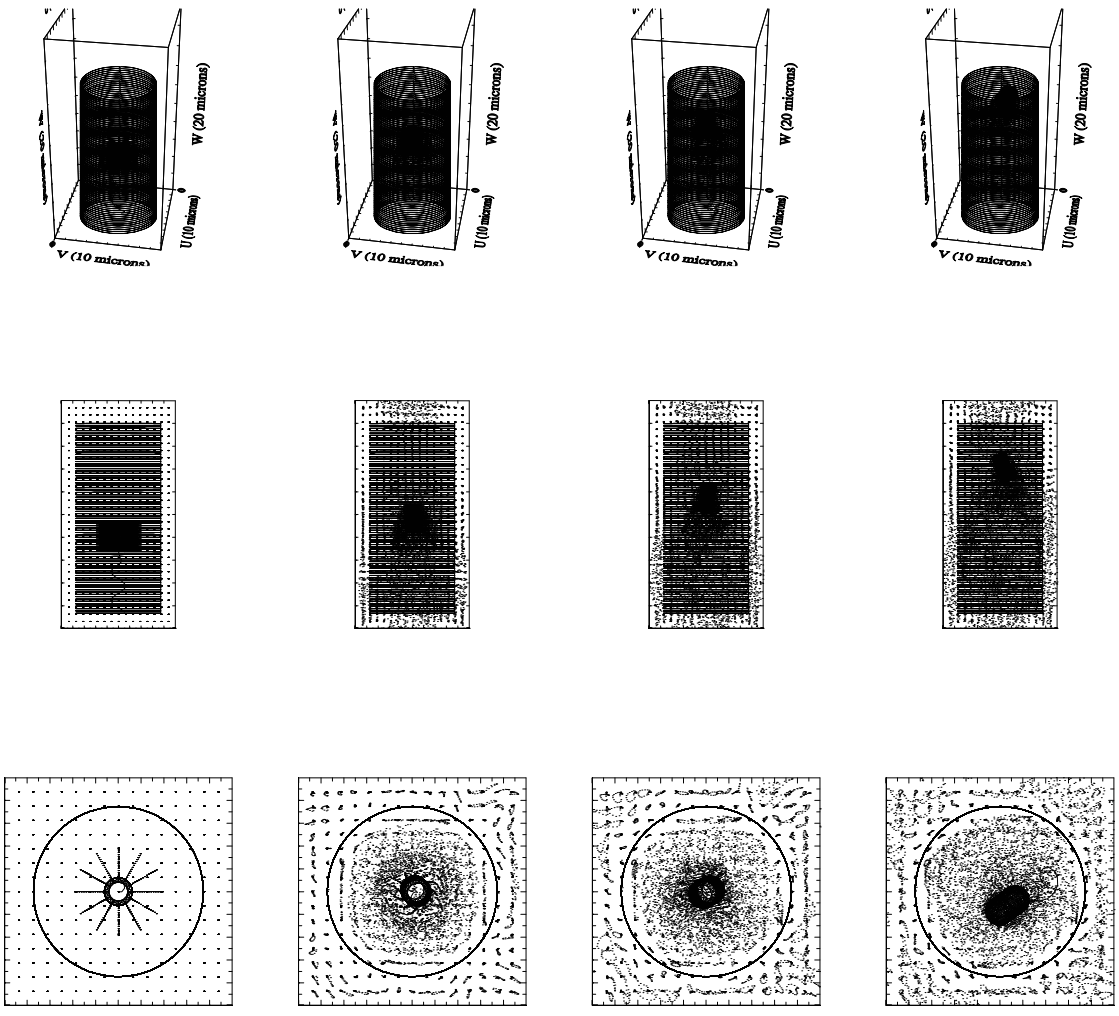

Figure 4.11: Swimming inside a cylinder with increased swimming speed.

4.3.3 Swimming Inside a Cylinder Near the Cylinder Wall

In the simulations shown in Chapter 4.3.2, we found that the model cell swimming speed was significantly reduced in the cylinder. Here we increase the model cell swimming speed by setting the flagellar force parameter to $c_f = 1.0 \times 10^{-3}$ pN. The objective is to visualize wall effect on the trajectory of the model cell.

In this simulation, the model cell is 2.1 μm away from the cylinders wall. The tube with height 16.67 μm comprised of 150 immersed boundary points on each 81 rings. We summarize the simulation results in Table 4.7:

Simulation information	Data	Unit
Computational domain	$10 \times 10 \times 20$	μm^3
Diameter of the cylinder	7.46	μm
Flagellar force c_f	1.0×10^{-3}	pN
Frames interval	0.325	sec
Total swimming time	0.65	sec
Swimming speed with cylindrical wall influence	3.40	μm/sec.

Table 4.7: Swimming near a cylindrical wall.

In the 3D view shown in Figure 4.12 (top) and in the XZ-view shown in Figure 4.12 (middle) we see that the model cell swims upwards with the cell body tilted toward cylindrical wall. In the XY-view from the top we can see that the cell orientation moves away from the Z-axis as well. In order to observe the bacterial cell swimming pattern when it swims nearby the cylinder, a larger flagellar force c_f taken. The bacterium swims at a speed of 3.40 μm/sec.

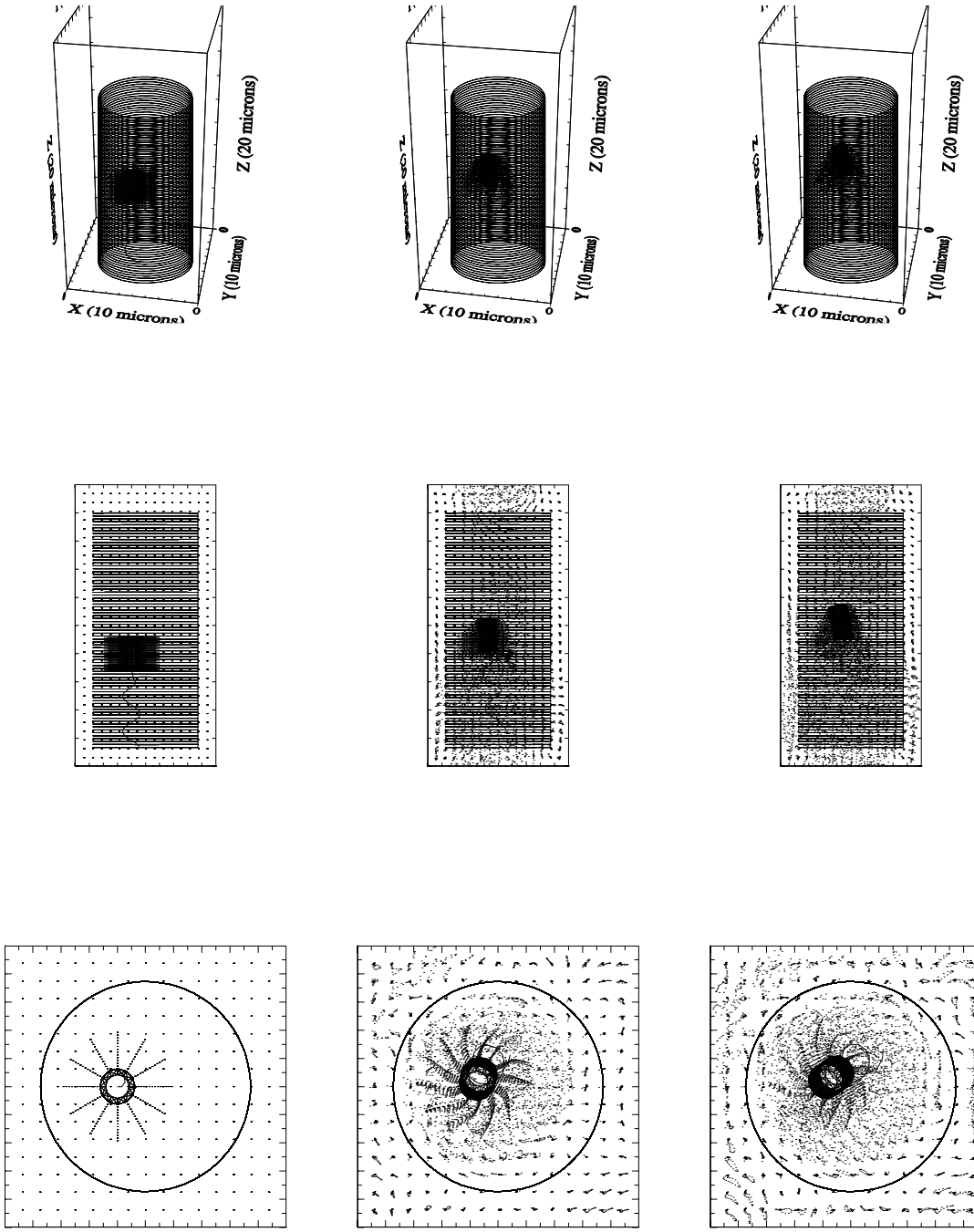

Figure 4.12: Swimming near the internal wall of a cylinder.

4.3.4 Near the Inner Wall of a Tethered Cylinder

In this simulation, the computational domain is $20 \times 20 \times 20$ μm^3 with a $32 \times 32 \times 32$ grid. The diameter of the cylinder is increased to 7.96 μm from the previous one of 7.46 μm in Chapters 4.3.1-4.3.3. The tube with height of 16.67 μm is comprised of 160 immersed boundary points on each of the 81 rings. The initial spacing between cell wall and cylindrical wall is 1.355 μm. The flagellar force $c_f = 0.8 \times 10^{-3}$ pN. The simulation data is summarized Table 4.8:

Simulation information	Data	Unit
Computational domain	$20 \times 20 \times 20$	μm^3
Diameter of the cylinder	7.96	μm
Flagellar force c_f	0.8×10^{-3}	pN
Frames interval	0.2167	sec
Total swimming time	0.433	sec
Swimming speed near internal cylindrical wall	2.28	μm/sec.

Table 4.8: Swimming near an internal wall.

The bacterial swimming speed is strongly influenced by the no-slip condition of the cylinder wall, because the initial cell to wall spacing is small. The simulation results are shown in Figure 4.13.

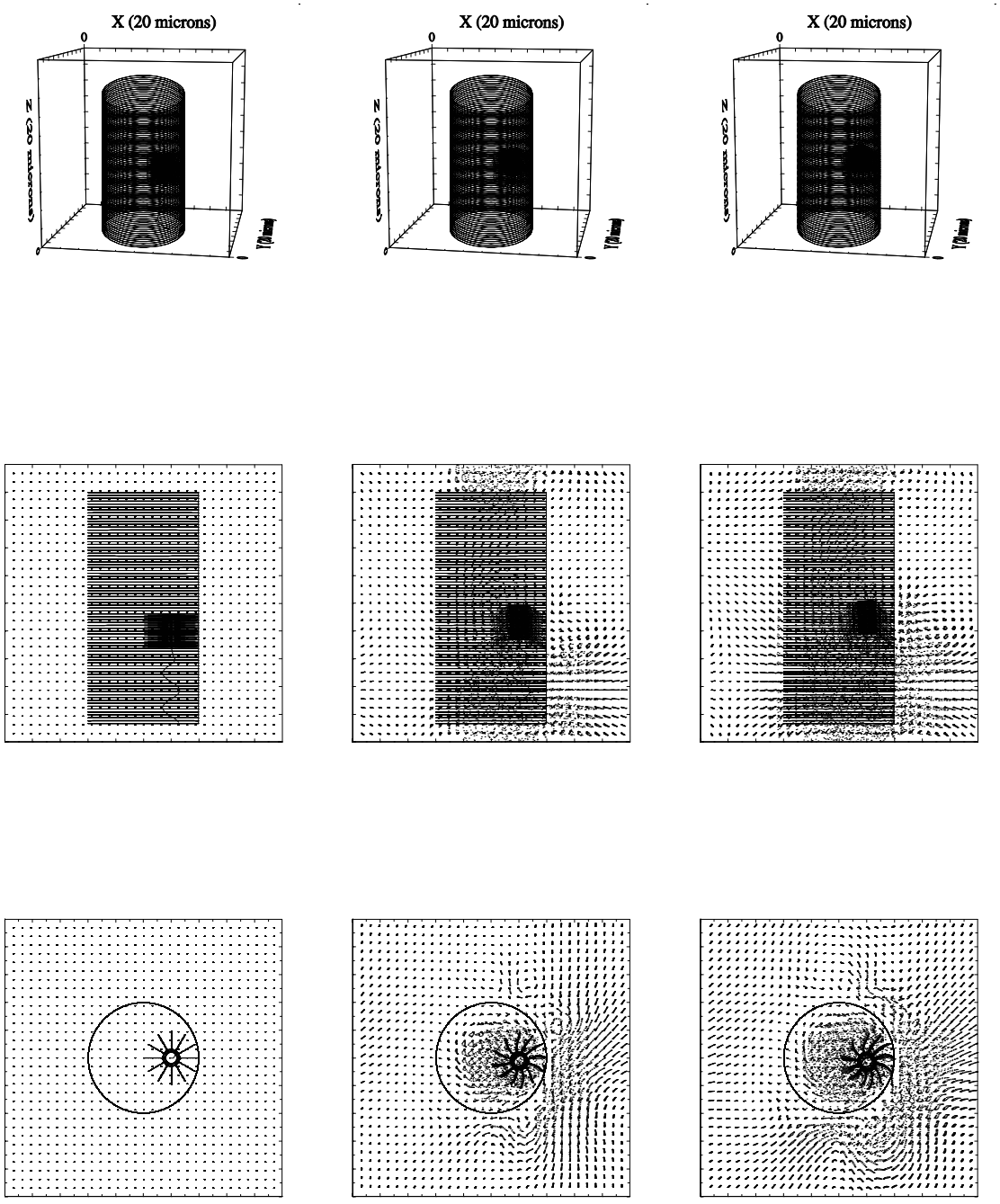

Figure 4.13: Swimming near an internal cylindrical wall.

4.3.5 Near the External Wall of the Fixed Cylinder

In the following simulation, we consider a model bacterial cell swimming outside a cylinder. The computational domain is $20 \times 20 \times 20$ μm^3 with a $32 \times 32 \times 32$ grid. The diameter of the cylinder is 5.97 μm. It is comprised of 120 immersed boundary points on each of the 81 rings with a height of 16.67 μm. In this simulation, the bacterium is swimming outside the cylinder with an initial spacing of 2.052 μm between the cell wall and the cylindrical wall.

Simulation information	Data	Unit
Computational domain	$20 \times 20 \times 20$	μm^3
Diameter of the cylinder	5.97	μm
Flagellar force c_f	0.8×10^{-3}	pN
Frames interval	0.2167	sec
Total swimming time	0.433	sec
Swimming speed with cylindrical wall influence	11.96	μm/sec.

Table 4.9: Swimming outside a tethered cylinder.

The total swimming time for the bacterial cell is 0.433 seconds with a swimming speed 11.96 μm/sec. We show the 3D results for the simulation in the top row of Figure 4.14. The cell swims upwards but tilted toward the right. We can compare the simulation results with that of Chapter 4.1.1. In Chapter 4.1.1, the cell swam near a planar wall, here the cell swims near a cylindrical wall. The flagellar force is the same in both simulation. The swimming speeds are comparable and in both cases the cells swim upwards with a tilt toward the right. The XZ-view with fluid markers is shown in the middle row of Figure 4.14 and the XY-view in the bottom row.

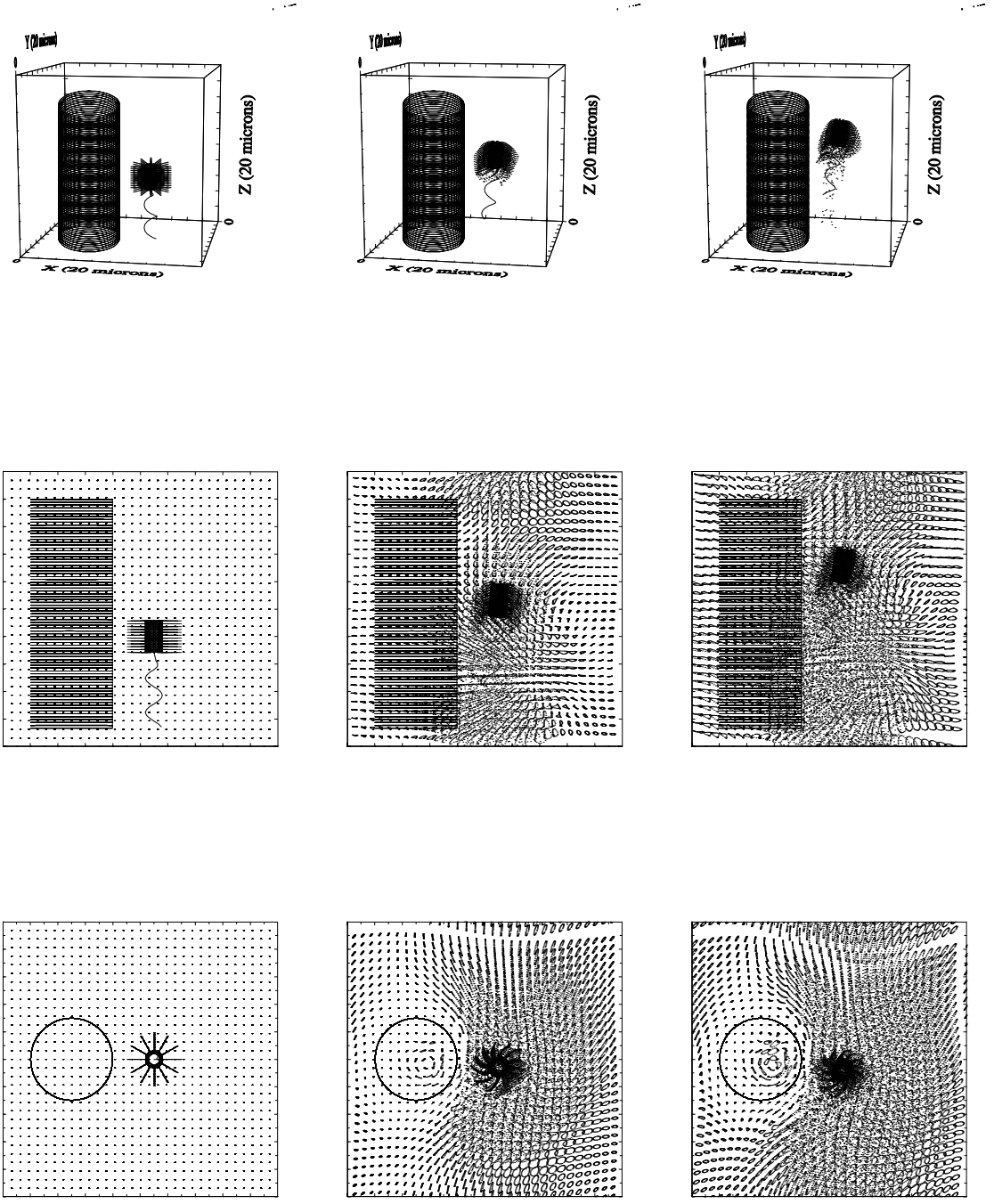

Figure 4.14: Swimming outside a cylinder.

4.3.6 Swimming Between Two Cylinders

Finally, we consider the model bacterial cell swimming between two cylinders in a computational domain of $20 \times 20 \times 20 \mu m^3$ with a $32 \times 32 \times 32$ grid. These two tethered cylinders are identical in design with diameters of 4.976 μm. Each cylinder's axis is aligned with the Z-axis. The spacing between two cylinders walls is 5.024 μm. These tubes are comprised of 100 immersed boundary points on each of 81 rings with a height of 16.67 μm. We use a large flagellar force of 1.8×10^{-3} pN in order to increase the swimming speed. The total run time is 0.4166 seconds and the average swimming speed is 22.077 μm/sec. The simulation details are summarized in Table 4.10.

Simulation information	Data	Unit
Computational domain	$20 \times 20 \times 20$	μm^3
Diameter of the cylinder	4.976	μm
Flagellar force c_f	1.8×10^{-3}	pN
Swimming speed	22.077	μm/sec.
Frames interval	0.2083	sec
Total swimming time	0.4166	sec

Table 4.10: Swimming between two cylinders.

We show the 3D view of the simulation results in Figure 4.15 (top) and see the cell swimming up and biased from its original swimming direction. In the XZ-view, Figure 4.15 (bottom), the fluid hydrodynamics can be observed with the fluid markers. In the XY-view, Figure 4.16(top) shows the model cell swimming toward the lower edge of the frame. In the YZ-view, Figure 4.16 (bottom), we see the cell swimming up with a direction that is biased away from its initial direction.

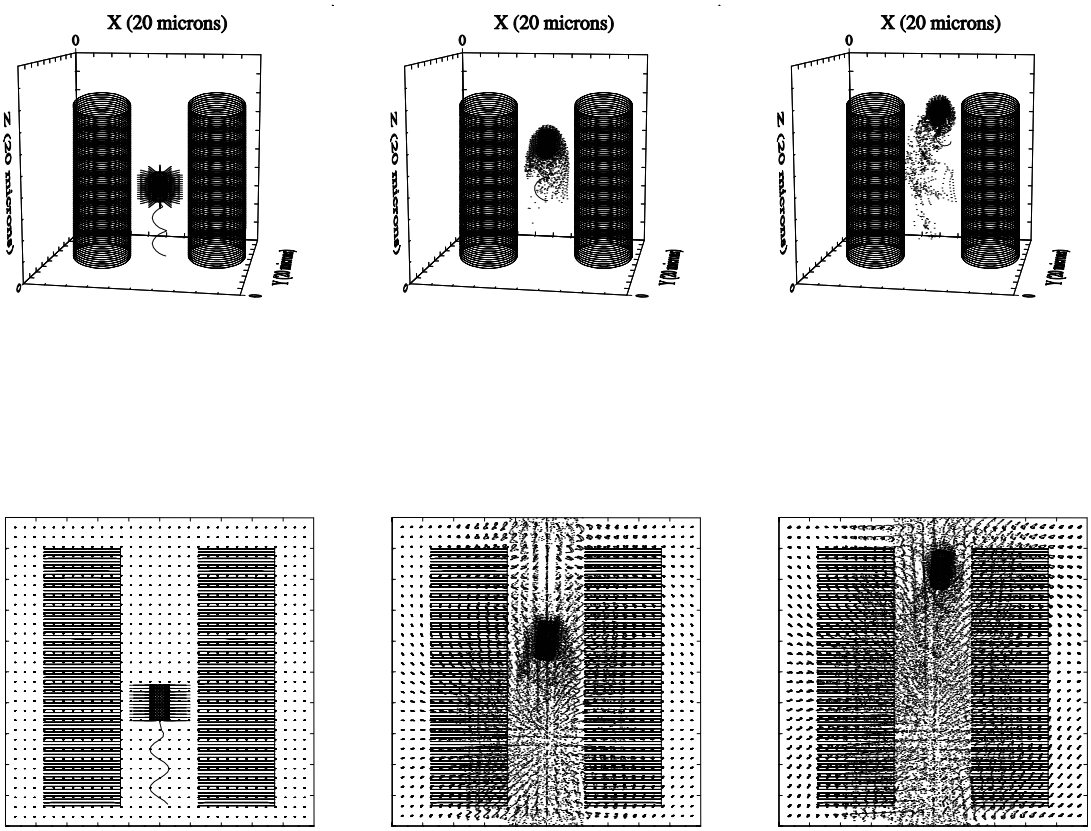

Figure 4.15: Swimming between two cylinders, (top) 3D, (bottom) XZ-view.

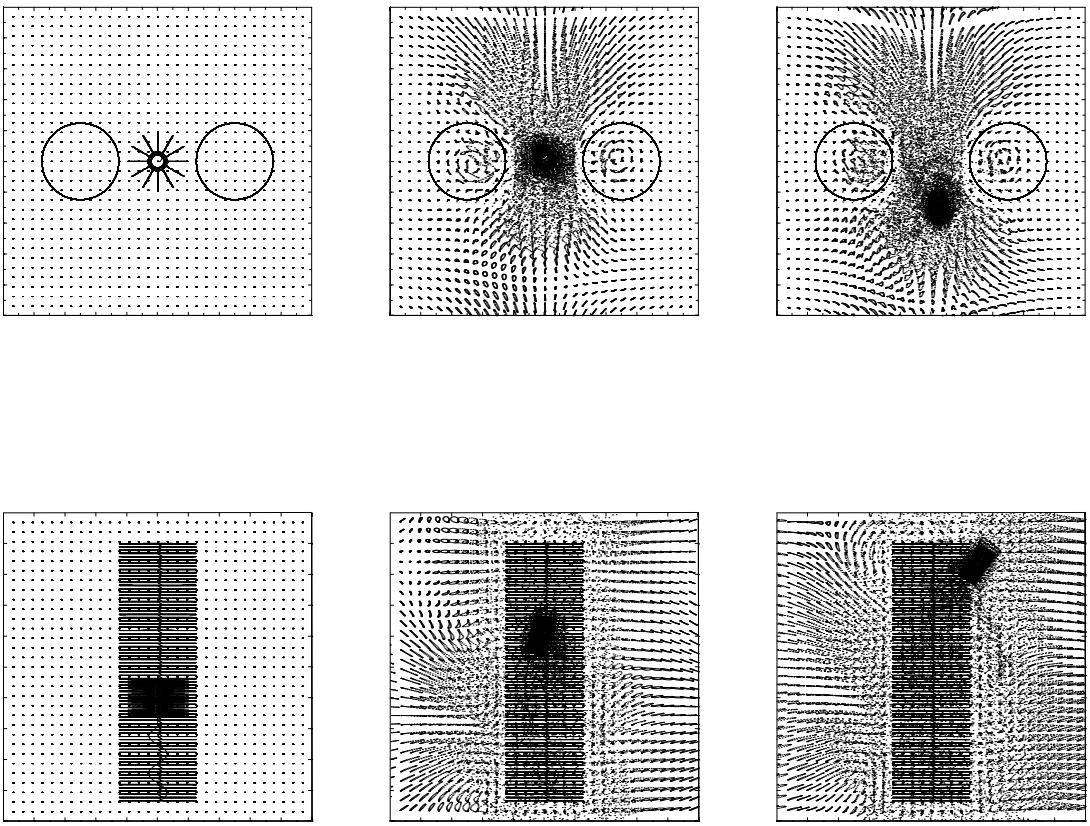

Figure 4.16: Swimming between two cylinders, (top) XY-, (bottom) YZ-view.

Chapter 5

Conclusions and Future Work

In this dissertation, a 3D rod-shaped flagellated bacterial swimming model has been successfully created to simulate the motility of monotrichous rod-shaped bacteria such as Pseudomonas aeruginosa. We have demonstrated the model bacterial cell's ability to swim forward by the propulsive forces of a rotating flagellum and the induced counter-rotation of the bacterial cell body. We presented a numerical convergence study of the numerical model and numerical methods. We presented a variety of simulation results including the swimming of a single model cell, interaction of two swimming cells, the interaction of several swimming cells, the hydrodynamic interaction of a single model cell with a nearby wall or walls and the bacterial swimming inside and outside of cylindrical tubes. We also investigated the model behavior due to the reversal of flagellar orientation by assuming a change in flagellar configuration from normal to semi-coiled as well as the associated change in handedness from left to right.

The 3D model was loosely based on the 2D bacterial swimming model developed by Dillon, Fauci and Gaver in 1995 [52] in which the flagellar forces were represented by a set of four to eight discrete forces and a spherical cell body was represented in

2D as a circular elastic structure. Here, we have developed a 3D rod-shaped cell body consisting of annular rings composed of immersed boundary points and interconnected with elastic links. The 3D bacterial cell body is constructed in the geometrical shape of a cylinder. The double layer of the cell body structure mimics the structure of the bacterial cell wall and provides rigidity for the cell body. In this model, the flagellum structure has been replaced by a set of forces which produces a fluid flow and propel the cell body forward or backward. The flagellar forces are applied to the fluid on a rotating curve of a helical flagellum. We have assumed that the flagellum itself is rigid and inextensible. With this assumption we can model the flagellum in a simplified fashion and only represent the forces due to the flagellar rotation. The rotating flagellum consists a helix of constant diameter that is connected by a flagellar hook to the base of the cell body. The helical flagellar force distribution rotates at a predetermined rotational rate about the flagellar axis which is an extension of the cell's body axis. The normal rotating direction of the flagellum is CCW when viewed from behind the flagellar axis and the flagellum is given a left-handed helix. This produces forward swimming. It has been shown in studies by Shimada, Kamiya and Asakura [137], Macnab and Koshland [111] Taylor and Koshland [141] that a reversal of flagellar rotational direction typically involves a change in handedness from left- to right-. We have shown that reversing the rotational direction and handedness results in a backward swimming motion with approximately the same speed as in forward swimming. We provided a numerical experiment in which the reversal of rotational direction was accompanied by a reversal of handedness and an arc-length preserving change in amplitude and pitch. In this case, the bacterial model cell swam backwards in approximately the same direction but with a different swimming speed.

Diagrams of the forces on the cell body and on the flagellum were created to illustrate the flagellar forces, the torque generating forces and the swimming helical trajectory. We have developed a novel model for modeling the propulsive forces due to a rotating flagellum in which forces are applied to the fluid along a rotating helical filament that moves in the moving frame determined by the location and orientation of the bacterial cell body. The torque forces applied to the fluid by the flagellum are offset by torque forces applied to the cell body.

In all our simulations, total force and total torque applied to the fluid by the model bacterial cell sum to zero. For the cell structure, this condition was automatically satisfied because the link forces are produced in pairs so that the net contribution of each link is zero. The forces produced by the rotating flagellum were also produced in pairs in order to assure a zero force condition on the flagellum. The torque contribution of the flagellar forces with respect to the flagellar and cell axis are summed. The magnitude of the torque forces applied to the cell body is chosen to satisfy a torque balance equation for the entire model organism. The cell body torque forces produce a counter rotation of the cell body with respect to direction of flagellar rotation.

We provided many simulation results. In one set of simulations, we demonstrated the numerical convergence of the method as the computational grid was refined. In the convergence study we used a set of four computational grid on a N^3 cubic domain with grids of 16^3, 32^3, 64^3, and 128^3. With four grids, we were able to produce two convergence estimates. These results showed positive convergence rates for all measured quantities which included global fluid velocities in several norms, bacterial swimming and rotational velocities. The convergence results on the finer set of three grids ($N = 32, N = 64, N = 128$) produced numerical convergence results consistent

with first order convergence in the L_2 and L_∞ norms, second order in the L_1 norm in fluid velocities and roughly first order convergence in bacterial swimming and rotational velocities. These results are consistent with numerical convergence studies of other immersed boundary models. We showed the expected helical trajectory for a free swimming bacterial cell.

We have provided preliminary studies of the model cell behavior in forward and backward swimming, of the interaction of two swimming model cells, of a single model cell with one or two walls and one or two cylinders. Forward and backward swimming was investigated by Goto, et al. [114] using a boundary element method. They found that bacteria swim more slowly near a wall have trajectories that curve in the CCW direction when viewed from above. Our results, in Chapter 3.3, are in qualitative agreement with this study, and shows that a nearby wall reduced swimming speeds and produced changes in swimming direction. Lauga, et al in 2006 [92] found experimentally that bacteria swimming near a wall have curved trajectories. Our results in Chapter 4.1.2 found that the model cell trajectory was all curved in the CCW direction when the swimming in parallel to a nearby wall.

In future work, we plan to continue our development of the bacterial model cell. Several directions include:

- A more comprehensive study of two cell interaction in the rectangular parallelepiped as well as a study of two cell interaction within a cylinder.

- A comprehensive study of the interaction of bacterial swimming with walls. This study would also investigate the effect of wall and cylinder elasticity on the bacterial trajectory and the influence of cylindrical radius on cell swimming inside and outside of the cylinder.

- Reduction of the bacterial model by using a much smaller number of immersed boundary and flagellar points for the purpose of doing larger scale simulations of the collective swimming behavior of many bacteria seen in veil formation and bioconvection.

- A refinement of the current model to include a more detailed representation of the flagellum and bacterial motor [28] in which the material properties of the flagellum and motor are explicitly modeled by the immersed boundary method. The starting point for as model of this type is the immersed boundary model for a rotating filament introduced by Lim and Peskin [106, 152].

Bibliography

[1] M. Alam, M. Claviez, D. Oesterhelt and M. Kessel, "Flagella and Motility Behaviour of Square Bacteria". *The EMBO J.*. Vol.3, No.12, p.2899-2903, 1984.

[2] A. Arkhipov, P. Freddolino and K. Schulten, "Bacterial Flagellum: The Flagellum and Bacterial Motility". Available from: http://www.ks.uiuc.edu/Research/flagellum/

[3] A. Arkhipov, P. Freddolino, K. Imada, K. Namba and K. Schulten, "Coarse-Grained Molecular Dynamics Simulations of a Rotating Bacterial Flagellum". *Biophys. J.*. Vol. 91, p.4589-4597, Dec.2006.

[4] G.K. Batchelor, "Slender-body theory for particles of arbitrary cross-section in Stokes flow". *J. Fluid Mech.*. Vol.44, Part 3, p.419-440, 1970.

[5] H.C. Berg, "Dynamics properties of bacterial flagellar motors". *Nature*. Vol.249, p.77-79, May.1974.

[6] H.C. Berg, "Bacterial behavior" *Nature*. Vol.254, p.389-392, Apr.1975.

[7] H.C. Berg, "Chemotaxis in Bacteria". *Annual Reviews*. p.119-136, 1975.

[8] H.C. Berg, "How Bacteria Swim". *Sci. Am.*. Vol.233, p.36-44, 1975.

[9] H.C. Berg, "Motile Behavior of Bacteria". *Physics Today on the Web-Cover Story*. Available from: http://www.aip.org/pt/jcn00/berg.htm

[10] H.C. Berg, "Chemotaxis Gene Unveiled". *Nature*. Vol.321, p.200-201, May.1986.

[11] H.C. Berg, "Random Walks in Biology: Expanded Edition". *Princeton University Press*. 1993.

[12] H.C. Berg, "Symmetries in Bacterial Motility". *Proc. Natl. Acad. Sci. USA*.. Vol.93, p.14225-14228, Dec.1996.

[13] H.C. Berg, "The Rotary Motor of Bacterial Flagella". *Annu. Rev. Biochem*.. Vol.72, p.19-54, 2003.

[14] H.C. Berg and D.A. Brown, "Chemotaxis in Escherichia coli Analysed by Three-Dimensional Tracking". *Nature*. Vol.239, p.500-504, Oct.1972.

[15] H.C. Berg and R.A. Anderson, "Bacteria Swim by Rotating their Flagellar Filaments". *Nature*. Vol.245, p.380-382, 1973.

[16] H.C. Berg and L. Turner, "Movement of Microorganisms in Viscous Environments". *Nature*. Vol.278, p.349-351, Mar.1979.

[17] H.C. Berg and L. Turner, "Chemotaxis of Bacteria in Glass Capillary Array: Escherichia coli, Motility, Microchannel Plate and Light Scattering". *Biophys. J.*. Vol.58, p.919-930, Oct.1990.

[18] H.C. Berg and L. Turner, "Torque Generated by the Flagellar Motor of Escherichia coli". *Biophys. J.*. Vol.65, p.2201-2216, Nov.1993.

[19] H.C. Berg and L. Turner, "Cells of Escherichia coli Swim Either End Forward". *Cell Biology*. p.477-479, 1994.

[20] R.M. Berry, L. Turner and H.C. Berg, "Mechanical Limits of Bacterial Flagellar Motors Probed by Electrorotation". *Biophys. J.*. Vol.69, p.280-283, Jul.1995.

[21] R.M. Berry and H.C. Berg, "Torque Generated by the Flagellar Motor of Escherichia coli While Driven Backward". *Biophys. J.*. Vol.76, p.580-587, Jan.1999.

[22] R.P. Beyer, Jr., "A Computational Model of the Cochlea Using the Immersed Boundary Method". *J. Comput. Phys.*. Vol.98,No.1, p.145-162, Jan.1992.

[23] J.R. Blake, "A Note on the Image System for a Stokeslet in a No-Slip Boundary". *Proc. Camb. Phil. Soc.*. Vol.70, p.303-310, 1971.

[24] J.R. Blake, "A Model for the Micro-Structure in Ciliated Organisms". *J. Fluid Mech.*. Vol.55, p.1-23, 1972.

[25] J.R. Blake and A.T Chwang, "Fundamental Singularities of Viscous Flow". *J. Eng. Math.*. Vol.8, No.1, p.23-29, Jan.1974.

[26] D.F. Blair, "The Bacterial Rotary Motor". *Nanotechnology*. Vol.2, p.123-133, 1991.

[27] D.F. Blair, "How Bacteria Sense and Swim". *Annu. Rev. Microbiol.*. Vol.49, p.489-520, 1995.

[28] S.M. Block and H.C. Berg, "Successive Incorporation of Force-Generating Units in the Bacterial Rotary Motor". *Nature*. Vol.309, p.470-472, May.1984.

[29] D.C. Bottino, "Modeling Viscoelastic Networks and Cell Deformation in the Context of the Immersed Boundary Method". *J. Comput. Phys.*. Vol.147, p.86-113, 1998.

[30] A. Boyd and M. Simon, "Bacterial Chemotaxis". *Ann. Rev. Physiol.*. Vol.44, p.501-517, 1982.

[31] A. Bren and M. Eisenbach, "Changing the Direction of Flagellar Rotation in Bacteria by Modulating the Ratio Between the Rotational States of the Switch Protein Flim". *J. Mol. Biol.*. Vol.312, p.699-709, 2001.

[32] C.J. Brokaw, "Swimming with Three-Dimensional Flagellar Bending Waves". Available from: http://www.cco.caltech.edu/∼brokawc/Suppl3D/Swim3D.pdf

[33] S. Childress, "Mechanics of Swimming and Flying". *Cambridge University Press*. 1977.

[34] A.J. Chorin and J.E. Marsden, "A Mathematical Introduction to Fluid Mechanics: Third Edition". *Springer*. 2000.

[35] A.J. Chorin, "Numerical Solution of the Navier-Stokes Equations". *Math. Comput.*. Vol.22, p.745-762, 1968.

[36] A.J. Chorin, "On the Convergence of Discrete Approximations to the Navier-Stokes Equations". *Math. Comput.*. Vol.23, p.341-353, 1969.

[37] N.G. Cogan and C.W. Wolgemuth, "Pattern Formation by Bacteria-Driven Flow". *Biophys. J.*. Vol.88, p.2525-2529, Apr.2005.

[38] R. Cortez, L.J. Fauci, N. Cowen and R. Dillon, "Simulation of Swimming Organisms: Coupling Internal Mechanics with External Fluid Dynamics". *Comput. Sci. and Eng.*. Vol.6, No.3, p.38-45, 2004.

[39] R. Cortez, "The Method of Regularized Stokeslets". *SIAM. J. Sci. Comput.*. Vol.23, No.4, p.1204-1225, 2001.

[40] R. Cortez and M. Minion, "The Blob Projection Method for Immersed Boundary Method". *J. Comput. Phys.*. Vol.161, p.428-453, 2001.

[41] R.G. Cox, "The Motion of Long Slender Bodies in a Viscous Fluid. Part 1. General Theory". *J. Fluid Mech.*. Vol.44, Part 4, p.791-810, 1970.

[42] A.T. Chwang, T.Y. Wu and H. Winet, "Locomotion of Spirilla". *Biophys. J.*. Vol.12, p.1549, 1972.

[43] A.T. Chwang, H. Winet and T.Y. Wu, " A Theoretical Mechanism for Spirochetal Locomotion". *J. Mechanochem, Cell Motil.*. 1973.

[44] A.T. Chwang and T.Y. Wu, "Hydromechanics of Low-Reynolds-Number Flow. Part 1. Rotation of Axisymmetric Prolate Bodies". *J. Fluid Mech.*. Vol.63, p.607-622, 1974.

[45] A.T. Chwang and T.Y. Wu, "Hydromechanics of Low-Teynolds-Number Flow. Part 2. Singularity Method for Stokes Flows". *J. Fluid Mech.*. Vol.67, p.787-815, 1975.

[46] A.T. Chwang, "Hydromechanics of Low-Reynolds-Number Flow. Part 3. Motion of a Speroidal Particle in Quadratics Flows". *J. Fluid Mech.*. Vol.72, p.17-34, 1975.

[47] A.T. Chwang and T.Y. Wu, "Hydromechanics of Low-Reynolds-Number Flow. Part 4. Translation of Spheroids". *J. Fluid Mech.*. Vol.75, p.677-689, 1976.

[48] C.V. Delden amd B.H. Iglewski, "Cell-to-Cell Signaling and Pseudomonas aeruginosa Infections". *Emerging Infectious Diseases*. Vol.4, No.4, p.551-560, 1998.

[49] M.L. DePamphilis and J. Adler, "Fine Structure and Isolation of the Hook-Basal Body Complex of Flagella from Escherichia coli and Bacillus subtilis". *J. Bact.*. Vol.105, No.1, p.384-395, Jan.1970.

[50] M.L. DePamphilis and J. Adler, "Attachment of Flagellar Basal Bodies to the Cell Envelope: Specific Attachment to the Outer, Lipopolysaccharide Membrance and the Cytoplasmic Membrane". *J. Bact.*. Vol.105, No.1, p.396-407, Jan.1971.

[51] D. DeRosier, "The Turn of the Screw: The Bacterial Flagellar Motor". *Cell*. Vol.93, p.17-20, Apr.1998.

[52] R. Dillon, L.J. Fauci and D. Gaver III, "A Microscale Model of Bacterial Swimming, Chemotaxis and Substrate Transport". *J. Theor. Biol.*. Vol.177, p.325-340, 1995.

[53] R. Dillon, L.J. Fauci, A.L. Fogelson and D. Gaver, "Modeling Biofilm Processes Using the Immersed Boundary Method". *J. Comput. Phys.*. Vol.129, p.57-73, 1988.

[54] R. Dillon and L.J. Fauci, "A Microscale Model of Bacterial and Biofilm Dynamics in Porous Media". *John Wiley and Sons, Inc.*. 2000.

[55] R. Dillon and L.J. Fauci, "An Integrative Model of Internal Axoneme Mechanics and External Fluid Dynamics in Ciliary Beating". *J. Theor. Biol.*. Vol.207, p.415-430, 2000.

[56] R. Dillon and H.G. Othmer, "A Mathematical Model for Outgrowth and Spatial Patterning of the Vertebrate Limb Bud". *J. Theor. Biol.*. Vol.197, p.295-330, 1999.

[57] R.N. Doetsch and R.D. Sjoblad, "Flagellar Structure and Function in Eubacteria". *Ann. Rev. Microbiol.*. Vol.34, p.69-108, 1980.

[58] T.B. Doyle, A.C. Hawkins and L.K. McCarter, "The Complex Flagellar Torque Generator of Pseudomanas aeruginosa". *J. Bact.*. p.6341-6350, 2004.

[59] C.D. Eggleton and A.S. Popel, "Large Deformation of Red Blood Cell Ghosts in a Simple Shear Flow". *Phys. Fluids*. Vol.10, No.8, p.1834-1845, 1998.

[60] R. Erban and H.G. Othmer, "Taxis Equations for Amoeboid Cells". *J. Math. Biol*. Vol.54, p.847-885, 2007.

[61] L.J. Fauci and C.S. Peskin, "A Computational Model of Aquatic Animal Locomotion". *J. Comput. Phys.*. Vol.77, No.1, p.85-108, Jul.1988.

[62] L.J. Fauci and A. McDonald, "Sperm Motility in the Presence of Boundaries". *Bull. Math. Biol.*. Vol.57, No.5, p.679-699, 1995.

[63] L.J. Fauci, "Computational Modeling of the Swimming of Biflagellated Algal Cells". *Contemporary Mathematics*. Vol.141, 1993.

[64] L.J. Fauci, "A Computational Model of the Fluid Dynamics of Undulatory and Flagellar Swimming". *Amer. Zool.*. Vol.36, p.599-607, 1996.

[65] L.J. Fauci and A.L. Fogelson, "Truncated Newton Method and the Modeling of Complex Immersed Elastic Structures". *J. Communications on Pure and Applied Mathematics*. Vol.XLVI, p.787-818, 1993.

[66] H. Flores, E. Lobaton, S. Mendez-Diez, S. Tlupova and R. Cortez, "A Study of Bacterial Flagellar Bundling". *Bull. of Math. Bio.*. Vol.67, p.137-168, 2005.

[67] A.L. Fogelson, "A Mathematical Model and Numerical Method for Study Platelet Adhesion and Aggregation during Blood Clotting". *J. Comput. Phys*. Vol.56, No.1, Oct.1984.

[68] A.L. Fogelson, "Continuum Models of Platelet Aggregation: Mechanical Properties and Chemically-Induced Phase Transitions". *Fluid Dynamics*

in Biology. Contemporary Mathematics Series, American Mathematical Society. 1993.

[69] P.D. Frymier, R.M. Ford, H.C. Berg and P.T. Cummings, "Three-Dimensional Tracking of Motile Bacteria Near a Solid Planar Surface". *Proc. Natl. Acad. Sci. USA.*. Vol.92, p.6195-6199, Jun.1995.

[70] E. Givelberg and J. Bunn, "A Comprehensive Three-Dimensional Model of the Cochlea". *J. Comput. Phys.*. Vol.191, No.2, p.377-391, 2003.

[71] T. Goto, K. Nakata, K. Baba, M. Nishimura and Y. Magariyama, "A Fluid-Dynamic Interpretation of the Asymmetric Motion of Singly Flagellated Bacteria Swimming Close to Boundary". *Biophys. J.*. Vol.89, p.3771-3779, 2005.

[72] R. Götz and R. Schmitt, "Rhizobium meliloti Swims by Unidirectional, Intermittent Rotation of Right-Handed Flagellar Helices". *J. Bact.*. p.3146-3150, Jul.1987.

[73] J. Gray, "Ciliary Movement". *Cambridge University Press*. 1928.

[74] J. Gray, "The Movement of Sea-Urchin Spermatozoa". *J. Exp. Biol.*. Vol.32, p.775-801, 1955.

[75] J. Gray, "Animal Locomotion". *Weidenfeld & Nicolson, London*. 1968.

[76] M.E. Gracheva and H.G. Othmer, "A Continuum Model of Motility in Ameboid Cells". *Bull. Math. Bio.*. Vol.66, p.167-193, 2004.

[77] B.E. Groffith and C. Peskin, "On the Order of Accuracy of the Immersed Boundary Method: Higher Order Convergence Rates for Sufficiently Smooth Prpoblems". *J. Comput. Phys.*. Vol.208, p.75-105, 2005.

[78] G.J. Hancock and J. Gray, "The Propulsion of Sea-Urchin Spermatozoa". *J. Exp. Biol.*. Vol.32, p.802, 1955.

[79] G.J. Hancock, "The Self-Propulsion of Microscopic Organisms Through Liquids". *Proc. Roy. Soc. A.*. Vol.217, p.96-121, 1953.

[80] M. Hines and J.J. Blum, "Bend Propagation in Flagella I: Derivation of Equations of Motion and Their Simulation". *Biophys. J.*. Vol.23, p.41-57, 1978.

[81] J.J.L. Higdon, "A Hydrodynamics Analysis of Flagellar Propulsion". *J. Fluid Mech.*. Vol.90, Part 4, p.685-711, 1979.

[82] J.J.L. Higdon, "The Hydrodynamics of Flagellar Propulsion: Helical Waves". *J. Fluid Mech.*. Vol.94, Part 2, p.331-351, 1979.

[83] J.J.L. Higdon, "The Gegeration of Feeding Currents by Flagellar Motions". *J. Fluid Mech.*. Vol.94, Part 2, p.305-330, 1979.

[84] M.M. Hopkins and L.J. Fauci, "A Computational Model of the Collective Fluid Dynamics of Motile Micro-organisms". *J. Fluid Mech.*. Vol.455, p.149-174, 2002.

[85] T. Ishikawa and M. Hota, "Interaction of Two Swimming Paramecia". *J. Exper. Biol.*. Vol.209, p.4452-4463, 2006.

[86] C.J. Jones and S.I. Aizawa, "The Bacterial Flagellum and Flagellar Motor: Structure, Assembly and Function". *Adv. Microb. Phys.*. Academic Press Limited, 1991.

[87] M. Kim, J.C. Bird, A.J.Van Parys, K.S. Breuer and T.R. Powers, "A Macroscopic Scale Model of Bacterial Flagellar Bundling". *PNAS*. Vol.100, No.26, p.15481-15485, Dec.2003.

[88] J.B. Keller and S.I. Rubinow, "Slender-Body Theory for Slow Viscous Flow". *J. Fluid Mech.*. Vol.75, Part 4, p.705-714, 1976.

[89] J.B. Keller and S.I. Rubinow, "Swimming of Flagellated Microorganisms". *Biophys. J.*. Vol.16, p.151-170, 1976.

[90] M.C. Lai and C. Peskin, "An Immersed Boundary Method with Formal Second Order Accuracy and Reduced Numerical Viscosity". *J. Comput. Phys.*. Vol.160, p.705-719, 2000.

[91] S.H. Larsen, R.W. Reader, E.N. Kort, W.W. Tso, J. Adler, "Change in Direction of Flagellar Rotation in the Basis of the Chemotactic Response in Escherichia coli". *Nature*. Vol.249, p.75-77, 1974.

[92] E. Lauga, W.R. DiLuzio, G.M. Whitesides and H.A. Stone, "Swimming in Circles: Motion of Bacteria Near Solid Boundaries". *Biophys. J.*. Vol.90, p.400-412, Jan.2006.

[93] P. L*ä*uger, "Torque and Rotation Rate of the Bacterial Flagellar Motor". *Biophys. J.*. Vol.53, p.53-65, Jan.1988.

[94] D. Le, B.Khoo and J. Peraire, "An Immersed Interface Method for the Incompressible Navier Stokes Equations". *J. Comput. Phys.*. Vol.220, No.1, p.109-138, 2006.

[95] L. Lee, "An Immersed Interface Method for the Incompressible Navier Stokes Equations". *Ph.D. thesis*. University of Washington, Seattle, WA, 2002.

[96] L. Lee and R. LeVeque, "An Immersed Interface Method for the Incompressible Navier Stokes Equations". *SIAM Sci. Comp.*. Vol.25, No.3, p.832-856, 2003.

[97] R. LeVeque and Z. Li, "Immersed Interface Methods for Elliptic Equations with Discontinuous Coefficients and Singular Sources". *SIAM J. Numer. Anal.*. Vol.31, p.1019-1044, 1994.

[98] R. LeVeque and Z. Li "Immersed Interface Methods for Stokes Flow with Elastic Boundaries or Surface Tension". *SIAM J. Sci. Comput.*. Vol.18, No.3, p.709-735, 1997.

[99] Z. Li, "The Immersed Interface Method-A Numerical Approach for Partial Differential Equations with Interfaces". *Ph.D. thesis*. University of Washington, Seattle, WA, 1994.

[100] Z. Li and M.C. Lai, "An Immersed Interface Method for the Navier-Stokes Equations with Singular Forces". *J. Comput. Phys.*. Vol.171, p.822-842, 2001.

[101] J. Lighthill, "Mathematical Biofluiddynamics". *SIAM*. CBMS 17, 1975.

[102] J. Lighthill, "Flagellar Hydrodynamics". *SIAM Review*. Vol.18, No.2, p.161-229, Apr.1976.

[103] Z. Liu and K.D. Papadopoulos, "Unidirectional Motility of Escherichia coli in Restrictive Capillaries". *Appl. Env. Microb.*. Vol.61, No.10, p.3567-3572, Oct.1995.

[104] Z. Liu and K.D. Papadopoulos, "A Method for Measuring Bacterial Chemotaxis Parameters in a Microcapillary". *Biotech. and Bioeng.*. Vol.51, p.120-125, 1996.

[105] Z. Liu, W. Chen and K.D. Papadopoulos, "Bacterial Motility, Collisions and Aggregation in a 3-μm-Diameter Capillary". *Bioteh. and Bioeng.*. Vol.53, p.238-241, 1997.

[106] S. Lim and C.S. Peskin, "Simulations of the Whirling Instability by the Immersed Boundary Method". *SIAM J. Sci. Comput.*. Vol.25, No.6, p.2066-2083, 2004.

[107] G. Lowe, M. Meister and H.C. Berg, "Rapid Rotation of Flagellar Bundles in Swimming Bacteria". *Nature*. Vol.325, p.637-640, Feb.1987.

[108] K.E. Machin, "Wave Propagation Along Flagella". *J. Exp. Biol.*. Vol.35, p.796-806, 1958.

[109] R.M. Macnab, "Bacterial Falgellar Rotating in Bundles: A Study in Helical Geometry". *Proc. Nat. Acad. Sci. USA*. Vol.74, No.1, p.221-225, 1977.

[110] R.M. Macnab, D.E. Koshland, "The Gradient-Sensing Mechanism in Bacterial Chemotaxis". *Proc. Nat. Acad. Sci. USA*. Vol.69, No.9, p.2509-2512, 1972.

[111] R.M. Macnab, D.E. Koshland, "Bacteria Motility and Chemotaxis: Light Induces Tumbling Response and Visualization of Individual Flagella". *J. Molec. Biol.*. Vol.84, p.399-406, 1974.

[112] R.M. Macnab, "The Bacterial Flagellum: Reversible Rotary Propellor and Type III Export Apparatus". *J. Bact.*. p.7149-7153, Dec.1999.

[113] R.M. Macnab, "How Bacteria Assemble Flagella". *Annu. Rev. Micobiol.*. Vol.57, p.77-100, 2003.

[114] Y. Magariyama, M. Ichiba, K. Nakata, K. Baba, T.Ohtani, S. Kudo and T. Goto, "Difference in Bacterial Motion between Forward and Backward Swimming Caused by the Wall Effect". *Biophys. J.*. Vol.88, p.3648-3658, May.2005.

[115] N. Maki, J.E. Gestwicki, E.M. Lake, L.L. Kiesslingm and J. Adler, "Motility and Chemotaxis of Filamentous Cells of Escherichia coli ". *J. Bact.*. Vol.182, No.15, p.4337-4342, Aug.2000.

[116] A. Mayo and C.S. Peskin, "An Implicit Numerical Method for Fluid Dynamics Problem with Immersed Elastic Boundaries". *In Fluid Dynamics in Biology: Proc. AMS-IMS-SIAM Joint Summer Research Conf. Biofluiddynamics*. Vol.141 of Contemporary Mathematics, AMS, p.261-277, 1993.

[117] D.M. McQueen and C.S. Peskin, "A Three-Dimensional Computer Model of the Human Heart for Studying Cardiac Fluid Dynamics". *Computer Graphics*. Vol.34, p.56-60, 2000.

[118] D.M. McQueen and C.S. Peskin, "Heart Simulation by an Immersed Boundary Method with Formal Second-Order Accuracy and Reduced Numerical Viscosity". *Mechanics for a New Millennium, Proceedings of the International Conderence on Theoretical and Applied Mechanics (ICTAM) 2000*. Kluwer Acdemics Publishers, 2001.

[119] N. Mittal, E.O. Budrene, M.P. Brenner and A.V. Oudenaarden, "Motility of Escherichia coli Cells in Clusters Formed by Chemotactic Aggregation". *PNAS*. Vol.100, No.3, p.13259-13263, Nov.2003.

[120] K. Namba, " Revealing the Mystery of the Bactreial Flagellum-A self Assembling Nanomachine with Fine Switching Capability". *Japan Nanonet Bulletin-Nanonet Interview*. 11th Issue, Feb.2004.

[121] L. M. Prescott, J. P. Hartley and D. A. Klein, "Microbiology: 2nd edition". *Brown Publishers*. 1993.

[122] C.S. Peskin, "Flow Patterns Around Heart Valves: A Numerical Method". *J. Comput. Phys.*. Vol.10, p.252-271, 1972.

[123] C.S. Peskin, "Numerical Analysis of Blood Flow in the Heart". *J. Comput. Phys.*. Vol. 25, No.3, p.221-249, Nov.1977.

[124] C.S. Peskin, "The Immersed Boundary Method". *Acta Numerica*. p.1-39, 2002.

[125] C.S. Peskin and D.M. McQueen, "A Three Dimensional Computational Model for Blood Flow in the Heart: I. Immersed Elastic Fibers in a Viscous Incompressible Fluid". *J. Comput. Phys.*. Vol.81, p.372-405, 1989.

[126] C.S. Peskin and D.M. McQueen, "Computational Biofluid Dynamics". *Contemporary Mathematics*. Vol.141, p.161-186, 1993.

[127] C.S. Peskin and D.M. McQueen, "A General Method for the Computer Simulation of Biological Systems Interacting with Fluids". *Bio. Fluid Dynamics*. C.P. Ellington and T.J. Pedley, ed. Company of Biologists Ltd., 1995. Available from: http://math.nyu.edu/~mcqueen/Public/papers/seb/SEB_19971216/SEB_19971216.html

[128] C.S. Peskin and B.F. Printz, "Improved Volume Conservation in the Computation of Flow with Immersed Elastic Boundaries". *J. Comput. Phys.*. Vol.105, p.33-46, 1993.

[129] Phan-Thien, Tran-Cong and M. Ramia, "A Boundary-Element Analysis of Flagellar Propulsion". *J. Fluid Mech.*. Vol.184, p.533-549, 1987.

[130] T.T. Powers, "Role of Body Rotation in Bacterial Flagellar Bundling". *Phys. Review E.*. Vol.65, p.040903-1-040903-4, 2002.

[131] E.M. Purcell, "Life at Low Reynolds Number". *Amer. J. Phys.*. Vol.45, No.1, p.3-11, Jan.1977.

[132] E.M. Purcell, "The Efficiency of Propulsion by a Rotating Flagellum". *Proc. Natl. Acad. Sci. USA.*. Vol.94, p.11307-11311, 1997.

[133] M. Ramia, D.L. Tullcok and N. Phan-Thien, "The Role of Hydrodynamic Iinteraction in the Locomotion of Microorganisms". *Biophys. J.*. Vol.65, p.755-778, Aug.1993.

[134] F.F. Roberts,Jr and R.N. Doetsch, "Some Singular Properties of Bacterial Flagella, with Special Reference to Monotrichous Forms". *J. Bact.*. Vol.91, No.1, p.414-421, Jan.1965.

[135] M.E. Rosar and C.S. Peskin, "Fluid Flow in Collapsible Elastic Tubes: A Three-Dimensional Numerical Model". *New York J. Math.*. Vol.153, p.509-534, 2001.

[136] L. Savas, N. Duran, N. Savas, Y. Önlen and S. Ocak, "The Prevalence and Resistance Patterns of Pseudomonas aeruginosa in Intensive Care Units in a University Hospital". *Turk J. Med. Sci.* 2005.

[137] K. Shimada, R. Kamiya and S. Askura, "Left-Handed to Right-Handed Helix Conversion in Salmonella Flagella". *Nature*. Vol.254, p.332-334, Mar.1975.

[138] M. Silverman and M. Simon, "Flagellar Rotation and the Mechanism of Bacterial Motility". *Nature*. Vol.249, p.73-74, 1974.

[139] P.A. Spiro, J.S. Parkinson and H.G. Othmer, "A Model of Excitation and Adaptation in Bacterial Chemotaxis". *Proc. Natl. Acad. Sci. USA*. Vol.94, p.7263-7268, Jul.1997.

[140] A.M. Spormann, "Gliding Motility in Bacteria: Insights from Studies of Myxococcus xanthus". *Microb. Mol. Bio. Rev.*. Vol.63, No.3, p.621-641, Sep.1999.

[141] B. Taylor and D.E. Koshland, Jr., "Reversal of Flagellar Rotation in Monotrichous and Perichous Bacteria: Generation of Changes in Direction". *J. Bact.*. Vol.119, No.2, p.640-642, Aug.1974.

[142] G.I. Taylor, "The Action of Waving Cylindrical Tails in Propelling Microscopic Orginisms". *Proc. Roy. Soc. A.*. Vol.211, p.225-239, 1951.

[143] G.I. Taylor, "Analysis of the Swimming of Microscopic Organisms". *Proc. Roy. Soc. A.*. Vol.209, p.447-461, 1951.

[144] R. Thar and T. Fenchel, "True Chemotaxis in Oxygen Gradients of the Sulfur-Oxidizing Bacterium Thiovulum majus". *Appl. Env. Microb.*. p.3299-3303, Jul.2001.

[145] R. Thar and M. K*ü*hl, "Conspicuous Veils Formed by Vibrioid Bacteria on Sulfidic Marine Sediment". *Appl. Env. Microb.*. p.6310-6320, Dec.2002.

[146] R. Thar and M. K*ü*hl, "Bacteria Are Not Too Small for Spatial Sensing of Chemical Gradients: An Experimental Evidence". *PNAS*. Vol.100, p.5748-5753, May.2003.

[147] R. Thar and M. K*ü*hl, "Complex Pattern Formation of Marine Gradient Bacteria Explained by a Simple Computer Model". *FEMS Microbiology Letters*. Vol.246, p.75-79, 2005.

[148] C.C. Vesier and A.P. Yoganathan, "A Computer Method for Simulation of Cardiovascular Flow Fields: Validation of Approach". *J. Comput. Phys.*. Vol.99, p.271-287, 1992.

[149] Y. Wang, T. Hayat and A.M. Siddiqui, "Gliding Motion of Bacteria on Power-Law Slime". *Math. Meth. Appl. Sci.*. Vol.28, p.329-347, 2005.

[150] N.T. Wang and A.L. Fogelson, "Computational Methods for Continuum Model of Platelet Aggregation". *J. Comput. Phys.*. Vol.151, p.649-675, 1999.

[151] C.W. Wolgemuth and N.W. Charon, "The Kinky Propulsion of Spiroplasma". *Cell*. Vol.122, No.6, p.827-827, 2005.

[152] C.W. Wolgemuth, T.R. Powers and R.E. Goldstein, "Twirling and Whirling: Viscous Dynamics of Rotating Elastic Filaments". *Physical Review Letters*. Vol.84, No.7, 2000.